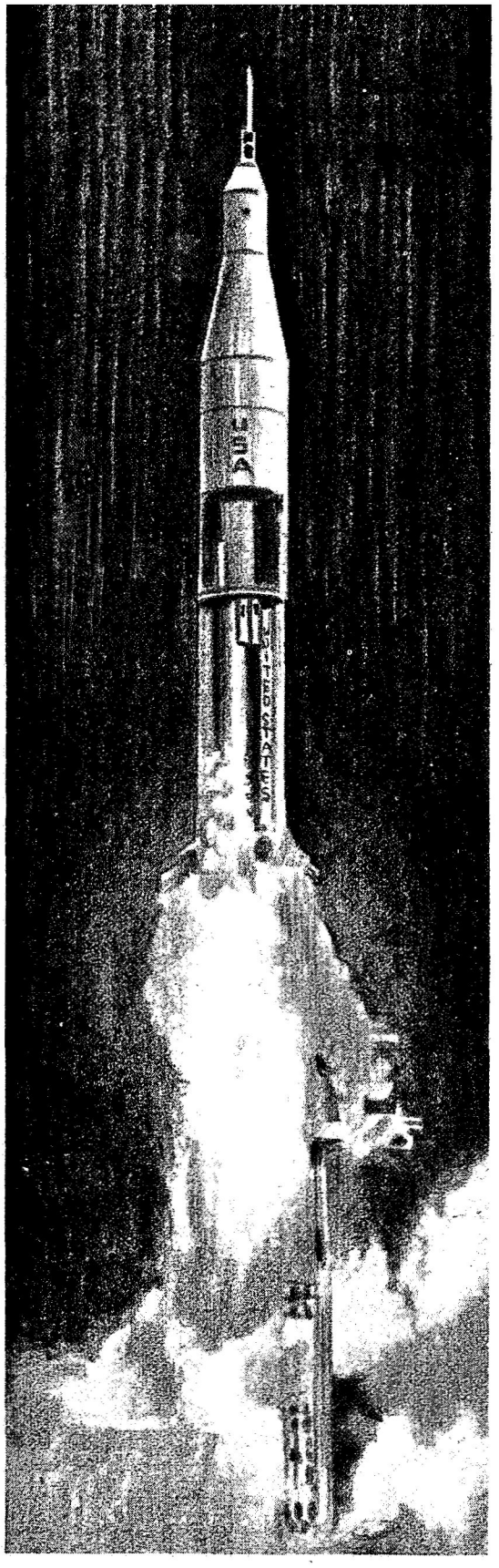

~~BB-3.1.3-15-201~~

PART II

DUR-R-AERO-4

(TN-AP-68-338)

contract NAS8-4016 schedule I vehicle systems integration

AS-205/CSM-101 LAUNCH VEHICL DYNAMICS ANALYSES

SEPTEMBER 3, 1968

SPACE DIVISION CHRYSLER CORPORATION

BB-3.1.3-15-201
Part II
DUR-R-AERO-4
(TN-AP-68-338)

AS-205/CSM-101 LAUNCH VEHICLE DYNAMICS ANALYSES

September 3, 1968

Prepared By

Vehicle Controllability Unit

and

Launch Vehicle Dynamics Unit

of the

AEROSPACE PHYSICS BRANCH
CHRYSLER CORPORATION SPACE DIVISION

Edited By

C. L. Colwell, Supervisor
Vehicle Controllability Unit

R. J. Dinger, Managing Eng.
Rigid Body Control Group

J. S. Keith, Managing Eng.
Vehicle Dynamics Group

J. G. Swider, Manager
Flight Mechanics Section

C. R. Wells, Manager
Flight Dynamics Section

R. H. Ross, Chief Engineer
Aerospace Physics Branch

FOREWORD

This report provides a comprehensive summary of detailed trajectory and flight dynamics analyses data which are applicable to the Saturn IB launch vehicle for the AS-205/CSM-101 mission. All analyses documented herein were generated in the Aerospace Physics Branch, Chrysler Corporation Space Division by authorization of Marshall Space Flight Center, National Aeronautics and Space Administration, under Contract NAS8-4016, Schedule II, Modification MSFC-1, Amendment 87, BB Item 3.1.3-15-201, DUR-R-AERO-4.

ABSTRACT

Contained in the report are the summary of results and description of detailed trajectory (rigid body) and flight dynamics (flexible body) analyses which are applicable to the Saturn IB launch vehicle for the Apollo-Saturn 205/CSM-101 mission. The documentation is divided into two sections. Section 1, SUMMARY OF RESULTS, is an integrated summary of conclusions obtained from each analysis. Section 2, ANALYSES, is a collection of technical presentations in each of which are described the study assumptions, mathematical models, analytical approaches and the results obtained. The specific analyses which are included pertain to:

1) Liftoff Motion
2) Rigid Body Boost Flight Wind Limits
3) Flexible Body Flight Simulation for Real and Synthetic Winds
4) H-1 Engine Out Controllability
5) S-IB/S-IVB Stage Separation Relative Motion
6) Auxiliary Propulsion System Orbital Propellant Requirements

The data results for the nominal and off nominal vehicle flights are presented in the form of time histories and envelopes of extreme values for significant detailed trajectory and flight dynamics parameters. For flights in which the vehicle is subjected to extreme winds or system malfunctions, there are additional displays in the form of flight limitations imposed by launch pad obstructions, vehicle controllability requirements, vehicle structural integrity, and stage separation clearance distance.

INTRODUCTION

The primary mission for the AS-205/CSM-101 Saturn IB launch vehicle is to inject the manned Block II Apollo spacecraft into an elliptical near earth orbit having a 120 nautical mile perigee and a 150 nautical mile apogee. The primary objective of this mission is to verify the spacecraft/crew operations and subsystems performance for an orbital mission.

The AS-205/CSM-101 Saturn IB, which is comprised of an S-IB first stage, an S-IVB second stage, an Instrument Unit, and a payload consisting of the Launch Escape System (LES), Command Module (CM), Service Module (SM), and a Spacecraft Lunar Module Adapter (SLA) is to be launched from Cape Kennedy Launch Facility 34. After rising vertically for 10 seconds, the booster initiates a roll maneuver from the 100 degree launch azimuth to the 72 degree flight azimuth simultaneously with a time dependent pitch program. The S-IB stage propels the vehicle essentially in a gravity turn flight path until an approximate S-IB/S-IVB Separation time of 144.5 seconds. At S-IB/S-IVB separation, the predicted range, altitude, inertial velocity, and inertial flight path angle are approximately 62.0 kilometers, 62.0 kilometers, 2326 meters per second, and 63.4 degrees, respectively. After S-IB/S-IVB stage separation, the S-IVB stage is roll stabilized by the Auxiliary Propulsion System while steering signals are provided in the pitch and yaw planes by the Iterative Guidance Mode. The S-IVB stage propels the payload until an approximate Guidance Cutoff Signal time of 614.6 seconds after liftoff. At Guidance Cutoff Signal, the predicted range, altitude, inertial velocity, and inertial flight path angle are approximately 1870 kilometers, 228 kilometers, 7781 meters per second, and 90 degrees, respectively. The nominal AS-205/CSM-101 mission trajectory which is used as the basis for the analyses reported herein, is documented in Reference 38.

TABLE OF CONTENTS

TABLE OF CONTENTS (CONT'D.)

LIST OF FIGURES

LIST OF FIGURES (CONT'D.)

LIST OF FIGURES (CONT'D.)

LIST OF FIGURES (CONT'D.)

LIST OF FIGURES (CONT'D.)

LIST OF FIGURES (CONT'D.)

LIST OF TABLES

SECTION 1

SUMMARY OF RESULTS

1.1 LIFTOFF MOTION

The clearance distance between the AS-205/CSM-101 launch vehicle drift envelope during liftoff motion and the Cape Kennedy Launch Facility 34 umbilical tower is conveniently expressed as percent of initially available clearance. The minimum percentage value occurs at two T.V. cameras mounted on the Apollo Access Arm Platform. At this level, there is a 3σ probability that the launch vehicle drift envelope will not use more than 82.8 percent of the initially available clearance distance during a November launch. Close ground support equipment constitutes less of a collision hazard than the umbilical tower. The worst case wind speed limits which will insure a 3σ conditional probability of tower clearance occurs for a wind azimuth of 196°. The maximum allowable steady-state wind speed for that azimuth is 10.1 meters per second (i.e., 14.1 meters per second peak wind speed) at the 60 ft. reference level. The maximum allowable steady-state wind speed for that azimuth with the T.V. cameras removed from the Apollo Access Arm Platform is 10.6 meters per second (i.e., 14.8 meters per second peak wind speed) at the 60 ft. reference level. If the AS-205/CSM-101 vehicle is subjected to 95 percentile design surface winds with a concurrent loss of thrust in Engine No. 1 prior to 3.50 seconds, collision with the Apollo Access Arm Platform will result. The same result applies to the occurrence of yaw control single actuator hardover on Engine No. 2 prior to 1.78 seconds.

1.2 RIGID BODY BOOST FLIGHT WIND LIMITS

Rigid body boost flight wind speed limits based upon the control system limitations and structural integrity of the AS-205/CSM-101 launch vehicle have been determined for the altitude interval between 5 and 15 kilometers. The wind limits are established for both the non wind biased and wind biased AS-205/CSM-101 mission first stage boost flight tilt programs. The former pitch program is designed to accommodate an August through October launch window. The latter pitch program is an alternative pitch program designed to accommodate a Winter month launch should the former pitch program prove inadequate for that purpose. As expected, the tilt program differences result essentially in a headwind-tailwind limit shift but have no appreciable effect on crosswind limits.

Wind speed limits for the non wind biased pitch program are most restrictive at an altitude of 11 kilometers for tailwinds. At that altitude, the tailwind limit is 92 meters per second. Thus, the AS-205/CSM-101 launch vehicle can be flown through design tailwinds. Disturbances other than wind speed used to establish this wind speed limit are 99 percent shears and gusts and 3σ C_1, C_2 variations. These disturbances are combined by the root sum square technique to establish the peak wind limit. The 99 percentile envelopes of predicted wind speeds for the months August through January do not exceed the 5 to 15 kilometer wind speed restrictions for the non wind biased tilt program. Therefore, the probability that an AS-205/CSM-101 launch using a non wind biased pitch program will be restricted by inflight winds is less than one percent for an August through January launch window.

1.3 FLEXIBLE BODY FLIGHT SIMULATION FOR REAL AND SYNTHETIC WINDS

The response parameter envelopes presented are based on synthetic wind profiles designed to be more severe than anticipated winds in the month of October so that peak response values associated with AS-205 flight through winds in that month should be below these envelopes. Response for flights through representative "October type" real winds are presented to complement the information furnished by the response parameter envelopes in the sense that the response values depicted are more representative of anticipated values. The results which include effects of bending, sloshing and control filters clearly show that winds should present no problem for the AS-205 flight unless the winds are unusually high for the month of October.

1.4 H-1 ENGINE OUT CONTROLLABILITY

There are no structural integrity or controllability problems associated with the occurrence of a single H-1 engine failure during AS-205/CSM-101 Saturn IB first stage boost flight with the AS-204 Saturn IB engine out steering compensation utilized. The controllability and structural loads estimates are based upon worst case design wind profiles superimposed upon worst case engine failures. Neither system nor environmental tolerances are considered in conjunction with engine failures. Therefore, the AS-204 Saturn IB engine out steering compensation is verified to be acceptable for the AS-205/CSM-101 mission.

1.5 S-IB/S-IVB STAGE SEPARATION RELATIVE MOTION

There are no S-IB/S-IVB stage separation relative motion problems. Potential problems considered are lateral relative motion of the J-2 bell with respect to the S-IB interstage wall during physical separation, and S-IVB post separation controllability. In the event of a single retro rocket failure, the probability of the J-2 bell clearing the S-IB interstage wall is estimated to be 99.82% provided an estimated 1025 kgm. of the residual S-IB propellants are unseated during retro action. The probability of the J-2 bell clearing the S-IB interstage wall is estimated to be 98.22% provided no residual S-IB propellants are unseated during retro action.

1.6 AUXILIARY PROPULSION SYSTEM ORBITAL PROPELLANT REQUIREMENTS

An analysis of the APS orbital propellant requirements reveals that there are sufficient APS propellant reserves to maintain controllability of the S-IVB stage through S-IVB/CSM separation. The estimated nominal and 3σ propellant consumption at the time of S-IVB/CSM separation are 25.9 lbs. and 36.3 lbs., respectively. The estimated nominal and 3σ propellant consumptions at the termination of guaranteed IU lifetime are 59.0 lbs. and 82.6 lbs., respectively. The nominal and 3σ times of propellant depletion are estimated to be 9.5 hours and 6.8 hours, respectively.

SECTION 2

ANALYSES

2.1 LIFTOFF MOTION

2.1.1 Objective

The drift envelope and active malfunction mode studies are conducted in order to establish criteria for safe liftoff conditions as determined by Cape Kennedy Launch Facility 34 umbilical tower proximity to the AS-205/CSM-101 launch vehicle during liftoff motion. A ground wind restriction is established for conditional probability levels ranging from zero sigma to three sigma. A ground wind restriction is also established for a 3σ conditional probability level of tower clearance in conjunction with the measured control deflection error. Also determined are the launch time intervals during which the occurrence of selected active malfunction modes can result in a AS-205/CSM-101 launch vehicle collision with a launch pad obstruction when subjected to concurrent 95 percentile design surface winds.

2.1.2 Discussion

The primary concern during the liftoff motion of the AS-205/CSM-101 vehicle is the clearance of the Cape Kennedy Launch Facility 34 umbilical tower as shown in profile on Figure 1. The Apollo Access Arm Platform, the Tower Top, the top of the Lightning Mast, and the close ground support equipment are the points in closest proximity to the AS-205/CSM-101 Launch Vehicle. These proximities are tabulated in Tables 1 and 2 and are determined from the dimensions obtained from References 2, 3, 4, 5, 6, and 7.

At the holddown arm release, the AS-205/CSM-101 vehicle orientation on LC-34 is shown on Figure 2 (See Reference 8). The vehicle is situated on the launch pedestal with the vehicle pitch plane oriented in the 100 degree azimuth plane and the inertial platform pitch plane oriented in the 72 degree azimuth plane. The sequence of events after holddown arm release entails a vertical rise for 10 seconds and subsequent simultaneous initiation of the pitch and roll maneuvers as defined in Reference 1. Inasmuch as these maneuvers are a factor in determining vehicle clearance with the umbilical tower during launch, the clearance of each vehicle fin adjacent to an umbilical tower obstruction is considered for the active malfunction modes.

All trajectories calculated for this study are generated with a digital flight mechanics computer routine which simulates rigid body vehicle motion in three dimensional space with six degrees of freedom. The simulation included variable mass characteristics, angle of attack dependent aerodynamics, multiple thrust vectors variable in both magnitude and direction, and an idealized control system which has proven adequate for calculating tower clearance in previous analyses. Included, however, are hardware control signal limits and control gimbal deflection limits which are significant during active malfunction modes. The computer input data which define launch vehicle physical characteristics and the data which describes the tilt maneuver and sequence of events conform to Reference 1. For the liftoff motion studies, angle

of attack dependent liftoff aerodynamics of Reference 9 are substituted for those of Reference 1.

Synthetic surface wind profiles (See Figure 3) are generated from the power law:

$$V = V_1\left(\frac{Z}{Z_1}\right)^P$$

where: V is the wind speed at any altitude Z; V_1 is the wind speed at the reference altitude Z_1; and P is the power law exponent as determined by the wind speed value at the reference altitude Z_1. The value of the wind speed in the azimuth of the umbilical tower direction is obtained from the wind rose of Reference 10. The power law exponent which is a function of V_1 is also obtained from Reference 10. The superimposed surface wind gust is a saw-tooth function which peaks at a wind speed value of 1.4 times the corresponding surface wind speed value as illustrated in Figure 3. The gust is initiated at holddown arm release, ramps up to the peak value at 2 seconds after holddown arm release, and ramps back down to the surface wind profile at 4 seconds after holddown arm release. A composite aerodynamic tolerance consisting of a 10% increase in normal force coefficient and a simultaneous .35 caliber forward CP shift is used to simulate distributed aerodynamics.

In order to determine the vehicle launch surface wind restriction, the partial derivatives of vehicle drift, with respect to each tolerance and wind magnitude, are obtained at the levels of closest proximity to each umbilical tower obstruction. The drift contribution due to a tolerance or wind is then generated by multiplying the appropriate partial by its corresponding parameter magnitude. The drift contributions are then root-sum-squared to yield a composite drift. Computation of the composite drift as a function of azimuth yields the desired envelope for each level of closest vehicle proximity to the respective umbilical tower obstruction. The AS-205/CSM-101 drift envelopes are developed for November steady state surface winds and those tolerances which are the primary drift contributors (See Reference 11). These tolerances include: a 2 inch lateral CG offset (See Reference 12), a .2[96] degree composite H-1 thrust misalignment (See Reference 13), and a .5[91] degree composite control deflection error (See Table 3). Comparison of the drift envelopes for each vehicle fin with the respective umbilical tower obstruction perimeters will furnish the resultant clearance distance for each obstruction. The obstruction having the least percentage of initially available clearance distance is then the obstruction for which the wind restriction is determined. The wind is found which results in reducing the obstruction clearance to zero when the drift contribution due to the wind is added to the root-sum-squared drift contribution due to a zero to three sigma range of primary drift contributors. A wind magnitude limit corresponding to a range of zero to three sigma conditional probability of umbilical

tower clearance during liftoff motion is thus generated as a function of wind azimuth.

The AS-205/CSM-101 launch vehicle is surface wind speed limited with respect to launch pad obstruction in conjunction with control deflection error levels. These limits are established by determining the surface wind speed for which the worst case obstruction clearance distance is reduced to zero. The limit is determined by adding the drift contributions of surface wind, a superimposed surface wind gust, distributed aerodynamics, and control deflection error to the root-sum-squared drift contributions of the 3σ values of the remaining primary drift contributors. The resulting surface wind speed limit for a 3σ conditional probability of tower clearance is specified as a function of wind azimuth.

In order to determine the time intervals during which an active malfunction mode results in an umbilical tower collision, the appropriate malfunctions are simulated for a spectrum of flight times of occurrence. Active malfunction mode umbilical tower collision is analyzed for the Apollo Access Arm Platform. All active malfunctions are assumed to occur in the presence of 95 percent design surface winds. The effects of surface winds on the active malfunction mode of single engine thrust failure (significant change in thrust to weight ratio) are determined by including the surface winds in the engine failure flight simulation. However, for malfunctions which do not significantly change the thrust to weight ratio, the effects of surface winds can be determined from the Apollo Access Arm Platform vehicle drift versus wind speed curve shown in Figure 4 (no additional flight simulation of winds is necessary). This curve was generated in the no malfunction liftoff analysis and is, therefore, based on a nominal thrust to weight ratio. The active malfunctions considered, which do not significantly change the thrust to weight ratio, are single control actuator hard-over and loss of hydraulic power. The time interval during which an active malfunction mode, with a concurrent 95 percent design surface wind, results in umbilical tower collision is then determined by interpolating for zero tower clearance from a graph of clearance distance versus the time of malfunction.

2.1.3 Results

The parameterization of drift due to a tolerance or wind magnitude shows that the drift versus tolerance magnitudes are linear and that the drift versus wind magnitude is non-linear. The drift versus wind magnitude at the critical obstruction levels of the umbilical tower are depicted in Figure 4. The clearance distance resulting from the root-sum-squared drift envelopes is presented in Tables 1 and 2. The minimum percent of initial clearance is found to be at the Apollo Access Arm Platform. The wind speed limits which will insure a zero sigma to three sigma range of conditional probability of tower clearance is shown in Figure 5. The worst case wind speed limit which will insure a 3σ conditional probability of tower clearance occurs for a wind azimuth of approximately 196°. The minimum allowable wind speed

for that azimuth is 10.1 meters per second (steady state, i.e., 14.1 meters per second peak wind speed) at the 60 ft. reference level. The maximum allowable steady-state wind speed for that azimuth with the T.V. cameras removed from the Apollo Access Arm Platform is 10.6 meters per second (i.e., 14.8 meters per second peak wind speed) at the 60 ft. reference level. The wind speed limit in conjunction with measured control deflection errors are shown in Figure 6 for a 3σ conditional probability of tower clearance with the T.V. cameras removed.

Engines No. 1, 5, and 6 constitute a potential thrust loss collision hazard as determined from previous analyses (See Reference 11). The launch time interval during which the occurrence of engine thrust losses can result in collision with the Apollo Access Arm Platform when the vehicle is subjected to concurrent 95 percent design surface winds is depicted in Figure 7. The AS-205/CSM-101 is wind limited for engine thrust loss occurrences as shown in Figure 8. The time required for the AS-205/CSM-101 launch vehicle to clear the LC 34 obstructions is shown in Figure 9 as a function of time of thrust loss occurrence.

Yaw control single actuator hardover constitutes the worst single actuator hardover collision hazard as determined from previous analyses (See Reference 11). Consequently, only yaw control single actuator hardover data is presented herein. The launch time interval during which the occurrence of single yaw actuator hardovers can result in collision with the Apollo Access Arm Platform when the vehicle is subjected to concurrent 95 percent design surface winds is depicted in Figure 10. The AS-205/CSM-101 is wind limited for single yaw actuator hardovers as shown in Figure 11.

2.2 RIGID BODY BOOST FLIGHT WIND LIMITS

2.2.1 Objective

The objective of the boost flight wind limits analysis is twofold. Envelopes of rigid body dynamic responses during first stage boost flight are established for the non wind biased AS-205/CSM-101 launch vehicle operational trajectory specified in Reference 38. In addition, wind speed limits are determined for both the non wind biased and wind biased AS-205/CSM-101 launch vehicle operational trajectories specified in Reference 38. The wind speed limits are defined as those at which restrictions must be placed upon the launch to assure a successful flight from a vehicle controllability and structural integrity point of view. Particular emphasis is placed upon the vehicle flight segment characterized by possible high wind speeds and concurrent high dynamic pressure. If a wind limit is exceeded by prelaunch measured winds, it is recommended that a controllability and structural loads trajectory analysis be conducted prior to launch. A final objective of the boost flight wind limits analysis is to provide an estimate of launch probability by comparing the computed wind limits with the probable wind speeds during the scheduled vehicle launch.

2.2.2 Discussion

All calculated trajectories for this study are generated using a digital flight mechanics computer routine which simulates rigid body vehicle motion in three dimensional space with six degrees of freedom. Those features included in the mathematical model, which are of particular importance to rigid body boost flight wind determination, are simulation of the aerodynamic forces and moments, and the simulation of the vehicle attitude control system of the S-IB stage. Features of the study which are paramount, however, are the methods used for computing vehicle structural loads indicators and the assumptions concerning the superposition of wind shear and gust disturbances upon normal boost flight. The analysis described herein is based upon the predicted flight of the AS-205/CSM-101 first stage as provided in Reference 38. The sequence of events pertinent to the predicted trajectory is presented in Table 4. The nominal flight vehicle parameter directly related to the launch vehicle dynamic response characteristics is shown in Figure 12. The parameter C_1 is the derivative, with respect to angle of attack, of angular acceleration due to aerodynamic moment. The parameter C_2 is the derivative, with respect to control engine gimbal deflection, of angular acceleration due to control moment. The $-C_1/C_2$ ratio reaches a local peak instability of .22 at approximately 50 seconds, a local peak instability of .[illegible] at approximately [illegible] seconds, and a local peak instability of 0.[illegible] at approximately 84 seconds. Figure 13 presents the nominal flight dynamic pressure and pitch angle of attack.

The aerodynamic center of pressure location, and the normal and axial force coefficients are computed as bivariate functions of both angle of attack and Mach number. Consideration of the nonlinearity with respect to angle of attack of these aerodynamic parameters is desirable for wind limit trajectory studies because the angle of attack

can become excessively large during the flight time in which the vehicle is subjected to a wind shear and gust disturbance. The vehicle aerodynamic data used in this study are applicable to the AS-205/CSM-101 vehicle and are extracted from References 14 and 15.

The attitude of the Saturn IB Launch Vehicle, S-IB stage, is maintained by a control system which utilizes: computed values for attitude error (i.e., deviations from commanded Euler angle values) in the pitch, yaw, and roll ordered rotations; the pitch, yaw, and roll body angular rates; and the accelerations normal to the vehicle pitch and yaw planes. The attitude error signals are obtained from the LVDC. The rate and acceleration signals are obtained from the body mounted rate gyro packages and accelerometers, respectively. These sensed signals are multiplied by their respective gains, modified by electrical shaping networks (filters), and combined to provide commanded values for pitch, yaw, and roll signals that in turn become mixed for pitch and yaw actuator commands to each of the four gimballed control engines. The logic, equations, and numerical data which are used in this study to simulate the overall control system are representative, within the limitations of digital simulation, of the actual control system aboard the AS-205/CSM-101 Launch Vehicle. Filter networks, internal limits, and engine actuator dynamics, with the exception of the engine actuator rate limits, are included in the mathematical model. The time histories of the control system gains (a_0, a_1, g_2) used are shown in Figure 14. The numerical values for each of the individual component transfer functions are extracted from Reference 16 and 17.

The structural limits criteria used are those presented in Reference 10. These limiting criteria indicate structural integrity limits in terms of control engine gimbal deflection and angle of attack for a specified Mach number, dynamic pressure, and time of flight. Given that for a specified Mach number the dynamic pressure is the same for all wind limit trajectories, angle of attack can be multiplied by the specified dynamic pressure and this product cross-plotted against Mach number and control engine gimbal deflection as illustrated in Figure 15. This product of angle of attack and dynamic pressure is the structural integrity limiting parameter and is designated as the limit. The trajectory flight mechanics computer routine simulation calculates the pitch and yaw $q\alpha$ limits as a bivariate table versus Mach number and pitch and yaw control engine gimbal deflection, respectively. The critical $q\alpha$ ratios for the pitch and yaw planes are computed by dividing the pitch and yaw trajectory simulated $q\alpha$ products by the limits.

Synthetic wind profiles are used to establish the boost flight wind limits. These synthetic wind profiles are comprised of a steady-state wind envelope, a wind shear buildup, and a superimposed gust. Steady-state wind envelopes are members of the family, "Scalar Wind Speed Profile Envelopes (Quasi-Steady-State) for Eastern Test Range" found in Reference 10. The 75% QSS, and 95% QSS steady-state wind envelopes are used in this analysis in the 5 to 15 kilometer altitude

region. Wind shears are defined by a linear wind speed buildup from zero speed at the surface of the earth to a point of tangency on a 99 percentile shear buildup envelope. The shear buildup envelope is followed to the intersection with the steady-state envelope. The 99 percentile shear envelopes for reference wind speeds (the reference wind speed is the value on the steady-state envelope at the altitude of intersection) are also provided in Reference 10. The superimposed gust is an extension of the shear buildup envelope to a peak value of 9 meters per second (99 percentile gust magnitude) above the steady-state wind speed. This peak value of the gust is held constant for a short interval of altitude and then the wind speed returns, in a linear fashion, to the steady-state value.

In order to establish the rigid body boost flight wind limits, the vehicle is subjected to a spectrum of synthetic headwind, tailwind and crosswind profiles as defined in the preceding paragraph. Gust altitudes are applied at one kilometer intervals between 5 and 15 kilometers. For each wind direction and for each gust altitude in the flight region of interest, vehicle flight is simulated for four different wind conditions. Those conditions are: 1) QSS design wind profile only, 2) 99% shear to QSS design wind profile, 3) 99% shear to QSS design wind profile with a superimposed 99% gust, and 4) 99% shear to QSS design wind profile and a superimposed 99% gust with concurrent center of pressure tolerance of .3 calibers. Trajectory and vehicle dynamic response data which corresponds to 75% QSS and 95% QSS wind speed profiles are generated. The monitored trajectory and vehicle dynamic response variables are control engine gimbal deflection, angle of attack and critical $q\alpha$ ratio. The time histories of control system sensor parameters are examined to determine if they have exceeded their limits. The trajectories that do not exceed these limits are used to determine the wind limits. The incremental variations in critical $q\alpha$ ratio for successive simulated conditions are root-sum-squared and added to the critical $q\alpha$ ratio due to the QSS design wind only. This composite critical $q\alpha$ ratio time history peak value for the 75% QSS and 95% QSS winds having the same direction and gust altitude are plotted against the corresponding steady-state wind magnitudes. The steady-state wind magnitudes at which the critical $q\alpha$ ratio equals one is the wind limit for that direction and altitude.

In order to establish the first stage boost flight rigid body dynamic response envelopes, the vehicle is also subjected to a nondirectional 1.75 degree thrust misalignment (per single engine) and a nondirectional .05 meter lateral CG offset. Only the 95% QSS wind profiles are used to generate the envelopes of rigid body dynamic responses. The envelopes are obtained by adding to the 95% QSS wind response the root sum square of the incremental responses due to shears, gusts, and tolerances.

2.2.3 Results

The wind limit results for the non-wind biased AS-205/CSM-101 trajectory are displayed in Figures 16 through 20. Displayed in Figure

16 are sample time histories of critical $q\alpha$ ratios for the four simulated wind conditions corresponding to the 95% QSS tailwinds at 11 kilometers. These time histories correspond to the worst case altitude and wind direction. The composite critical $q\alpha$ ratio for tailwinds at 11 kilometers is shown in Figure 17. The tailwind limit at 11 kilometers is 92 meters per second. It can be seen that the vehicle can be flown through tailwinds equalling the design wind speed.

Figures 18 and 19 depict the wind limit versus altitude determination for each wind direction. The inner curves on the wind limit figures obtained from Reference 19 depict the 99 percentile envelopes of predicted winds for the months of September, October, and November. The wind limit as a function of azimuth is shown in Figure 20 for the worst gust altitude. From Figure 20, it is apparent that the 99 percentile envelopes of wind speeds for the months of September, October and November do not exceed the wind limit for any wind direction. The incremental variations in angle of attack and control gimbal deflection for the four simulated wind conditions are summarized in Table 5.

The wind limit results for the wind biased AS-205/CSM-101 trajectory are displayed in Figures 21 through 23. Figures 21 and 22 depict the wind limit versus altitude determination for each wind direction. The inner curves on the wind limit figures obtained from Reference 19 depict the 99 percentile envelopes of predicted winds for the months of November, December, and January. The wind limit as a function of azimuth is shown in Figure 23 for the worst gust altitude. From Figure 23, it is apparent that the 99 percentile envelopes of wind speeds for the months of November, December, and January do not exceed the wind limits for any wind direction. The incremental variations in angle of attack and control gimbal deflection for the four simulated wind conditions are summarized in Table 6.

The graphs of the envelopes of rigid body dynamic responses during S-IB stage boost flight for the AS-205/CSM-101 non wind biased trajectory are shown in Figures 24 through 27. The attitude rate rigid body dynamic response envelopes shown in Figure 25 are expanded to account for variations observed in postflight data of previous Saturn IB flights.

2.3 FLEXIBLE BODY FLIGHT SIMULATION FOR REAL AND SYNTHETIC WINDS

2.3.1 Objective

This study was made to determine realistic envelopes for wind response parameters associated with AS-205 launch vehicle flight in the month of October.

2.3.2 Discussion

Flexible body response and loads for the AS-205 vehicle flight through real and synthetic winds have been obtained using a digital computer solution of the equations of motion. The effects of flexible body bending and liquid propellant sloshing are included. Seven bending and cluster modes and two sloshing modes are used to describe flexible body deformation and liquid propellant sloshing, respectively. The two sloshing modes simulate sloshing in the S-IVB LOX and S-IVB hydrogen tanks. The mathematical model used considers six rigid body degrees of freedom. Coupling between pitch, yaw and roll planes is, therefore, accurately accounted for. A complete simulation of the actual control system including filter transfer functions, time varying gains, and an actuator transfer function to account for engine compliance is used.

Trajectory data was taken from the AS-205 reference trajectory in Reference 1.

Synthetic Wind Response

AS-205 vehicle flights through a spectrum of synthetic wind profiles based on 95% wind speed envelopes for range and crossrange components in the 72° flight plane at Cape Kennedy for the month of October are simulated to determine extremum values for pertinent wind response parameters. A spectrum of five pitch plane (range) and five yaw plane (crossrange) synthetic wind profiles peaking at 6, 8, 10, 12 and 14 kilometers is considered. The synthetic wind profiles used are defined below:

1) The wind increases linearly from zero wind speed at the ground and merges tangentially into a wind buildup envelope which corresponds to a 99 percentile wind shear buildup envelope reduced by 15 percent.

2) Beginning at the point of tangency the wind follows the wind buildup envelope to the 95 percentile wind speed envelope associated with the month of October and 72° flight plane at Cape Kennedy. Data available for the 75° flight plane was used as approximate wind data for the 72° flight plane.

3) A 7.65 meter per second gust is superimposed by extending the wind buildup envelope 7.65 meters above the point where the buildup envelope joins the wind speed envelope. The gust value is held constant for a 300 meter altitude interval and returns to the value associated with the point where the buildup envelope joins the wind speed envelope. This constant value is maintained from this point on.

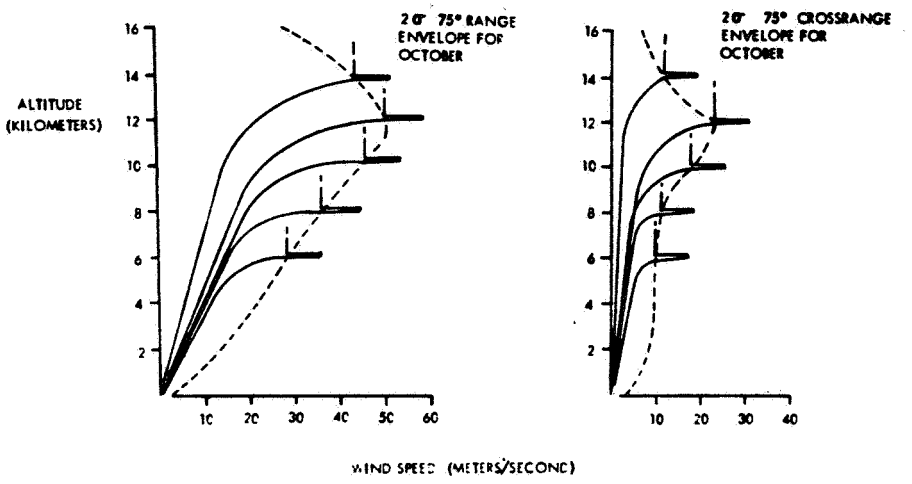

Real Wind Response

In addition to the synthetic winds, discussed above, a measured real wind was selected such that the peak wind speed values for the range components of the wind occurred between the 2σ and 3σ range wind speed envelopes and the peak values for the crossrange components occurred between 2σ and 3σ crossrange wind speed envelopes for October. AS-205 vehicle flight through this real wind is simulated and time histories of associated response parameters are presented as "representative" response for AS-205 flights through "October type" real winds.

2.3.3 Results

The results of this study are presented as time histories and envelopes of pertinent inflight response parameters. Figures 28 through 31 are envelopes of response parameters associated with the synthetic wind profiles. Peak response values for the corresponding real wind case is indicated on each plot. Time histories of response parameters for the real wind case are presented in Figures 32 through 39.

2.4 H-1 ENGINE OUT CONTROLLABILITY

2.4.1 Objective

The Engine Out Controllability Analysis is designed to verify the acceptability of the AS-204 Saturn IB engine out steering compensation for a single engine failure (See Reference 20) during the AS-205/CSM-101 Saturn IB first stage boost flight. The criteria used for verification are first stage boost flight controllability and structural integrity, as well as second stage post separation controllability.

2.4.2 Discussion

Deviations from the AS-205/CSM-101 mission trajectory due to single engine failure during first stage boost flight result in more severe environmental conditions, primarily large trim angles of attack. Further, control engine failures tend to result in greater extremes of environmental conditions than fixed engine failures due to control channel cross coupling and reduced control authority. These factors can lead to structural and controllability problems during S-IB boost flight and controllability problems during post stage separation S-IVB flight if no steering compensation for engine failure is provided.

In a preliminary engine out study (Reference 20) for the Saturn IB/Apollo configuration, it was found that the large aerodynamic moments and loads which accompany early engine failure may be effectively reduced to within tolerable limits by adopting a "chi-freeze" adjustment to the time history of the pitch attitude commands. In the chi-freeze steering mode, upon engine failure, the commanded pitch attitude value is frozen for an incremental duration and then the nominal (albeit, displaced in time) pitch program is resumed until S-IB outboard engine cutoff. The duration of the chi-freeze is chosen to be a variable function of the time of engine failure. The satisfactory value for the freeze interval is one approximately equal to the extended S-IB burning time (corresponding to outboard engine failure) which results from seven engines burning for the remainder of flight. Because chi-freeze is not required for late engine failure, at a flight time of 40 seconds the chi-freeze duration is ramped down from the extended burning time value to zero at 65 seconds; thereafter chi-freeze steering is not utilized. A further modification to the above described policy is related to very early failures. Because extended periods of vertical or near-vertical flight are objectionable near the launch complex, the chi-freeze mode is inhibited during the first 30 seconds of flight. During inhibited chi-freeze, the pitch attitude is not frozen until 30 seconds; the duration of the chi-freeze is, however, equivalent to the extended burn time for the time of engine failure (See Figure 40).

The nominal vehicle AS-205/CSM-101 trajectory, sequence of events, vehicle weight breakdown, control system, and bivariate aerodynamic

characteristics used for this engine out analysis are the same as that discussed in Section 2.2.2. Consideration of bivariate aerodynamics is desirable for engine out trajectory simulation because the angle of attack can become excessively large following an engine failure, particularly, with a superimposed wind shear and gust disturbance which is described in detail in a subsequent paragraph.

The nominal vehicle propulsion and propellant consumption used in this analysis are those specified in Reference 1. Two primary assumptions are made in order to readily facilitate simulation of the propulsion (vacuum thrust) and propellants consumption (mass loss) characteristics subsequent to single H-1 engine failures during first stage boost flight. The first assumption is that vacuum thrust levels on the individual H-1 engine are essentially independent of the difference in the vehicle acceleration profiles between an eight engine burn and a seven engine burn. The second assumption is that post engine out propellant consumption is uniformly distributed between the respective fuel and oxidizer tank clusters via the respective propellant tank cluster manifolds. The total seven engine propellant consumption rate is further assumed to be 7/8 of the nominal eight engine propellant consumption rate, and the total usable propellant is also assumed to be independent of the number of engines consuming the propellant.

The following equations are used to predict the times of inboard engines cutoff signal and outboard engines cutoff signal subsequent to single inboard H-1 engine failures and single outboard H-1 engine failures, respectively.

1) $$t_{OECO} = t_{IEO} + \frac{8}{7}(t_{PSLU} - t_{IEO}) + 3.1 + \frac{4 \times 3 + 3.1}{4}$$

2) $$t_{OECO} = t_{OEO} + \frac{8}{7}(t_{PSLU} - t_{OEO}) + 3.1 + \frac{4 \times 3 + 3.1}{3}$$

where:

t_{OECO} = flight time of outboard engine cutoff signal

t_{IEO} = flight time of single inboard engine failure

t_{OEO} = flight time of single outboard engine failure

t_{PSLU} = nominal flight time of propellant sensor level uncover

These equations are derivable by employing the second assumption. The sum of the first two terms in each equation is the predicted flight time of propellant sensor level uncover subsequent to a single engine failure. The sum of the first three terms in each equation is the predicted time

of inboard engine cutoff signal subsequent to a single engine failure. The first assumption culminates in merely dilating the time scale of the nominal vacuum thrust time histories subsequent to the single H-1 engine failure time. The scale factors for the time dilation are appropriately selected in order to duplicate the nominal engine cutoff vacuum thrust values at the predicted termination of extended burn time (t_{OECO}) due to the single H-1 engine failure. The second assumption culminates in merely dilating the time scale of the nominal propellant consumption time history subsequent to the single H-1 engine failure time. The scale factors for the time dilation are appropriately selected in order to achieve the main burn propellant consumption mass at both the predicted propellant sensor level uncover and predicted outboard engine cutoff signal subsequent to a single H-1 engine failure.

The S-IB stage control system is that described in Section 2.2.2. The S-IVB stage boost flight control system utilizes the same type of sensed signals as the S-IB stage except for the accelerometer signals. These signals are manipulated the same way as in the S-IB stage except the commanded pitch, yaw, and roll signals are not mixed. Instead, the pitch and yaw commanded signals are sent to the J-2 actuators as their commanded deflections, and the roll signal is sent to the Auxiliary Propulsion System. The Auxiliary Propulsion System was not simulated, consequently, a moment balance about the S-IVB stage roll axis is assumed. The time history curves of the S-IVB stage control system gains (a_0, a_1) are presented in Figure 41. The form and the numerical values for each of the individual S-IVB component transfer functions may be found in Reference 16.

A structural loads indicator well suited for malfunctioning vehicle trajectory analysis is the "bending moment critical ratio". Time histories of bending moment critical ratios are obtained by computing the bending moments and axial loads at several vehicle stations. The axial load values are used to compute the critical bending moment value. The critical bending moment at each station corresponds to that value for which a structural limit is violated. The bending moment critical ratio for each station is the quotient of the bending moment at that station and the corresponding critical bending moment for that station. Hence, a bending moment critical ratio equal to unity represents the limiting constraint for structural integrity. Bending moment critical ratios are used in this engine out controllability analysis rather than the critical $q\alpha$ ratios discussed in Section 2.2.2. The critical $q\alpha$ ratios cannot be used since the α,β structural limits data employed to compute these ratios is based upon eight engine flight. See Reference 22 for further details.

Design winds specified in Reference 10 are used with modifications established in Reference 23 to conform to the MSFC practice. Basically, this practice is to use wind shear values which will not be exceeded 99 percent of the time (reduced by 15 percent) to establish a wind speed build up to a quasi-steady-state, scalar wind speed envelope at a prescribed altitude. At the prescribed altitude, a trapezoidal gust, which will not be exceeded 99 percent of the time (reduced by 15

percent), is superimposed upon the wind profile. The percentile quasi-steady-state envelope is chosen to be compatible with September, October, and November winds in each direction referenced to the flight plane (Figure 42). The September, October and November wind envelopes are found in Reference 19. As shown in Figure 42, large magnitude winds are most probable in the directions corresponding to a tailwind and left crosswind. Consequently, only tailwinds and crosswinds are analyzed in this engine failure study.

In order to compare engine failure effects, it is first necessary to generate envelopes for loads and controllability parameters associated with eight engine flight. This objective is accomplished by subjecting an otherwise nominal flight to a spectrum of superimposed design winds. The eight engine flight data then are used to provide the basis for comparison with engine out flight. This comparative rather than absolute approach is convenient because the analysis is essentially a trajectory comparison. The structural loads indicators are calculated internally within the digital trajectory simulation by approximate loads computation formulas. These approximate loads computations, although more accurate than might be presupposed, serve primarily as a means for indicating the flight conditions and vehicle stations where possible structural problems are more likely to occur.

The second step in the engine out analysis is the simulation of vehicle flights which are otherwise normal but with an engine failed at selected times during first stage boost flight. The trajectories are computed with the AS-204 Saturn IB pitch attitude command engine out steering compensation utilized subsequent to the engine failure. This trajectory set provided the information useful for the preliminary verification of the acceptability of the AS-204 Saturn IB engine out steering compensation for the AS-205/CSM-101 mission. Examination of the peak "steady-state" (i.e., no wind) values for control gimbal deflection and bending moment critical ratios are indicative of the controllability and loads trends as a function of the time of engine failure. The engine out trajectory set also provides trend data of the post separation controllability of the second stage. The variation of stage separation $q\alpha$ as a function of engine out time is applicable toward verifying the acceptability of the AS-204 Saturn IB engine out steering compensation for AS-205/CSM-101 staging controllability requirements.

The final step in the technical approach is the final verification of the AS-204 Saturn IB engine out steering compensation for the AS-205/CSM-101 mission. This objective is accomplished by means of a comprehensive wind response and stage separation motion analyses. Envelopes of the peak transient values for loads and controllability parameters corresponding to each engine out time are generated by subjecting the vehicle to a spectrum of superimposed design wind shear and gust disturbances over the range of altitudes within the post engine out high $q\alpha$ flight region. Second stage trajectories are also simulated for each engine out time in order to determine peak dynamic response transients during the first few seconds following stage separation. The envelopes of extreme values for all parameters are used compatibly to provide final verification of the acceptability of the AS-204 Saturn IB engine out steering compensation for the AS-205/CSM-101 mission.

2.4.3 Results

The primary indicator of controllability during S-IB boost flight is the maximum control engine gimbal deflection. In Figures 44 and 43 are shown the envelopes of peak control gimbal deflection without engine failure for a spectra of superimposed 50 percent design crosswinds and 95 percent design tailwinds. The maximum value shown is 3.7 degrees at an altitude of 13 kilometers. Thus, 53.8 percent of the total available control gimbal deflection remains for accommodating an engine out malfunction.

Figures 46 and 45 present the envelopes of maximum bending moment critical ratios as a result of spectra of 50 percent design crosswinds and 95 percent design tailwinds superimposed during eight engine flights. Bending moments critical ratio is an indicator for structural integrity. A critical ratio value of unity or greater indicates the vehicle structural limis have been exceeded. The largest ratio which is shown in Figure 45 is approximately .67. All values presented in this figure are for the worst case vehicle station and for a safety factor of 1.40.

In Figures 47-49 are plotted versus time of engine failure, the envelopes of "steady-state" peak values (i.e., no wind) for control gimbal deflection and bending moment critical ratio (S.F. = 1.40). The peak values are the extremes found during the high q time of flight subsequent to the engine failure time for which the associated time of chi-freeze is shown in Figure 40. It is inferred that the trend behavior of these steady-state peak values due only to engine failure and steering compensation is indicative of the trend behavior of extrema exhibited by bending moment ratio and control gimbal deflection with superimposed wind induced transient conditions.

A preliminary verification of the acceptability of the engine out steering compensation shown in Figure 40 is accomplished through examination of the data shown in Figures 50 and 51. The data presented in these figures is based upon control engine No. 3 or No. 4 being failed during boost with a no wind condition. Particular note should be taken of Figure 50 in which the aerodynamic moment on the S-IVB stage at physical separation is shown versus the time of engine failure. The S-IVB post separation dynamic response transient peaks are increasing functions of the aerodynamic moment on the S-IVB stage at physical separation. The data in Figure 50 indicates that the worst engine failure time for S-IVB post separation controllability occurs at approximately 65 seconds of flight time. A comparison of Figure 50 (staging aero moment) with Figure 51 (staging $q\alpha$ product) illustrates the fact that staging aero moment is proportional to the staging $q\alpha$ product.

Plotted against time of H-1 engine failure in Figures 52-54 are the envelopes of maximum magnitudes of post separation J-2 engine pitch control gimbal deflection, S-IVB pitch attitude error, and pitch rate, respectively. The peak values represent extrema obtained from

second stage flight simulation over a time interval which begins at stage separation and terminates at the Iterative Guidance Mode (second stage steering) initiation. The initial conditions of the second stage flight simulations reflect only the effects of H-1 engine failure with its corresponding engine out steering compensation. Furthermore, H-1 engine failure occurs in the presence of a no wind condition. All three variables in the above figures exhibit similar trends in the dynamic response transient peak envelopes. For both pitch attitude error and pitch attitude rate the maximum magnitude occurs for an H-1 engine failure time of 65 seconds. The J-2 engine pitch control gimbal deflection is maximum for an H-1 engine failure at liftoff.

The prescribed limits for post separation controllability are 7 degrees J-2 control gimbal deflection, 15.3 degrees attitude error, and 10 degrees per second attitude rate. The last two limits may be associated with the S-IVB control system internal limits and the first limit is to be identified with the J-2 engine gimbal stops. As shown in the Figures 52-54 the maximum parameter magnitudes for engine out failure are 1.4 degrees, 2.4 degrees, and 0.73 degrees per second, respectively. Thus, the chi-freeze policy as shown in Figure 40 requires no change in order to accommodate acceptable post separation S-IVB controllability.

Final verification of the acceptability of the engine out steering compensation as depicted in Figure 40 is obtained from a comprehensive wind response rigid body analysis for engine out flights. The rigid body wind response data are obtained by subjecting the vehicle to an engine out malfunction and spectra of superimposed 50 percent design crosswinds and 95 percent design tailwinds. Shown in Figure 55 are the envelopes of peak control gimbal deflections in response to the above mentioned winds for different failure times of engine No. 4. Each of the points defining these envelopes is obtained by first selecting a particular wind direction and engine out time for engine No. 4 failures. Next, a series of trajectories are simulated for different wind gust initiation altitudes. Each of the series incorporates the same wind direction and engine failure time. For each trajectory (wind gust initiation altitude) the maximum value of control gimbal deflection is recorded. Finally, a plot is made of these recorded maximum control gimbal deflections versus gust initiation altitude. The peak value on this plot is the value presented in Figure 55. From Figure 55 it can be seen that the maximum control gimbal deflection encountered in an engine out flight with superimposed 95 percent design tailwinds is 6.9 degrees. (In comparison, the maximum gimbal deflection required for eight engine flight with the above winds is 3.7 degrees.) Thus, the chi-freeze policy as shown in Figure 40 requires no compromise in order to maintain adequate control capability for engine out flight.

In Figure 56 is shown the envelopes of peak bending moment critical ratios (S.F. = 1.40) in response to a spectrum of 50 percent design crosswinds and 95 percent design tailwinds for different Engine No. 4 failure times. Each of the points defining these envelopes is obtained by the same method used in defining the peak control gimbal deflection

envelopes of Figure 55. It can be seen from Figure 56 that engine out flight with superimposed 95 percent design tailwinds results in a maximum bending moment critical ratio of .70. (Eight engine flight with the above winds produces a maximum bending moment critical ratio of .67) Thus, there exists sufficient margin between the maximum ratio values and the limiting value of unity to preclude any possibility of vehicle loss by structural failure. Therefore, the chi-freeze policy as shown in Figure 40 requires no change in order to insure structural integrity for engine out flight.

In order to provide a more complete picture of the effects of engine failure upon vehicle dynamic response, Figure 57 shows envelopes of peak roll attitude error responses to a spectrum of 50 percent QSS crosswinds and 95 percent design tailwinds in combination with engine No. 4 failures. It is seen that the maximum roll attitude error experienced in an engine out flight with superimposed 50 percent QSS crosswinds is 4.6 degrees. Implicit in the roll attitude error excursions are the appreciable effects of control channel cross coupling. Therefore, the chi-freeze policy as shown in Figure 40 is proven to be adequate for all control considerations.

2.5 S-IB/S-IVB STAGE SEPARATION RELATIVE MOTION

2.5.1 Objective

The objective of the stage separation analysis is to verify S-IB/S-IVB staging capability for the AS-205/CSM-101 primary mission. S-IB/S-IVB stage separation capability is also investigated for single retro rocket ignition failures. Staging capability is assured if, during separation relative motion, lateral clearance of the J-2 engine bell with the S-IB interstage is accomplished and S-IVB post staging controllability is maintained. Envelopes of rigid body controllability dynamic responses during the entire S-IVB stage boost flight are also determined.

2.5.2 Discussion

The first requirements for successful AS-205/CSM-101 S-IB/S-IVB stage separation is lateral clearance of the J-2 bell with the S-IB interstage during the physical separation relative motion. Figure 58 depicts J-2 bell initial lateral clearance at the interstage exit plane and is based upon References 27 and 28. The second requirement of successful stage separation is retention of the S-IVB stage controllability during and after its physical separation from the S-IB stage.

Both potential separation problems of J-2 bell interstage collision and S-IVB stage controllability are mainly affected (assuming no retro failures) by large aerodynamic moments or attitude rates existing at first stage boost flight termination. These two problems can be minimized by appropriate first stage boost trajectory shaping which reduces to acceptable levels the dynamic pressure, angle of attack, and attitude rates at separation. Therefore, the AS-205/CSM-101 first stage boost flight is terminated by a nose down and subsequent chi-arrest maneuver such that the angle of attack is small and the attitude rate is essentially zero at S-IB/S-IVB first relative motion. The nose down is initiated at 134 seconds and the chi-arrest is initiated at 134.5 seconds as specified in Reference 30. Outboard engine cutoff occurs at 143.170 seconds and the subsequent S-IB/S-IVB stage separation sequence of events is as shown in Table 4 (See Reference 32).

The main contributor to the physical separation of the S-IB stage from the S-IVB stage is the thrust of the four retro rockets. To a very slight degree, the three ullage thrusts also contribute to the physical separation. Proper phasing of the retro thrust with respect to the separation signal and H-1 thrust decay is necessary for successful staging and is shown in Figure 59 (See Reference 32). The time histories of the retro and ullage thrusts are obtained from References 29 and 30, respectively. Reference 31 provides the H-1 thrust decay profiles. Impingement of the retro rocket plumes on the vehicle creates pressure distributions on the surface of the S-IB/S-IVB interstage and lower S-IVB stage. If a retro rocket fails to ignite, these pressure distributions then become asymmetric thereby causing imbalanced forces to act on the

stages as shown in Figures 60 and 61. This imbalanced force condition constitutes a potential S-IB/S-IVB collision hazard. Figure 59 indicates that the S-IVB stage is without effective J-2 control thrust for approximately 4.0 seconds after physical separation from the S-IB stage. It is during this time interval that S-IVB stage dynamic transients can become excessively large.

All trajectories for this analysis are generated with a digital flight mechanics computer routine which simulates rigid body vehicle motion in three dimensional space with six degrees of freedom. The computer input data which define launch vehicle physical characteristics and the data which describe the trajectory shape and sequence of events conform to Reference 32. Separation aerodynamic characteristics of the two launch vehicle stages correspond to those of Reference 32 and mass characteristics to those of Reference 33.

In order to verify post separation S-IVB stage controllability, envelopes of rigid body dynamic responses are generated during the S-IVB stage boost flight from separation structure severed to orbital injection. The data presented include a nominal time history with $\pm 3\sigma$ bands for each of eight S-IVB controllability parameters. The $\pm 3\sigma$ bands are determined from off nominal conditions. These off nominal conditions are simulated one at a time and include those which occur during first stage boost as well as those which occur during S-IVB flight. For a given flight time and S-IVB controllability parameter, the $+3\sigma$ deviation about the nominal is determined by adding to the nominal, the root-sum-square of the positive incremental excursions resulting from each off nominal condition considered independently. A similar method is used to obtain the -3σ deviation about the nominal. The tolerances which are the main contributors to S-IVB dynamic excursions during S-IB/S-IVB separation are those S-IB boost flight tolerances which have the greatest influence on $q\alpha$ product dispersions at staging, and S-IVB stage variations which increase the moments on the S-IVB stage. Table 7 shows the tolerance magnitudes considered for determining the S-IVB dynamic responses during separation motion (See Reference 34).

The S-IB/S-IVB potential collision problem subsequent to a single retro rocket failure is investigated with the latest available estimates for forces and their points of application which are representative of pressure distributions due to asymmetric plume impingements. The S-IB/S-IVB relative motion resulting from each of four retro rocket failures in combination with stage separation tolerances, subsequent to a nominal S-IB boost flight, is analyzed in order to ascertain successful retro out staging probability. The quoted probabilities are defined by the probability law:

$$P = \sum_{i=1}^{4} P_i \, P_i^*$$

where: $P \equiv$ probability of successful separation with one retro rocket failed

$P_i \equiv$ probability that retro rocket number "i" is the one which failed

$P_i^* \equiv$ probability of successful separation with retro rocket number "i" failed.

The P_i^* probabilities quoted pertain to the cumulative distribution function. Each P_i^* is determined by root-sum-squaring the incremental lateral travel due to each tolerance with retro rocket number "i" failed. Those stage separation tolerances which have the greatest influence on S-IB/S-IVB relative lateral motion are those which create significant moments on the S-IB stage. Aerodynamic moments resulting from aerodynamic tolerances are not large enough on either stage to be significant contributors to a potential S-IB/S-IVB collision. The stage separation tolerances considered in the retro out collision analysis are, therefore, retro rocket thrust variation (not composite), retro rocket thrust misalignment (not composite), and S-IB lateral CG deviation (no aerodynamic tolerances). Values for these tolerances are given in Table 8 and are derived from References 2°, 35 and 36, respectively.

2.5.3 Results

Figures 62 through 69 are a summary of the AS-205/CSM-101 S-IVB controllability from separation structure severed (CECO + 1.379 seconds) to orbital injection. These figures present a nominal time history with $\pm 3\sigma$ bands for each of eight S-IVB controllability parameters. The eight parameters shown are pitch, yaw, and roll attitude errors and body rates, and J-2 pitch and yaw control gimbal deflections. These parameters are influenced mainly by the S-IB boost tolerances (primary contributors to $q\alpha$ product staging dispersions), misalignment of the J-2 thrust with the S-IVB stage, and S-IVB CG lateral deviation. The widths of the 3σ envelopes for these eight parameters indicate that the AS-205/CSM-101 mission success will not be impaired.

The single retro rocket failure results are presented in Figure 58 and Figure 70, and Table 9. Table 9 gives the lateral clearance of the undeflected J-2 bell bottom (at interstage exit plane) with the S-IB interstage for each of the four single retro rocket failures possible, assuming that 1025 kgm of the residual S-IB propellants become unseated during retro action. These results are based upon all retro failures being simulated during an otherwise nominal separation subsequent to a nominal S-IB boost flight. The smallest lateral clearance is .255 meters which results when retro No. 3 fails. Figure 70 presents the J-2 bell lateral drifts in profile view for nominal and retro out conditions with the J-2 gimbal locked and the maximum expected required J-2 deflection of .8 degrees. In addition 3 sigma off nominal drifts for the above cases are also depicted. These results assume 1025 kgm of the residual S-IB propellants become unseated during retro rocket thrusting and retro out conditions are for the worst case, i.e., a failure of retro No. 3. Assuming 1025 kgm of the residual S-IB propellants are unseated during retro rocket thrusting, it is estimated that the probability (cumulative distribution) of the J-2 bell clearing the interstage

for a single retro failure in combination with stage separation tolerances is 99.82% (2.91 σ). Assuming that no residual S-IB propellants are unseated during retro rocket thrusting, it is estimated that the probability (cumulative distribution) of the J-2 bell clearing the interstage wall for a single retro failure in combination with stage separation tolerances is 98.22% (2.10σ).

2.6 AUXILIARY PROPULSION SYSTEM ORBITAL PROPELLANT REQUIREMENTS

2.6.1 Objective

The objective of the Auxiliary Propulsion System (APS) orbital propellant requirements analysis is to verify that there is sufficient APS propellant aboard the S-IVB stage to control the vehicle during the orbital maneuvers.

2.6.2 Discussion

The Auxiliary Propulsion System, shown in Figure 71, consists of two self-contained propulsion systems (modules) mounted on the S-IVB aft skirt 180 degrees apart approximately in the pitch plane. Each module contains three 150 lb. thrust hypergolic attitude control engines and individual fuel and oxidizer supply systems. Two engines, one in each module directed radially outward, are for pitch control. The remaining four engines, two per module, are opposed and directed nearly tangential to the vehicle surface. These latter four engines are for combined roll-yaw control during orbital flight, and during powered flight, are used in opposing pairs for roll control.

The APS control system and laws are found in Figure 72. The control laws attitude error gain (a_0) values are equal to 1.0 degrees per degree and the attitude rate gain (a_1) values are equal to 5.0 degrees per degree per second. The J-2 control system which remains active during orbital flight maintains the same gains which were scheduled at J-2 cutoff signal.

The desired attitude time lines are shown in Figure 73, (See Reference 38). The pitch, yaw, roll angles are ordered rotations defining the orientation between the vehicle coordinate system and the inertial platform system. Under zero roll conditions, pitch and yaw define the orientation of the vehicle longitudinal axis with the launch plane. Pitch attitude indicates the in-plane vehicle orientation and yaw attitude the out-of-plane orientation. Maneuvers required for the AS-205/CSM-101 Mission are included in Tables 4 and 10, (See References 37 and 38). Orbital J-2 thrust history is found in Figure 74 (See Reference 1).

The trajectories calculated for this analysis have been generated using a digital computer routine which simulates rigid body vehicle motion in three rotational degrees of freedom. The effects of vehicle dynamics inertial cross-coupling, APS logic, APS hardware characteristics, and the S-IVB stage J-2 control system characteristics are included.

2.6.3 Results

The APS orbital propellant requirements analysis reveals that the nominal APS propellant consumption for modules 1 and 3 are

as illustrated in Figure 73. The estimated nominal and 3-σ propellant consumption at the time of S-IVB/CSM separation are 25.9 lbs. and 36.3 lbs., respectively. The estimated nominal and 3-σ propellant consumptions at the termination of guaranteed IU lifetime are 59.0 lbs. and 82.6 lbs., respectively. The nominal and 3-σ times of propellant depletion are estimated to be 9.5 hours and 6.8 hours, respectively. The estimates are based upon a nominal and 3-σ propellant consumption of 4 lbs. and 5.6 lbs. during S-IVB stage powered flight.

FIGURE 1

CAPE KENNEDY LAUNCH FACILITY 34 UMBILICAL TOWER PROFILE

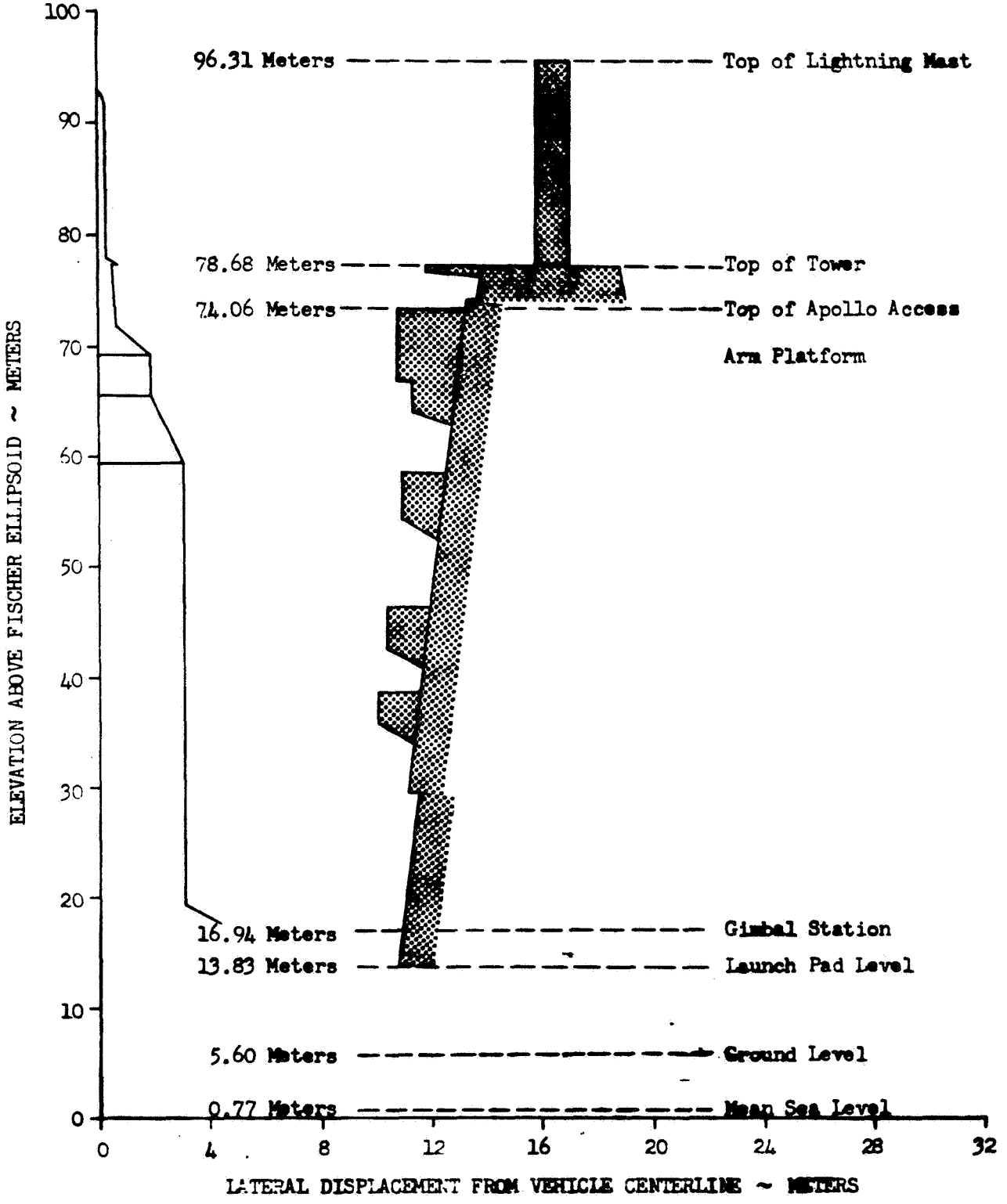

FIGURE 2

LIFTOFF GEOMETRY LC-34

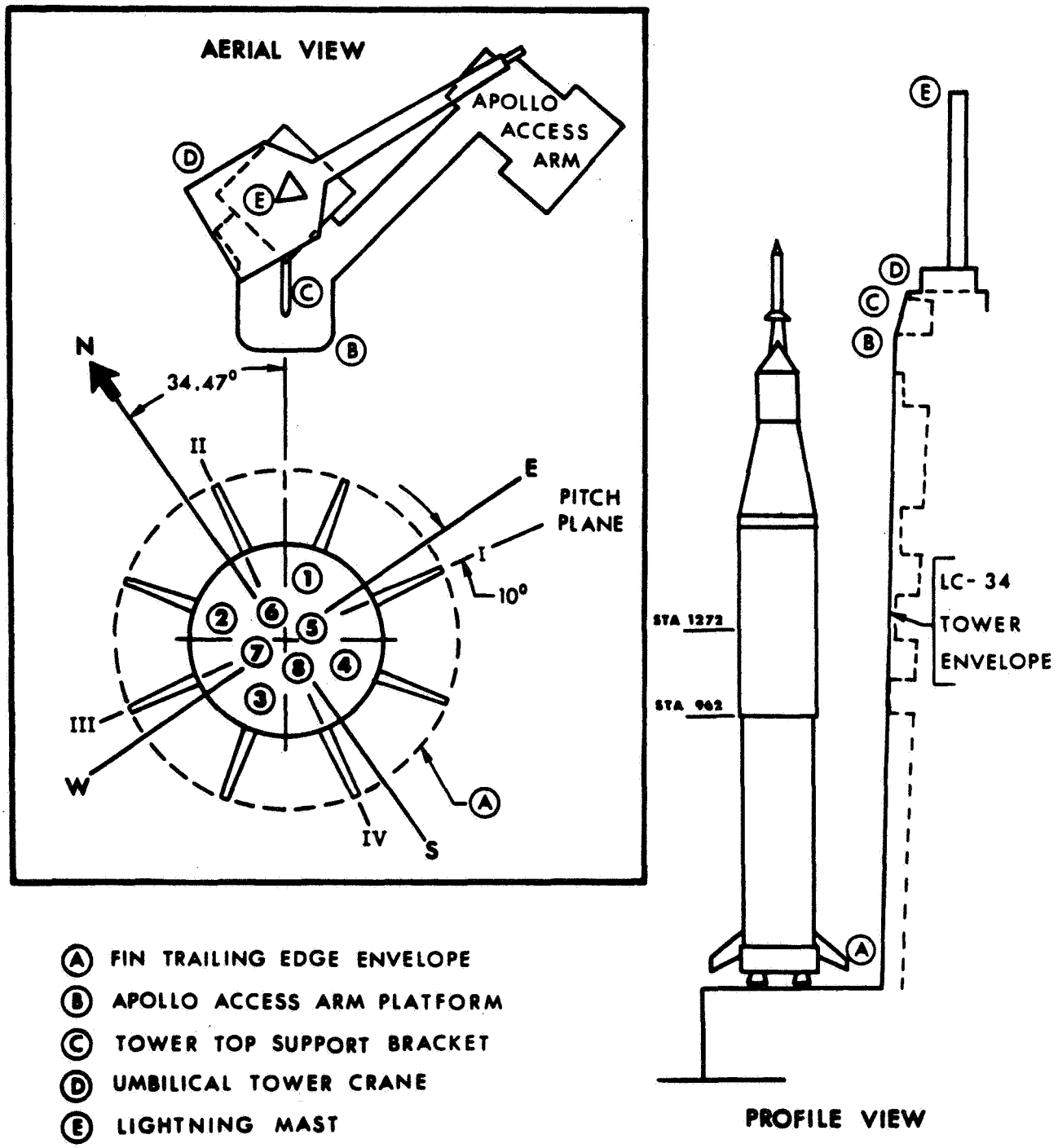

- (A) FIN TRAILING EDGE ENVELOPE
- (B) APOLLO ACCESS ARM PLATFORM
- (C) TOWER TOP SUPPORT BRACKET
- (D) UMBILICAL TOWER CRANE
- (E) LIGHTNING MAST

FIGURE 3
CAPE KENNEDY SURFACE WIND PROFILES

$$V = V_1 \left(\frac{Z}{Z_1}\right)^P$$

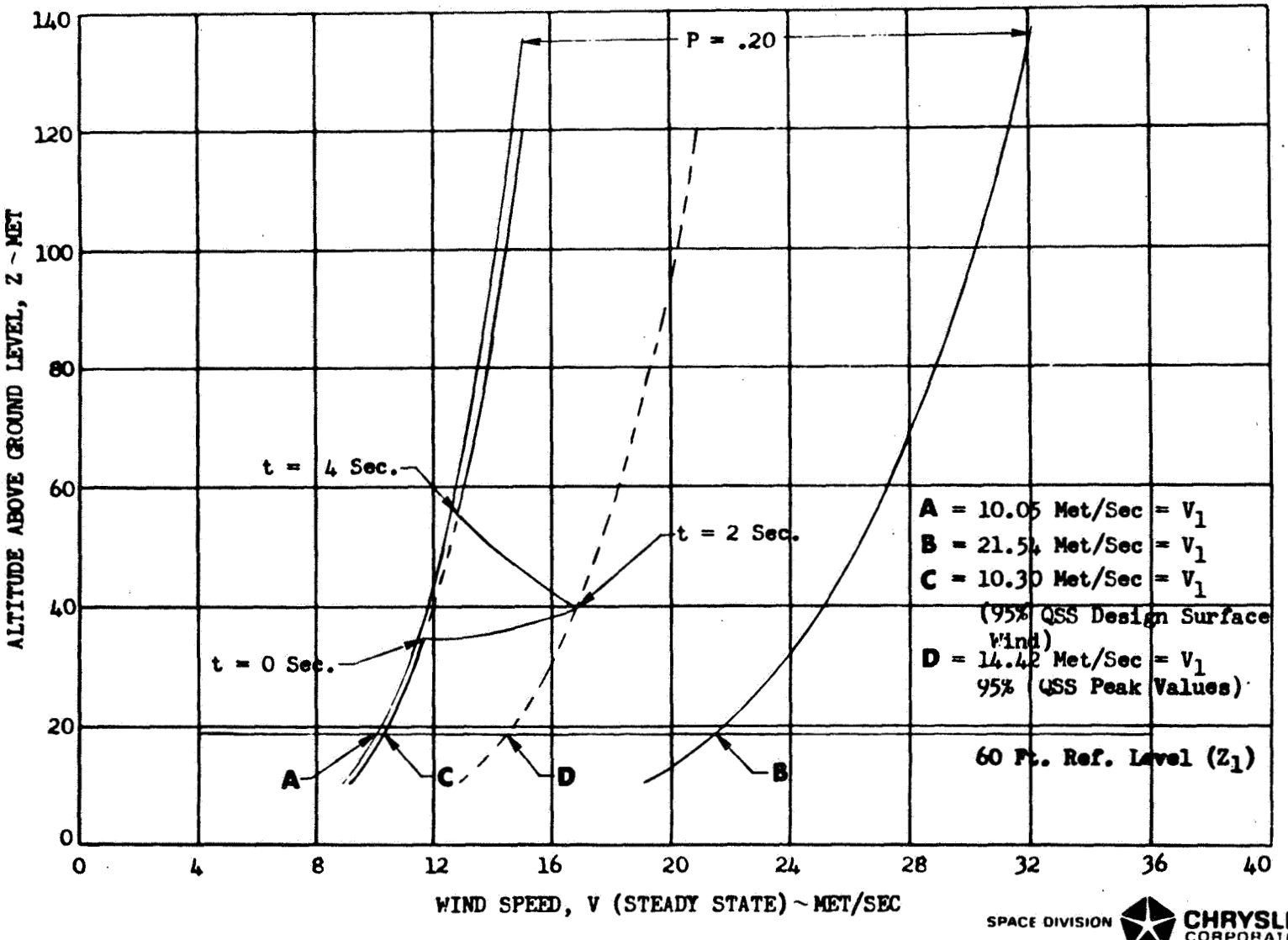

FIGURE 4

AS-205/CSM-101 DRIFT VERSUS WIND SPEED

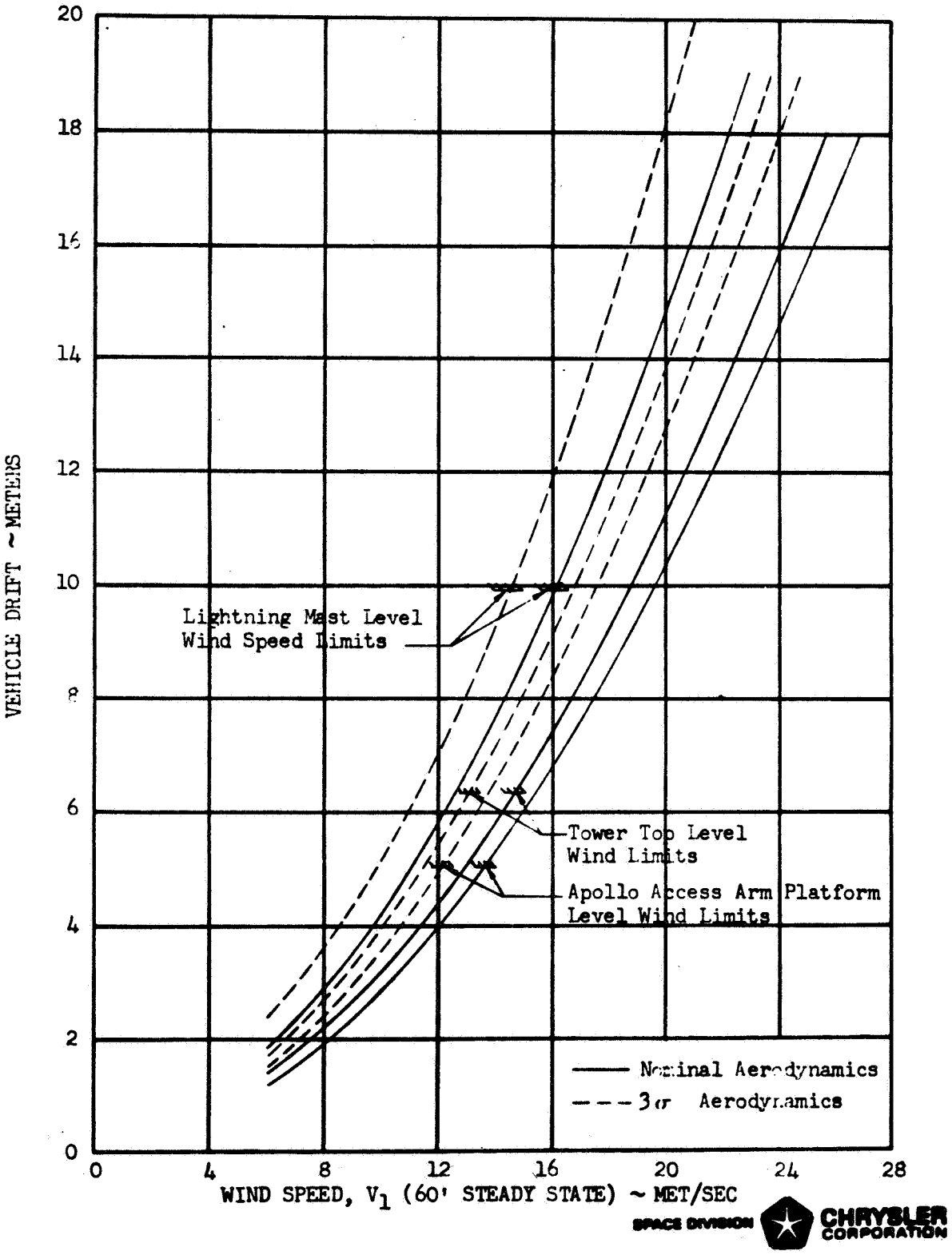

SPACE DIVISION CHRYSLER CORPORATION

FIGURE 5

AS-205/CSM-101 LIFTOFF UMBILICAL TOWER COLLISION
WIND LIMIT FOR APOLLO ACCESS ARM PLATFORM

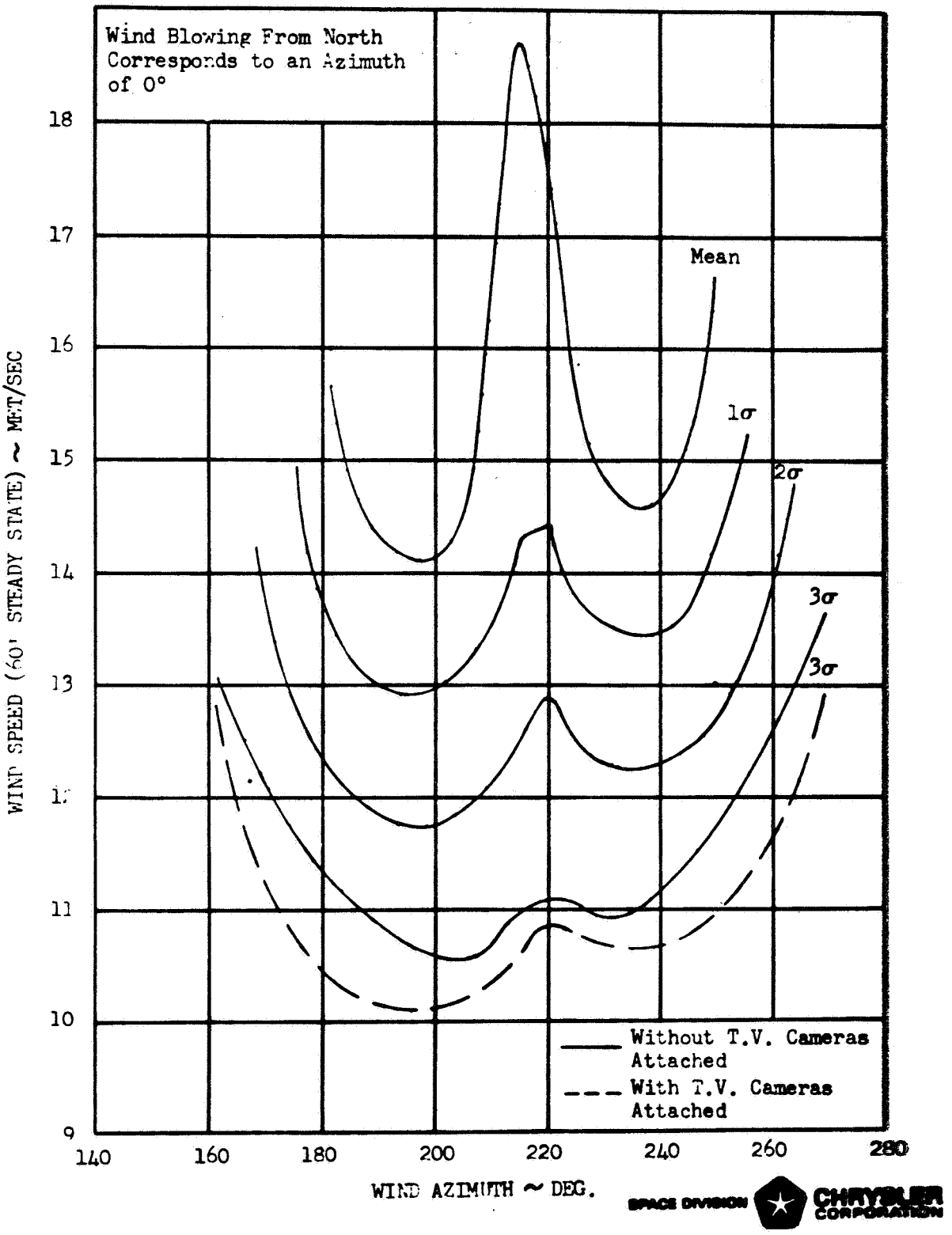

FIGURE 6

AS-205/CSM-101 LIFTOFF WIND SPEED AND COMPOSITE
CONTROL DEFLECTION COMBINATION LIMIT

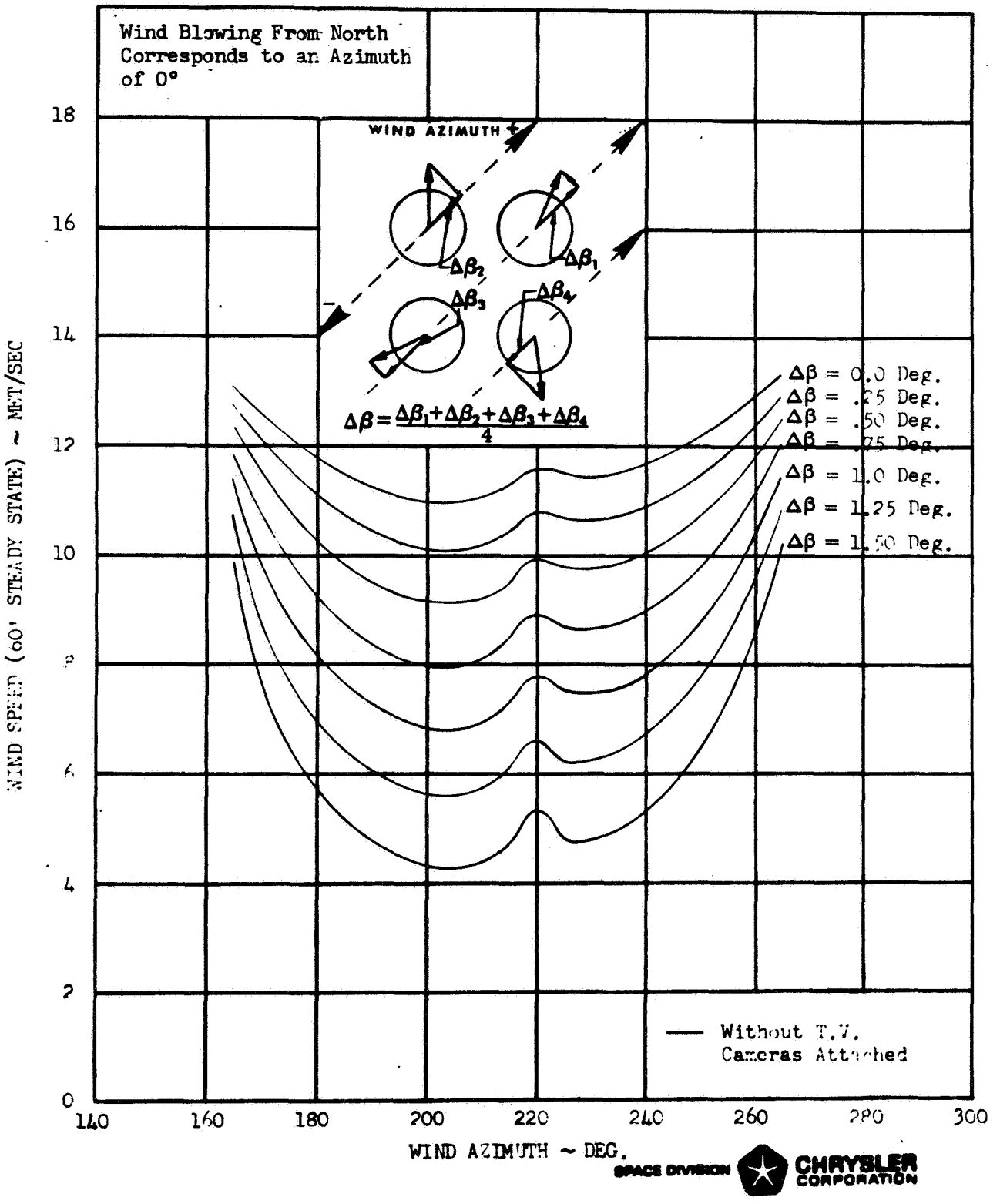

SPACE DIVISION CHRYSLER CORPORATION

AS-[illegible]/SM-101 LIFTOFF ENGINE FAILURE CRITICAL TIMES
FOR 95[illegible] KNOTS DESIGN SURFACE WIND

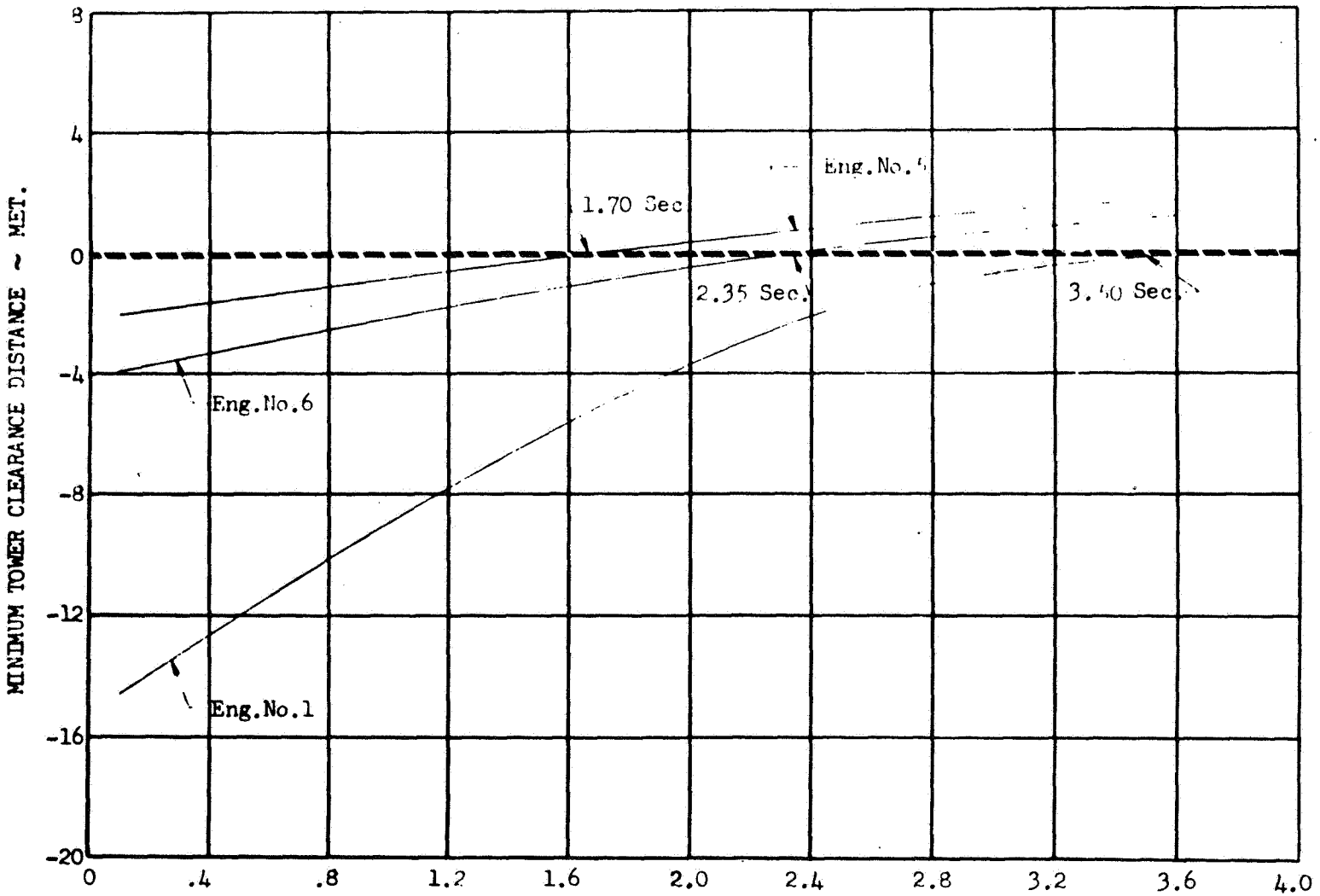

SPACE DIVISION CHRYSLER CORPORATION

FIGURE 8

AS-205/CSM-101 LIFTOFF ENGINE FAILURE WIND RESTRICTION

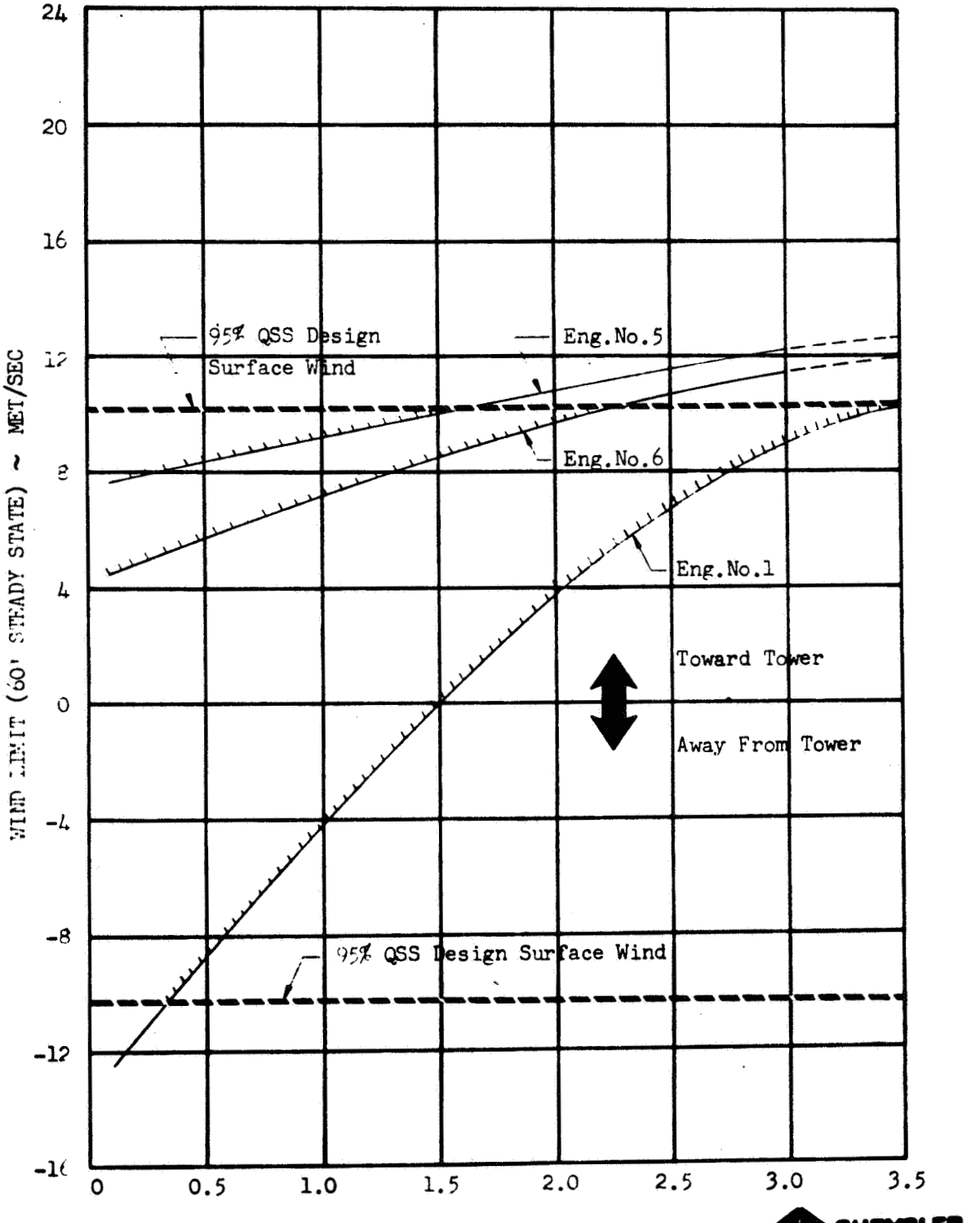

SPACE DIVISION CHRYSLER CORPORATION

FIGURE 6

AS-205/CSM-101 CLEARANCE TIME FOR ENGINE FAILURES

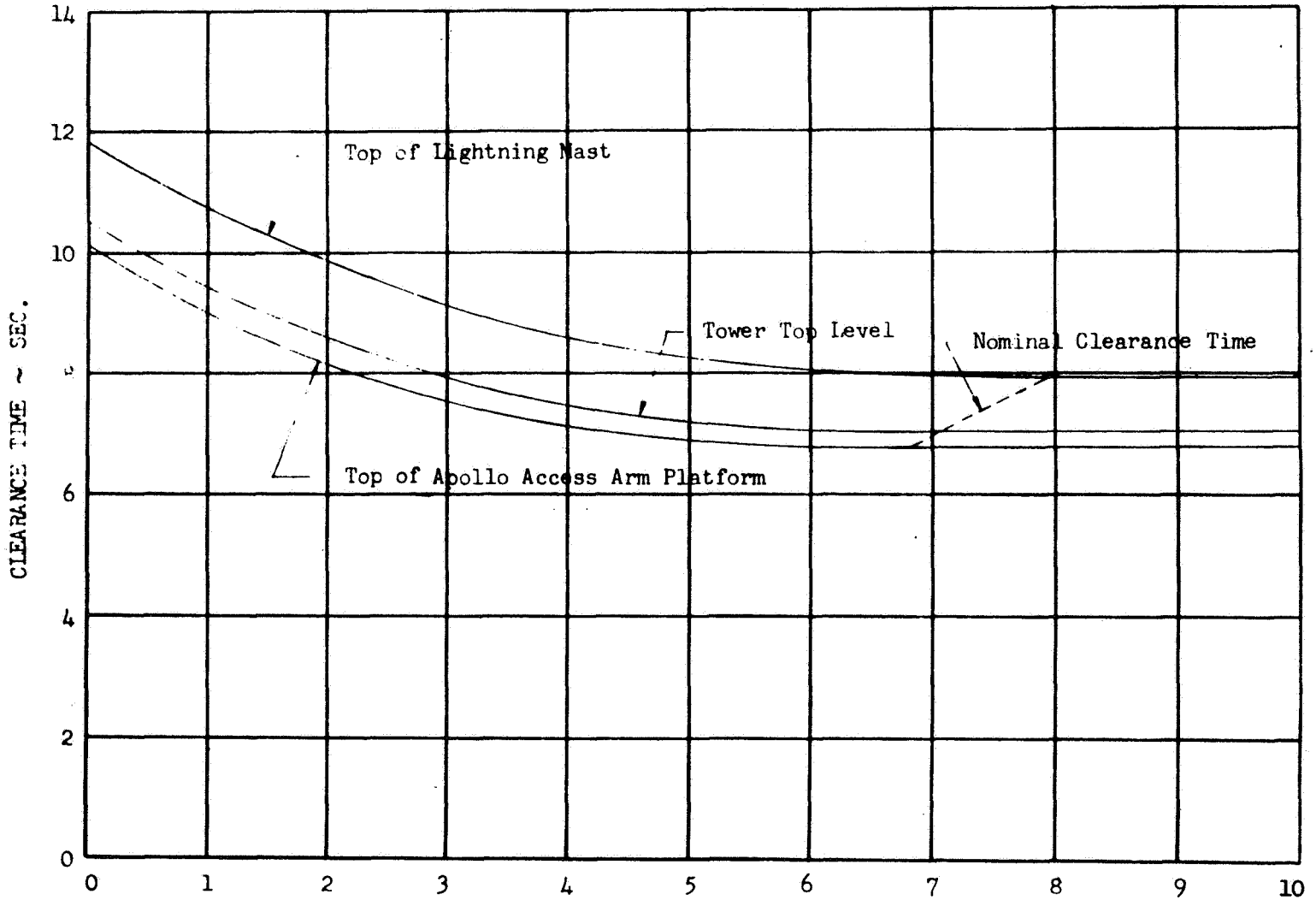

FIGURE 10

AS-205/CSM-101 LIFTOFF SINGLE ACTUATOR HARDOVER CRITICAL TIMES
FOR 95% DESIGN SURFACE WIND

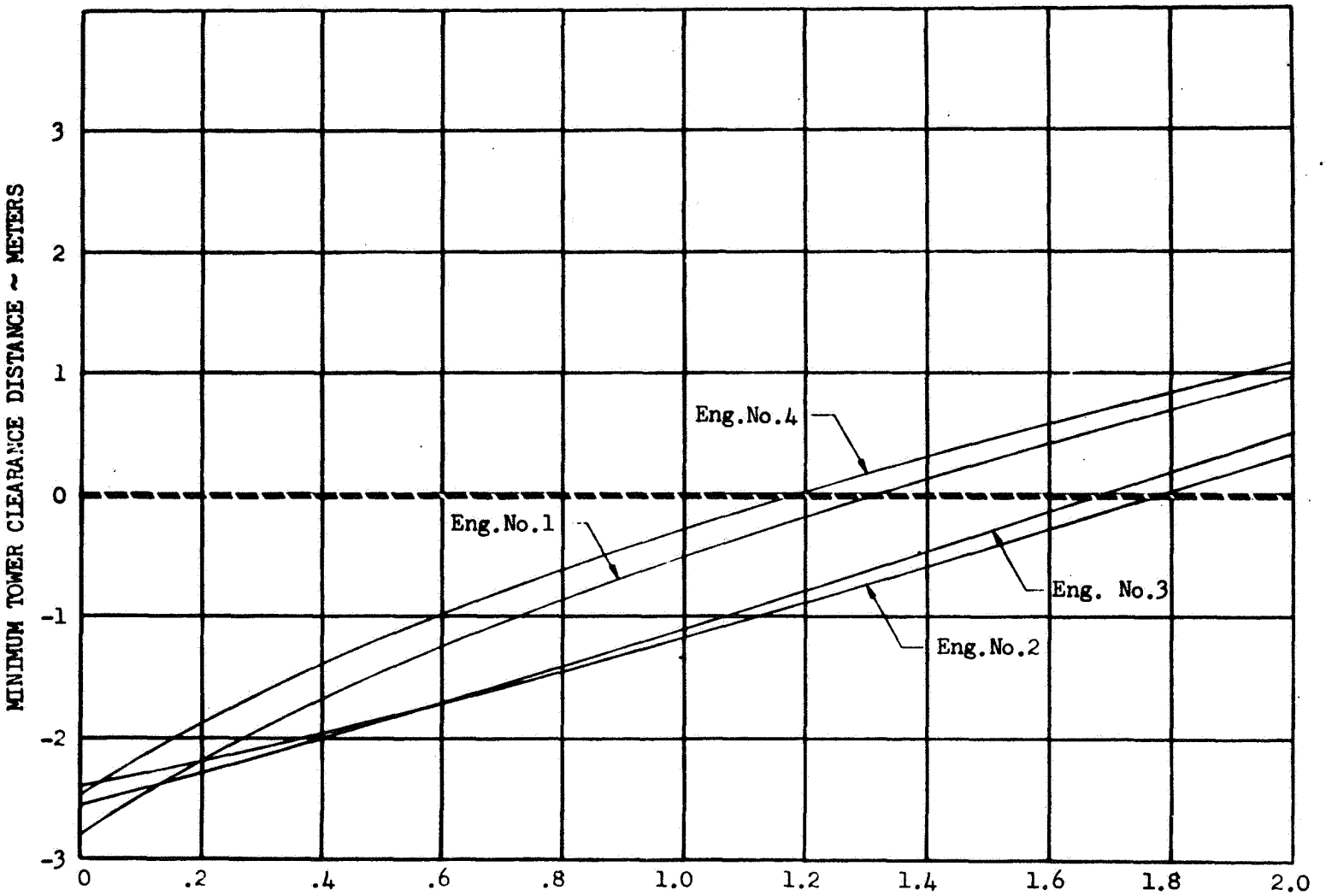

SPACE DIVISION CHRYSLER CORPORATION

FIGURE 11

AS-205/CSM-101 LIFTOFF SINGLE ACTUATOR HARDOVER WIND LIMITS

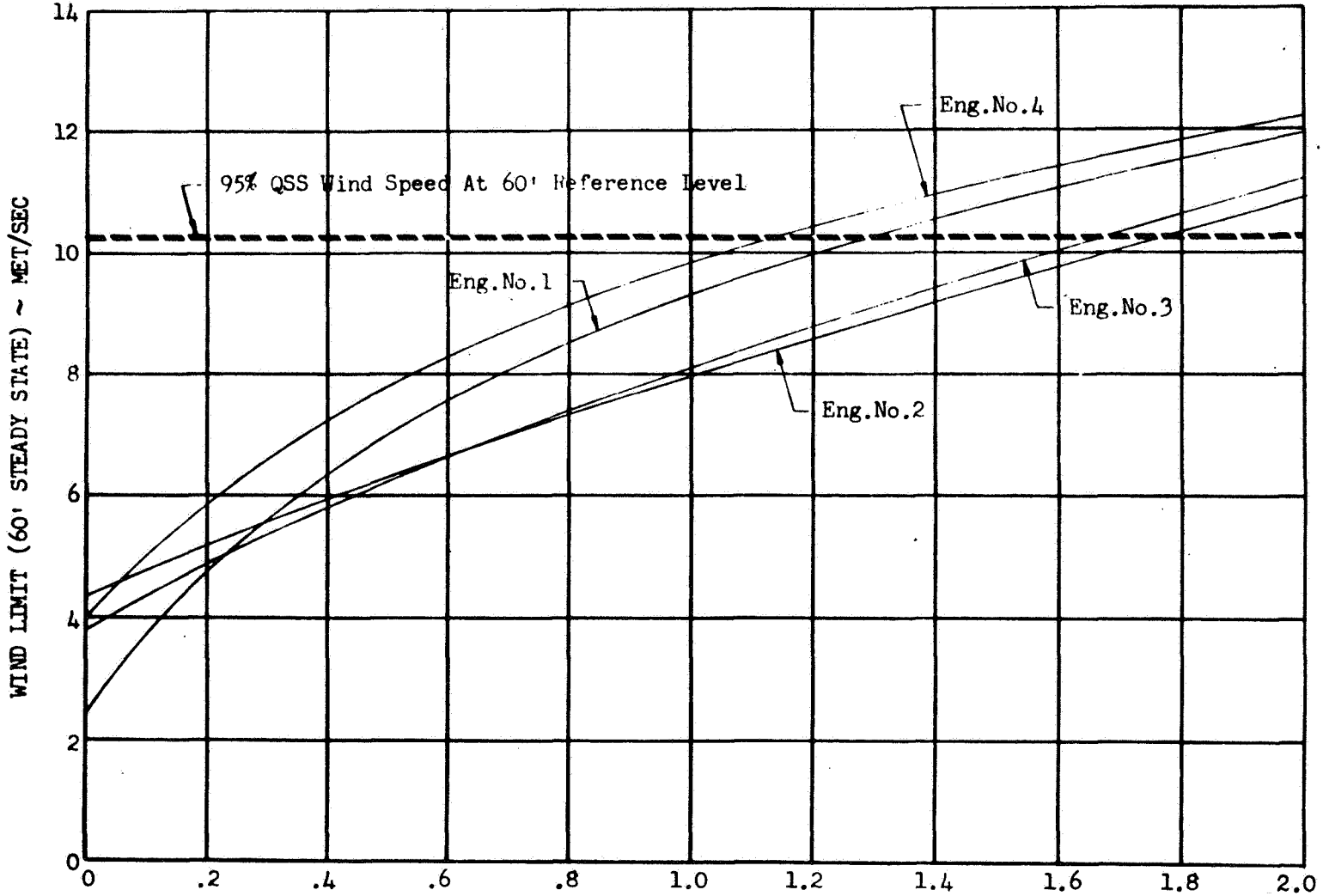

SPACE DIVISION CHRYSLER CORPORATION

FIGURE 12

AS-205/CSM-101 NOMINAL FLIGHT
RATIO OF CONTROL GIMBAL DEFLECTION TO ANGLE OF ATTACK
(STEADY STATE)

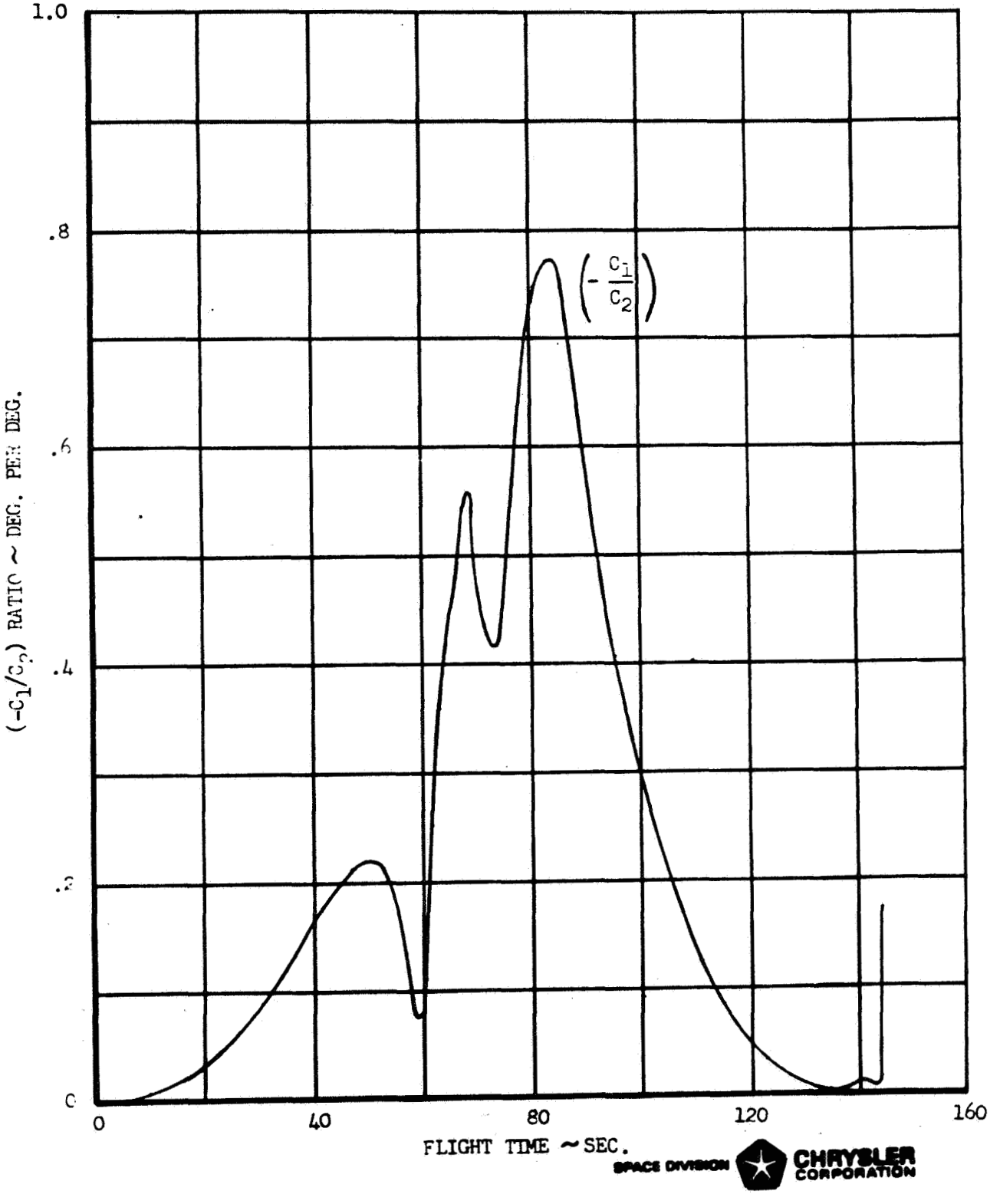

SPACE DIVISION CHRYSLER CORPORATION

FIGURE 13

AS-205/CSM-101 NOMINAL FLIGHT
DYNAMIC PRESSURE AND TRIM PITCH ANGLE OF ATTACK

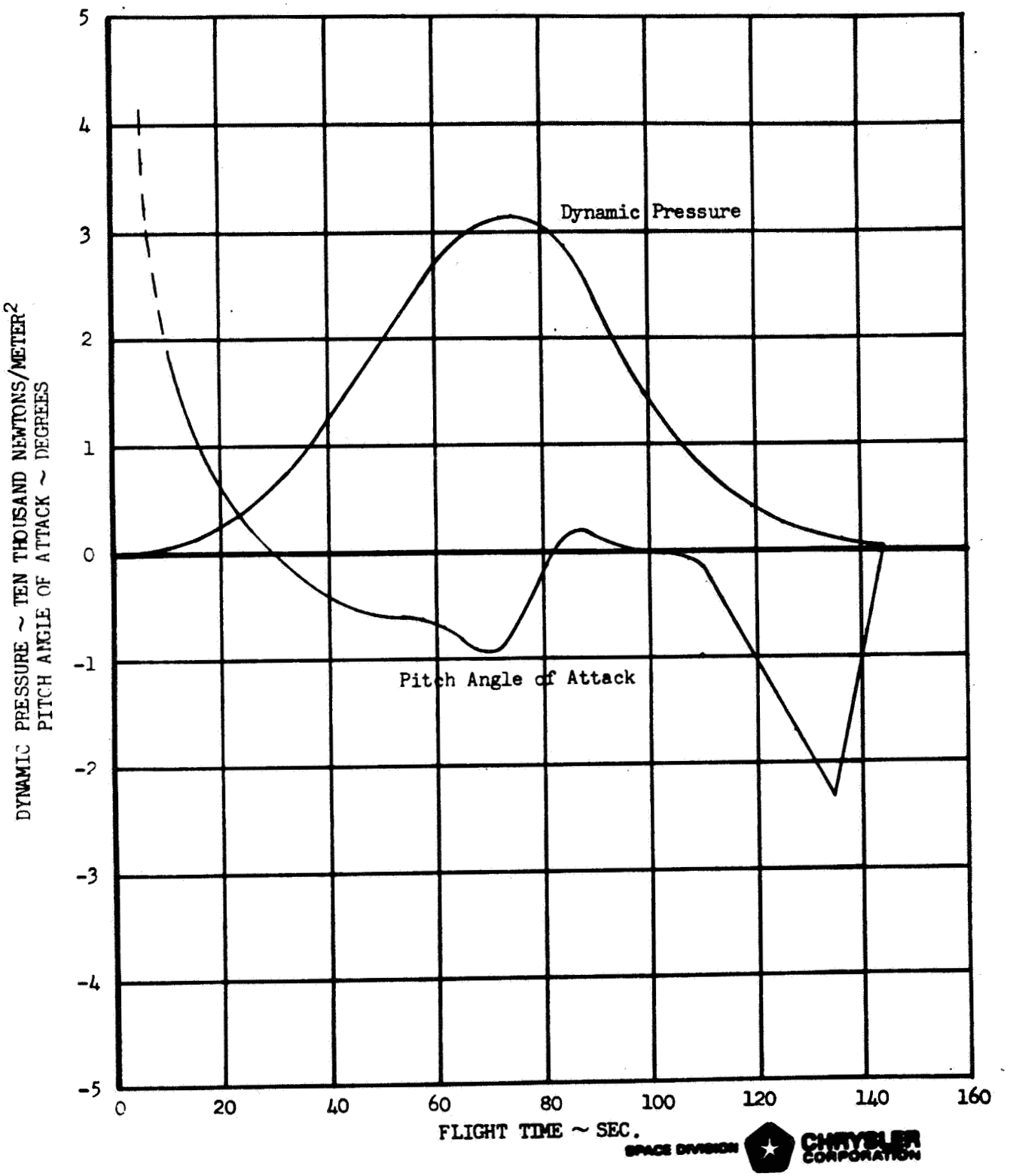

FIGURE 14
AS-205/CSM-101 CONTROL SYSTEM GAINS
S-IB STAGE

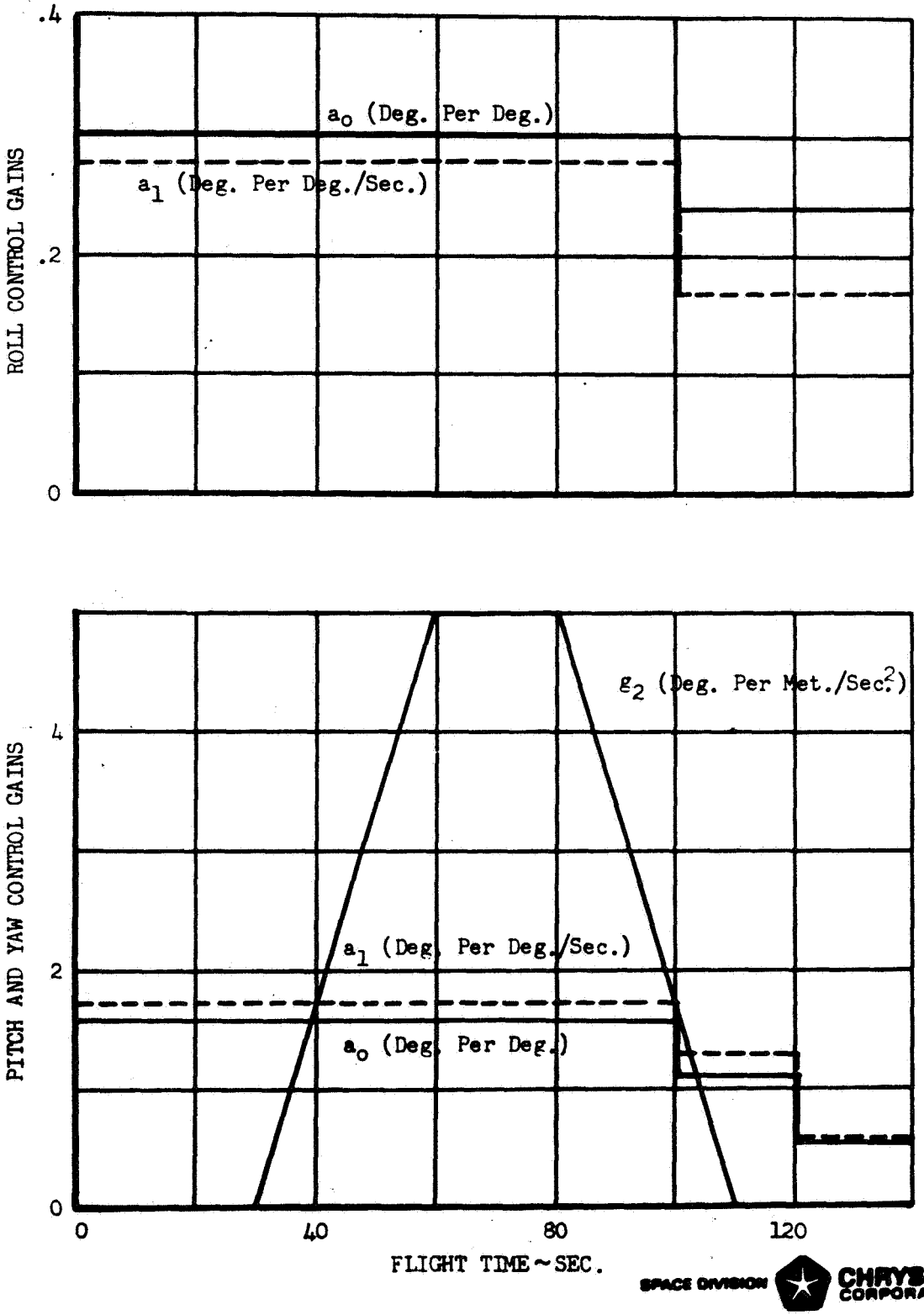

SPACE DIVISION CHRYSLER CORPORATION

FIGURE 15

AS-205/CSM-101 STRUCTURAL LIMITS FOR A 1.4 SAFETY FACTOR

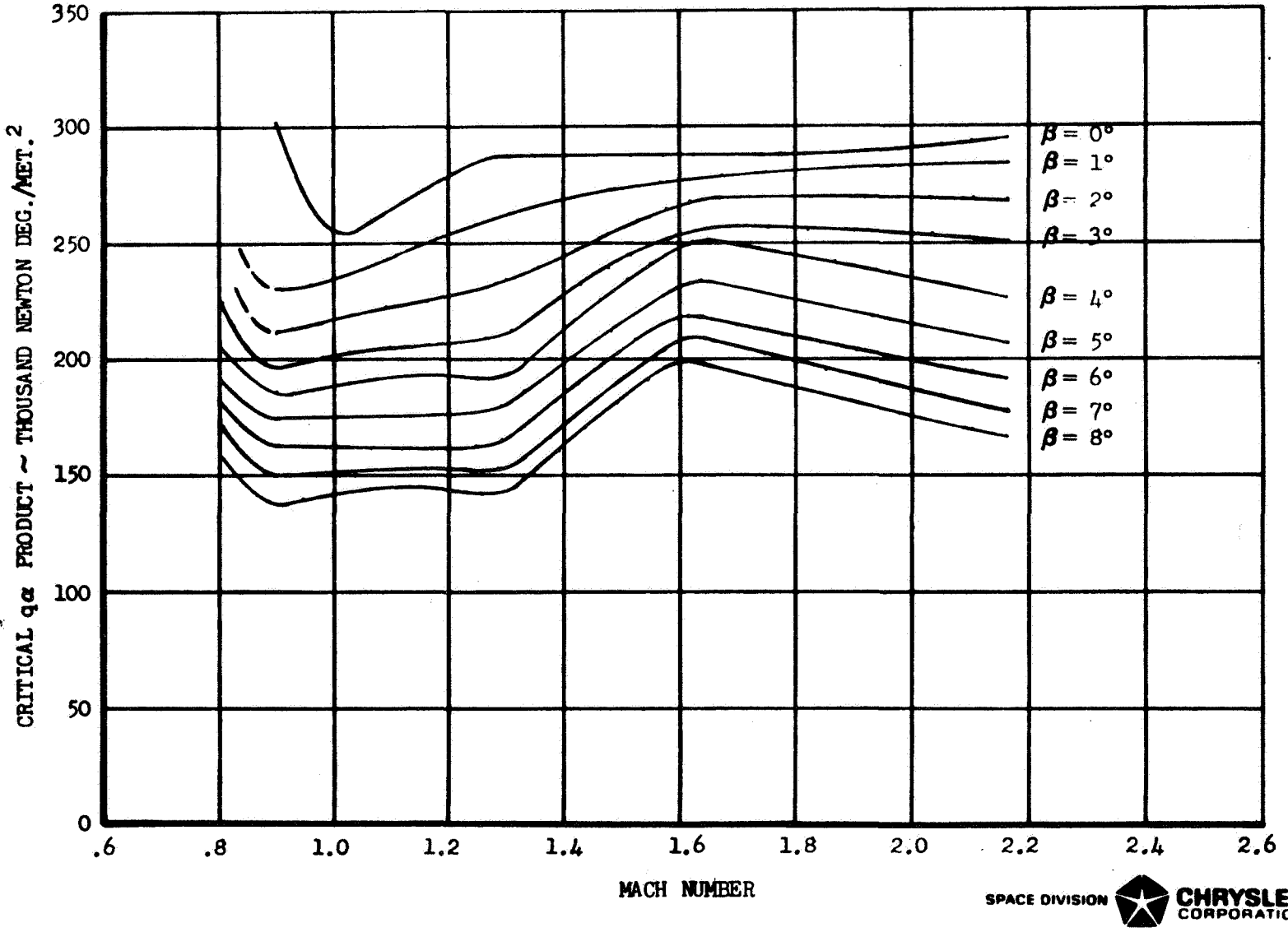

SPACE DIVISION CHRYSLER CORPORATION

FIGURE 16

AS-205/CSM-101 CRITICAL $q\alpha$ RATIO RESPONSE TO
THE MOST RESTRICTIVE 95% QSS AND DESIGN TAILWIND

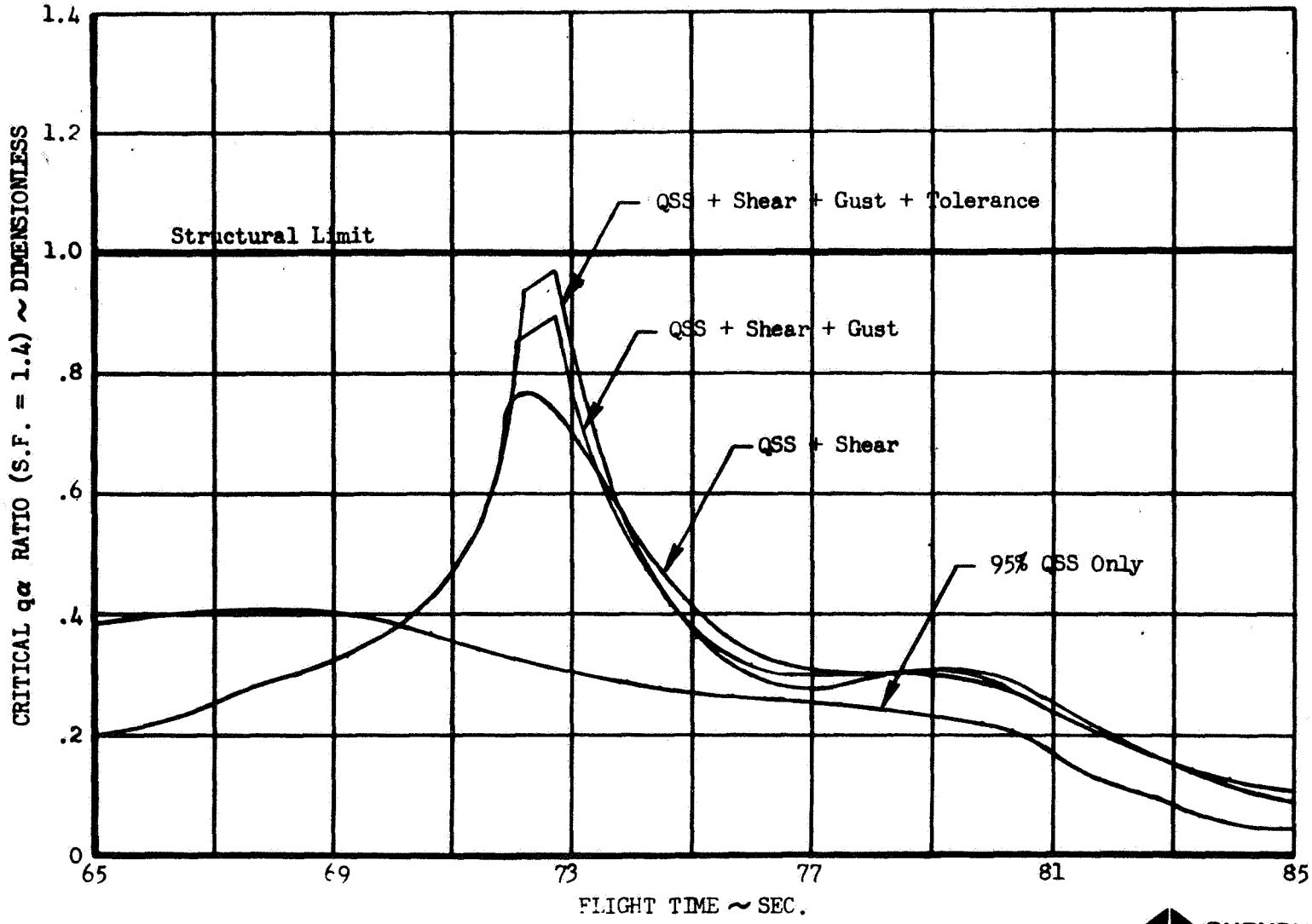

SPACE DIVISION CHRYSLER CORPORATION

FIGURE 17

AS-205/CSM-101 CRITICAL qα RATIO (S.F. = 1.4) vs. QSS WIND SPEED
FOR EACH WIND DIRECTION AT THE WORST ALTITUDE (11 KM.)

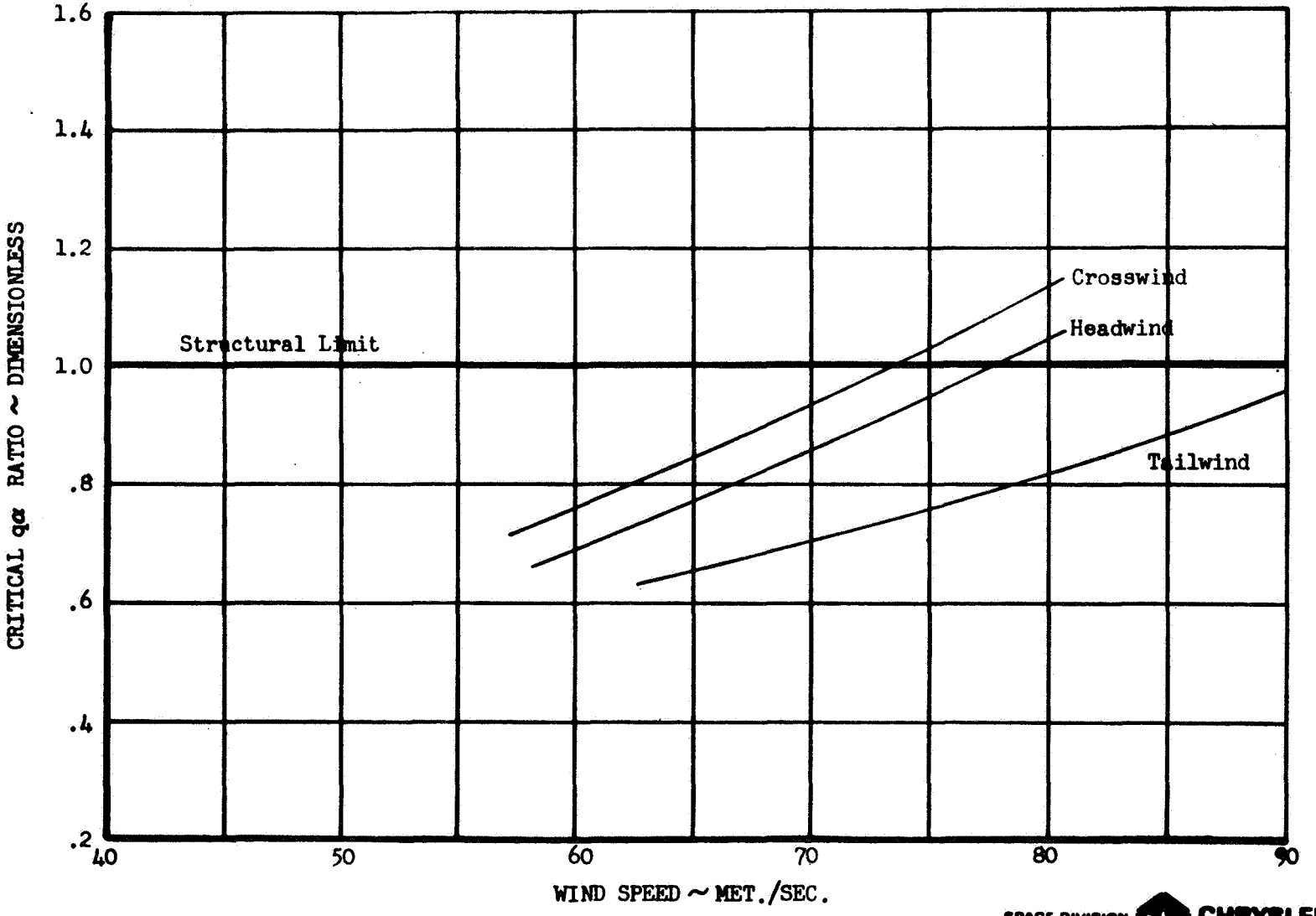

FIGURE 18

AS-205/CSM-101 BOOST FLIGHT HEAD-TAIL WIND SPEED LIMITS
FOR THE NON-WIND BIASED TRAJECTORY

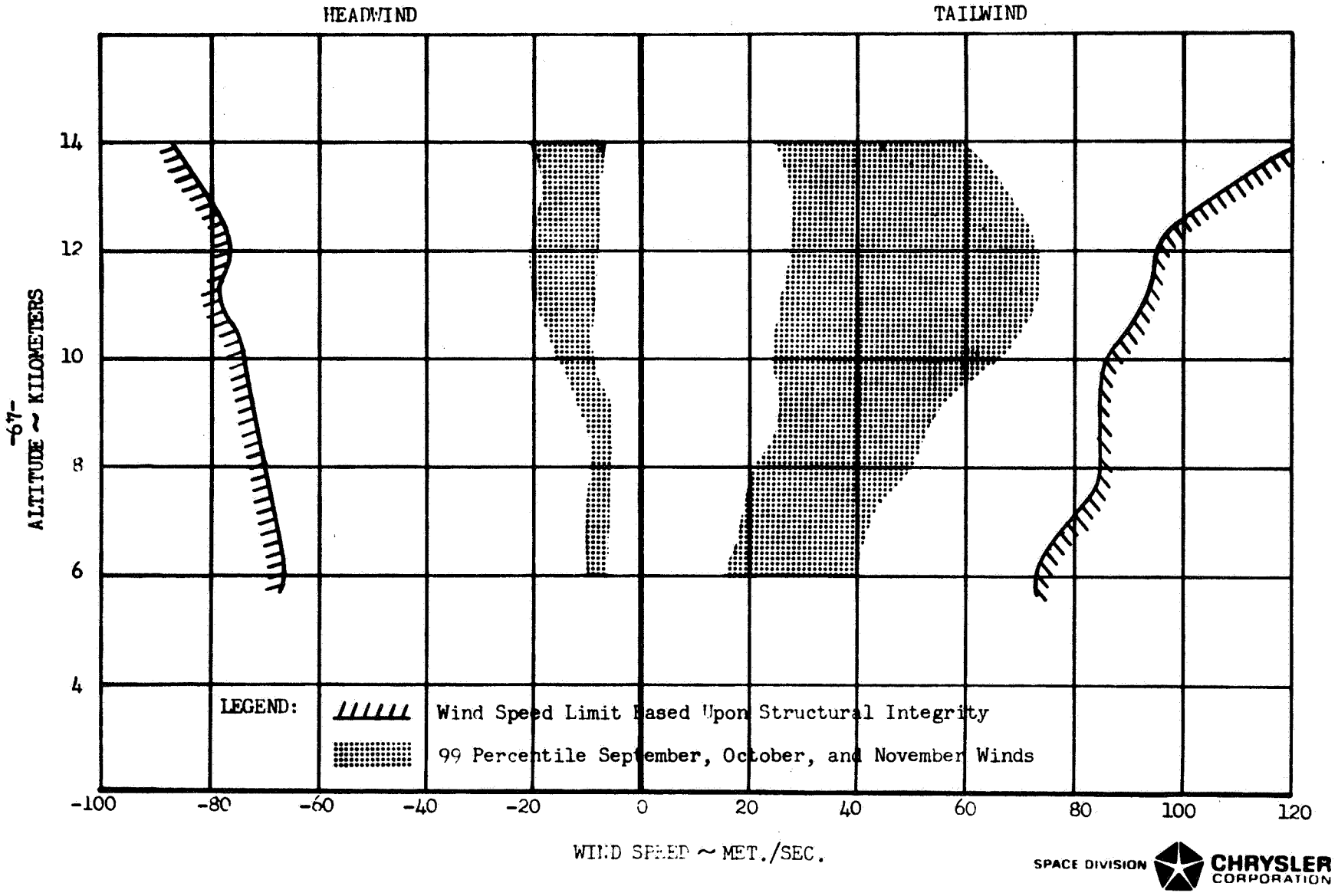

SPACE DIVISION CHRYSLER CORPORATION

FIGURE 19

AS-205/ SM-1[illegible] BOOST FLIGHT LEFT-RIGHT CROSSWIND SPEED LIMITS
FOR THE NON-WIND BIASED TRAJECTORY

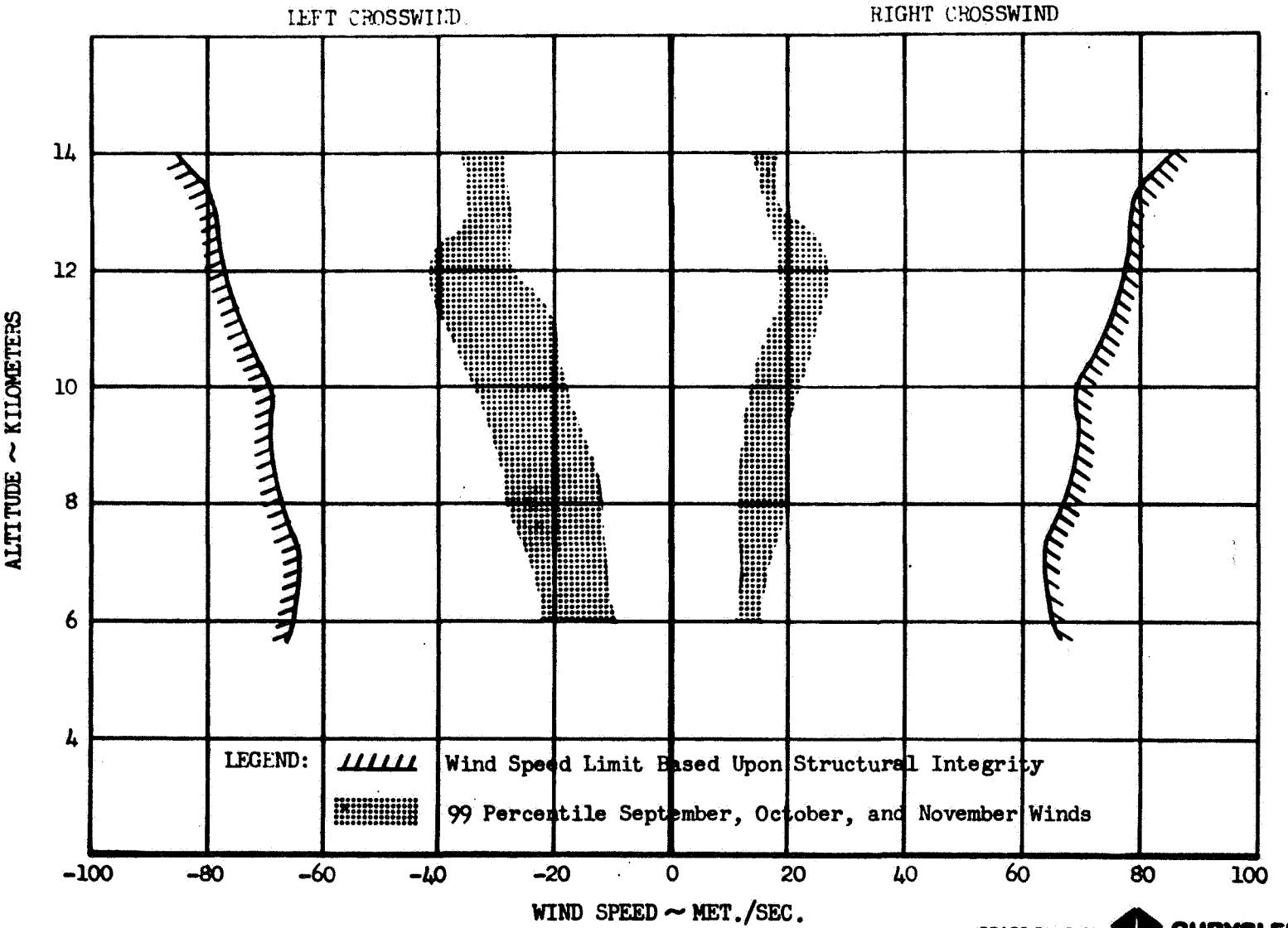

SPACE DIVISION CHRYSLER CORPORATION

FIGURE 20

AS-205/CSM-101 BOOST FLIGHT WIND SPEED LIMIT
AT MOST RESTRICTIVE ALTITUDE
OF THE NON-WIND BIASED TRAJECTORY

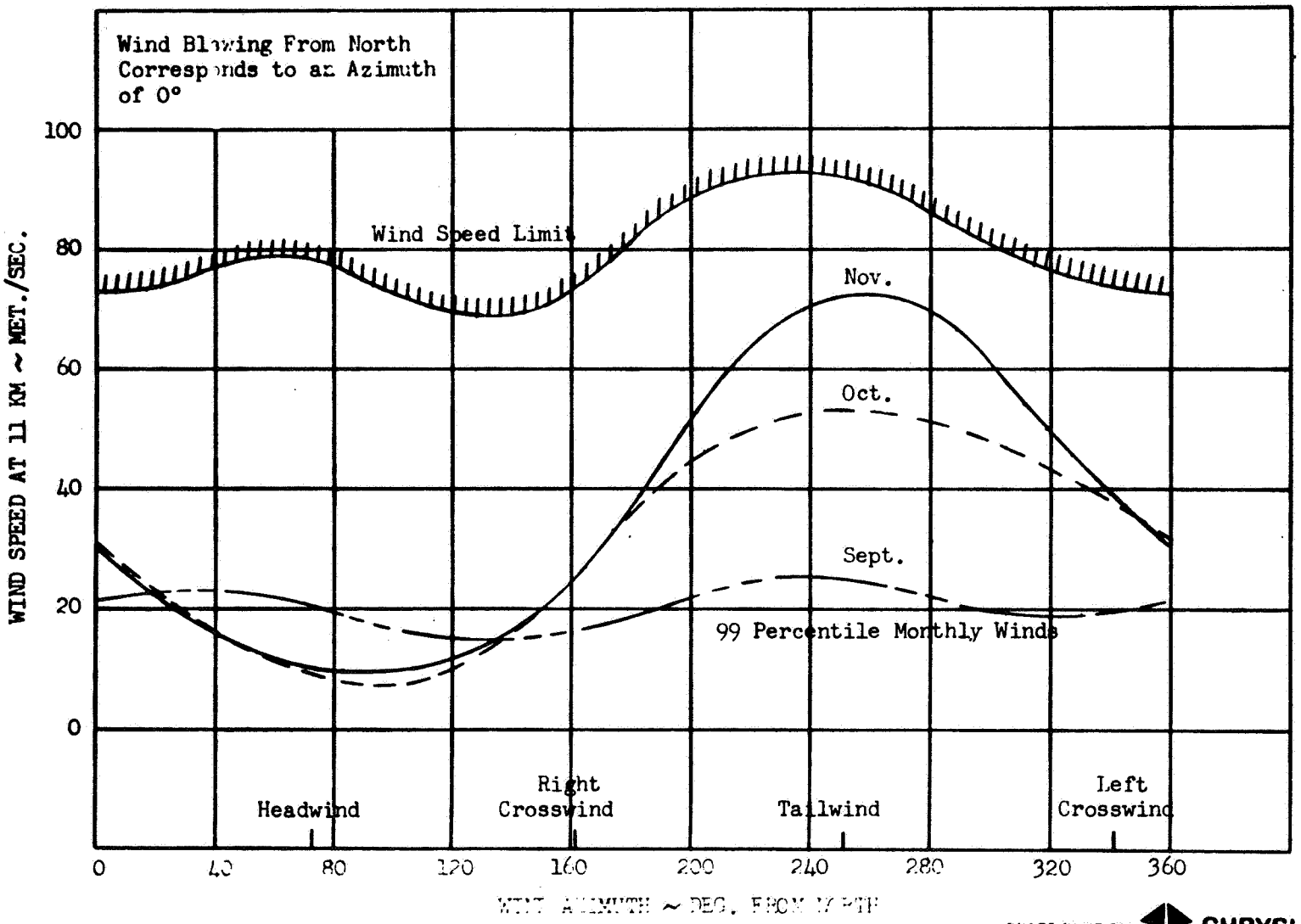

FIGURE 21

AS-205/CSM-101 BOOST FLIGHT HEAD-TAIL WIND SPEED LIMITS
FOR WIND BIASED TRAJECTORY

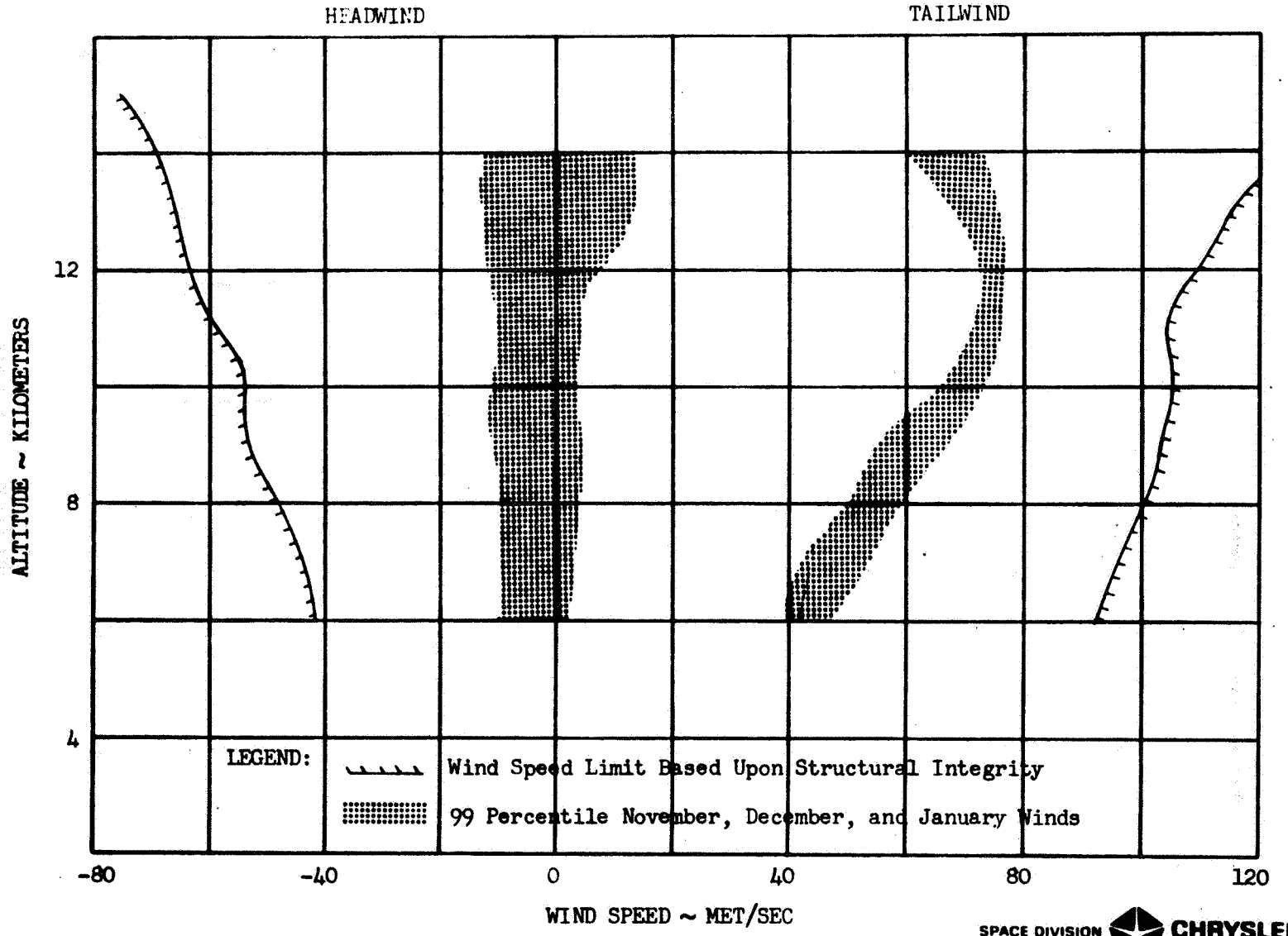

FIGURE 22

AS-205/CSM-101 BOOST FLIGHT LEFT-RIGHT CROSSWIND SPEED LIMITS
FOR WIND BIASED TRAJECTORY

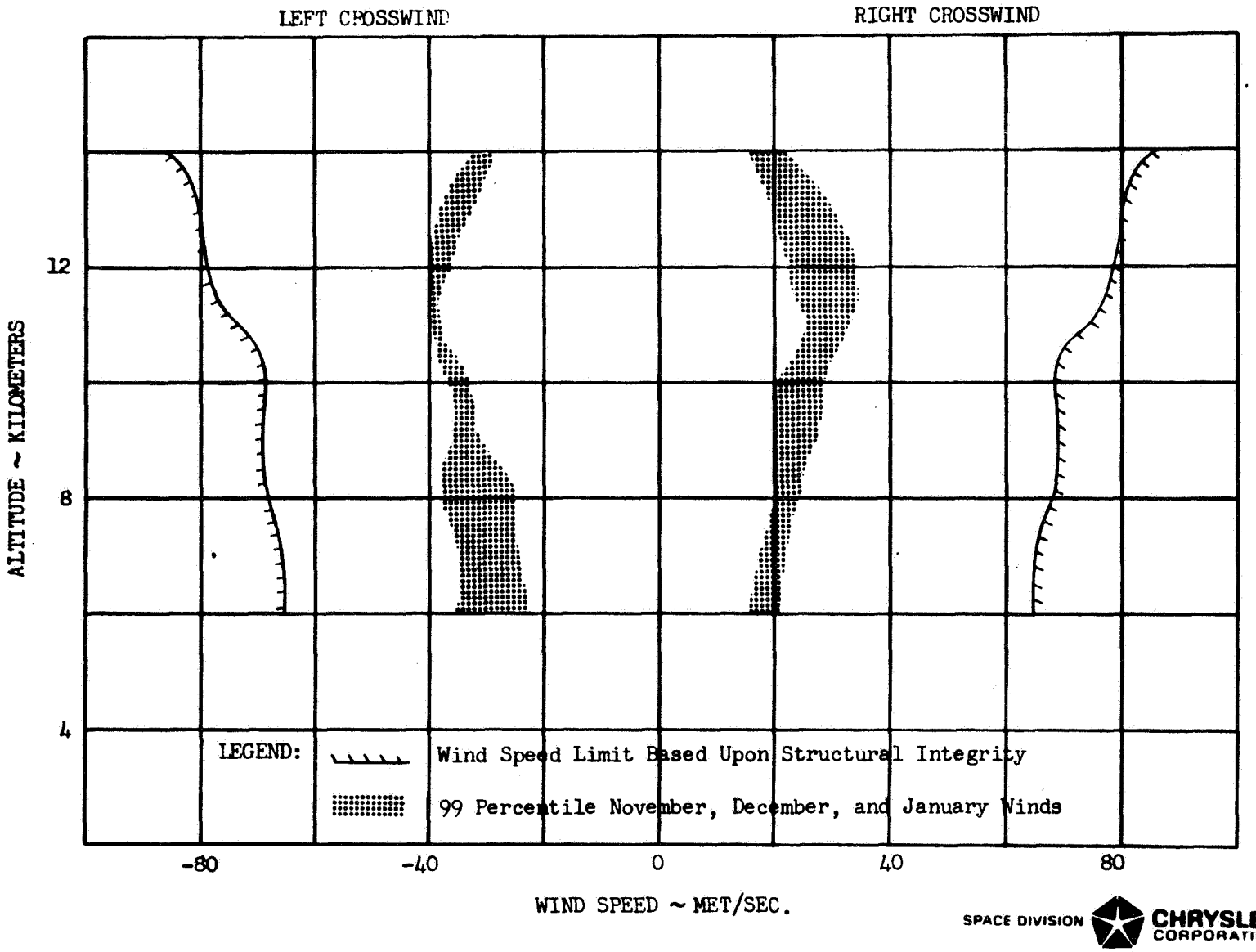

SPACE DIVISION CHRYSLER CORPORATION

FIGURE 23

AS-205/CSM-101 BOOST FLIGHT WIND SPEED LIMIT AT MOST RESTRICTIVE ALTITUDE (11 KM.) OF THE WIND BIASED TRAJECTORY

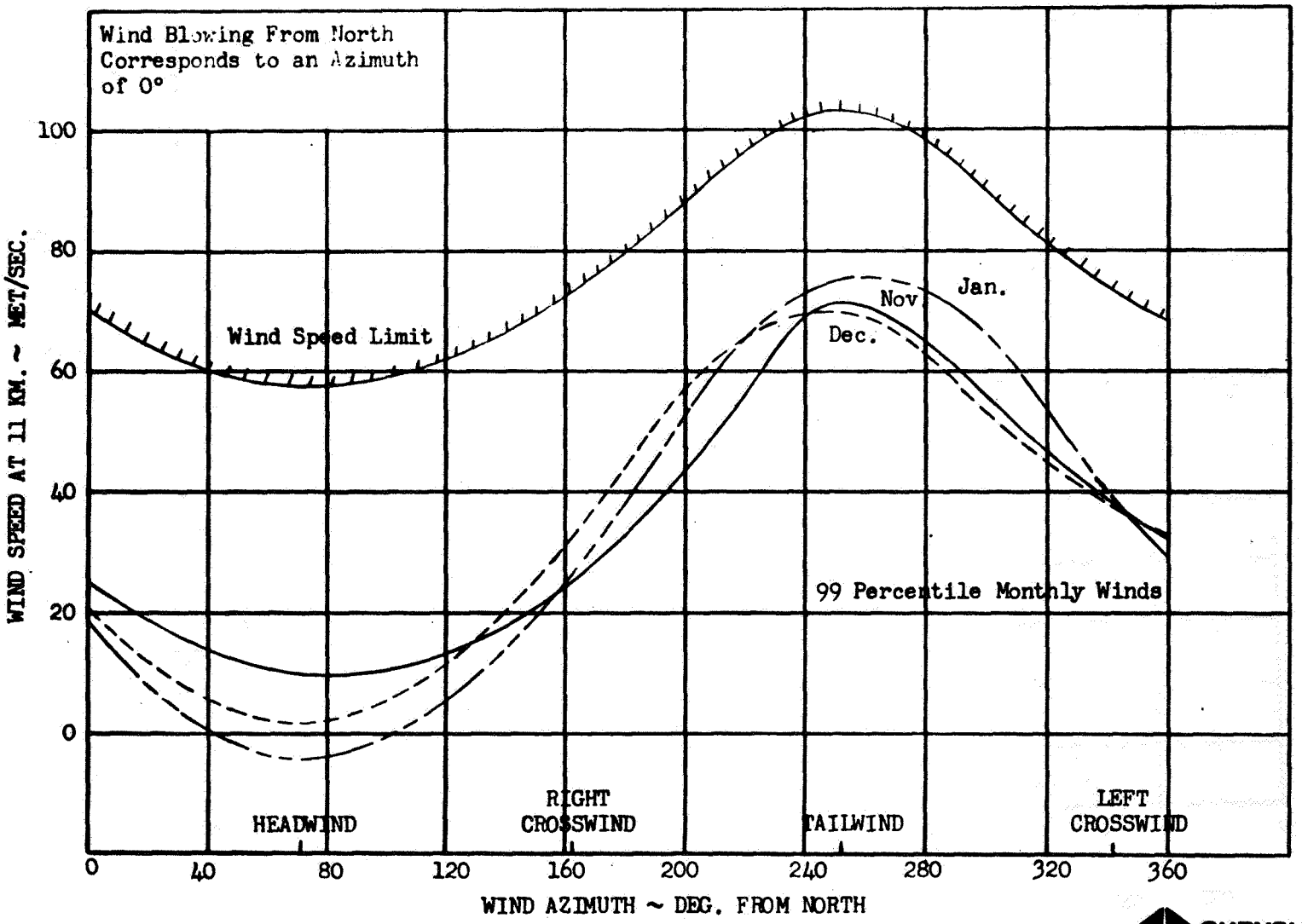

FIGURE 24

AS-205/CSM-101 ENVELOPES OF S-IB STAGE FLIGHT ATTITUDE ERRORS

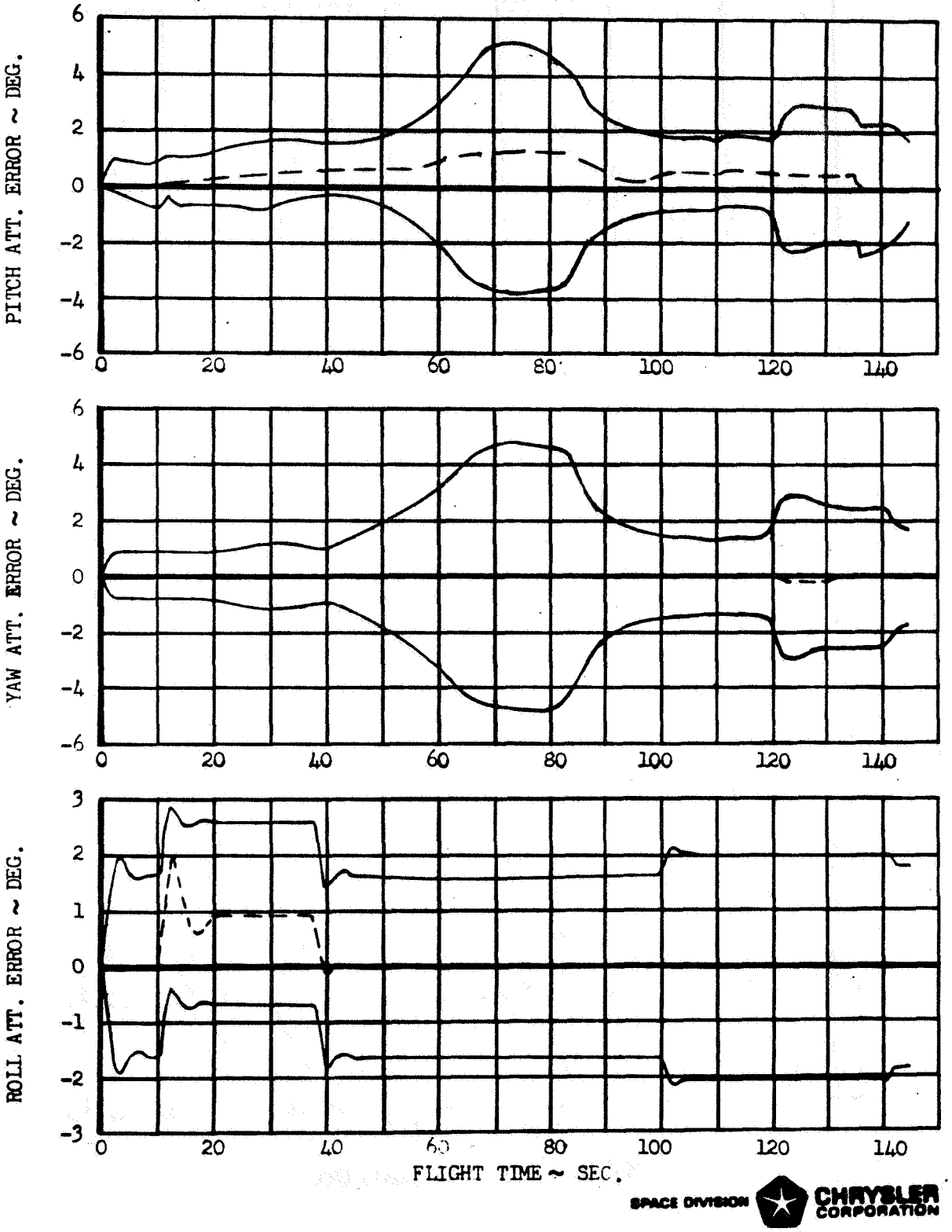

SPACE DIVISION CHRYSLER CORPORATION

FIGURE 25

AS-205/CSM-101 ENVELOPES OF S-IB STAGE FLIGHT ATTITUDE RATES

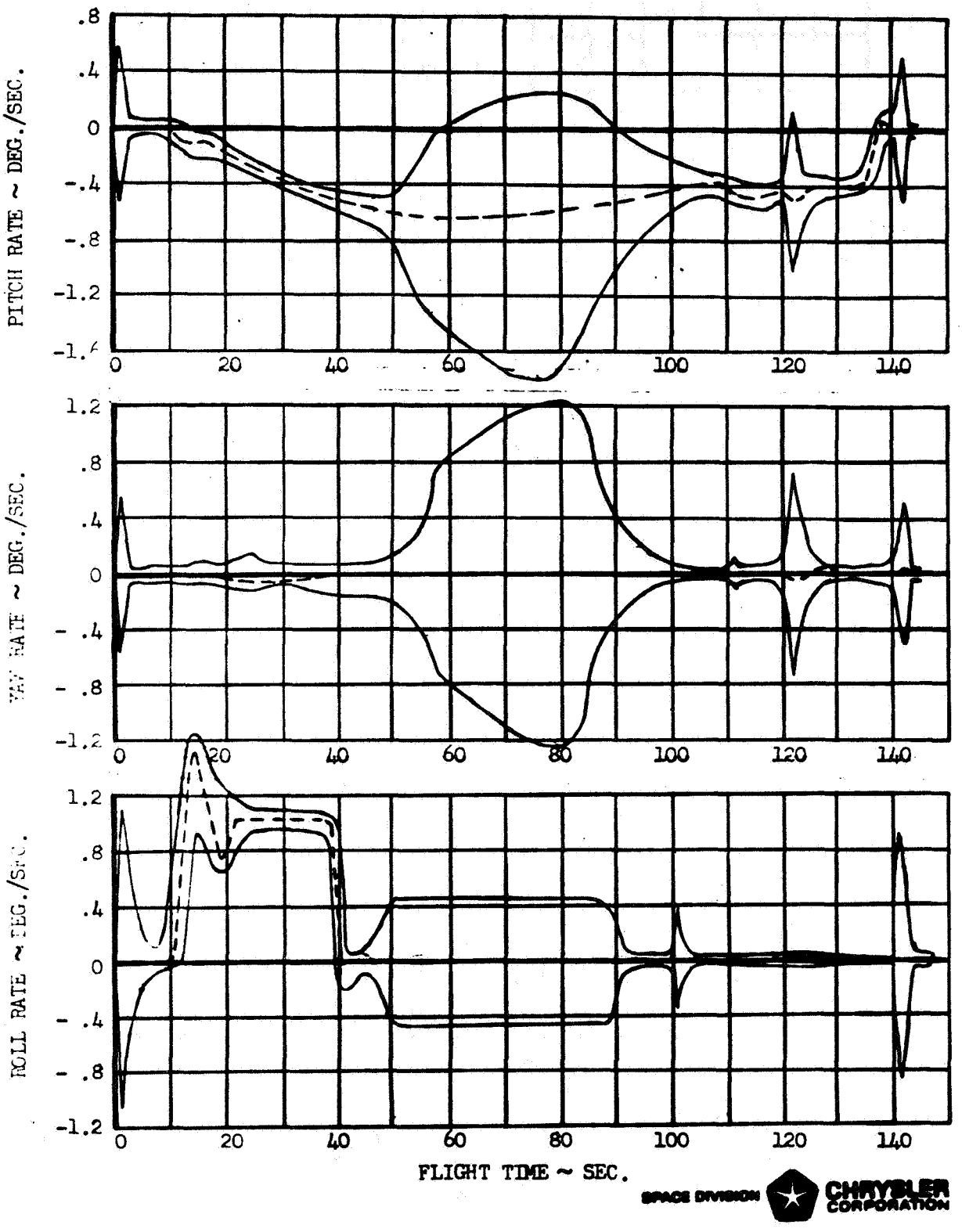

FIGURE 26

AS-205/CSM-101 ENVELOPES OF S-IB STAGE FLIGHT ANGLES OF ATTACK

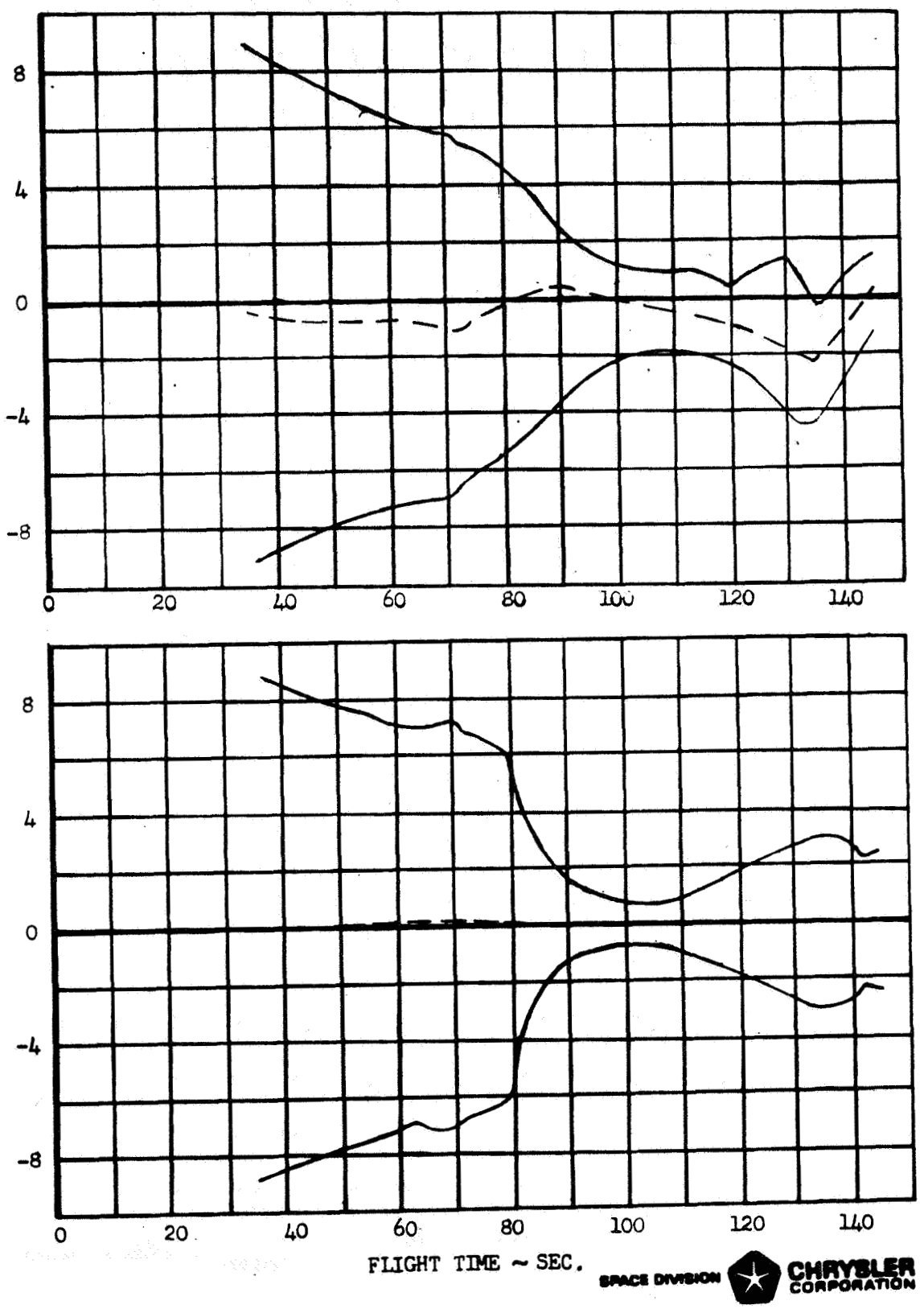

FIGURE 27

AS-205/CSM-101 ENVELOPES OF S-IB STAGE FLIGHT CONTROL DEFLECTIONS

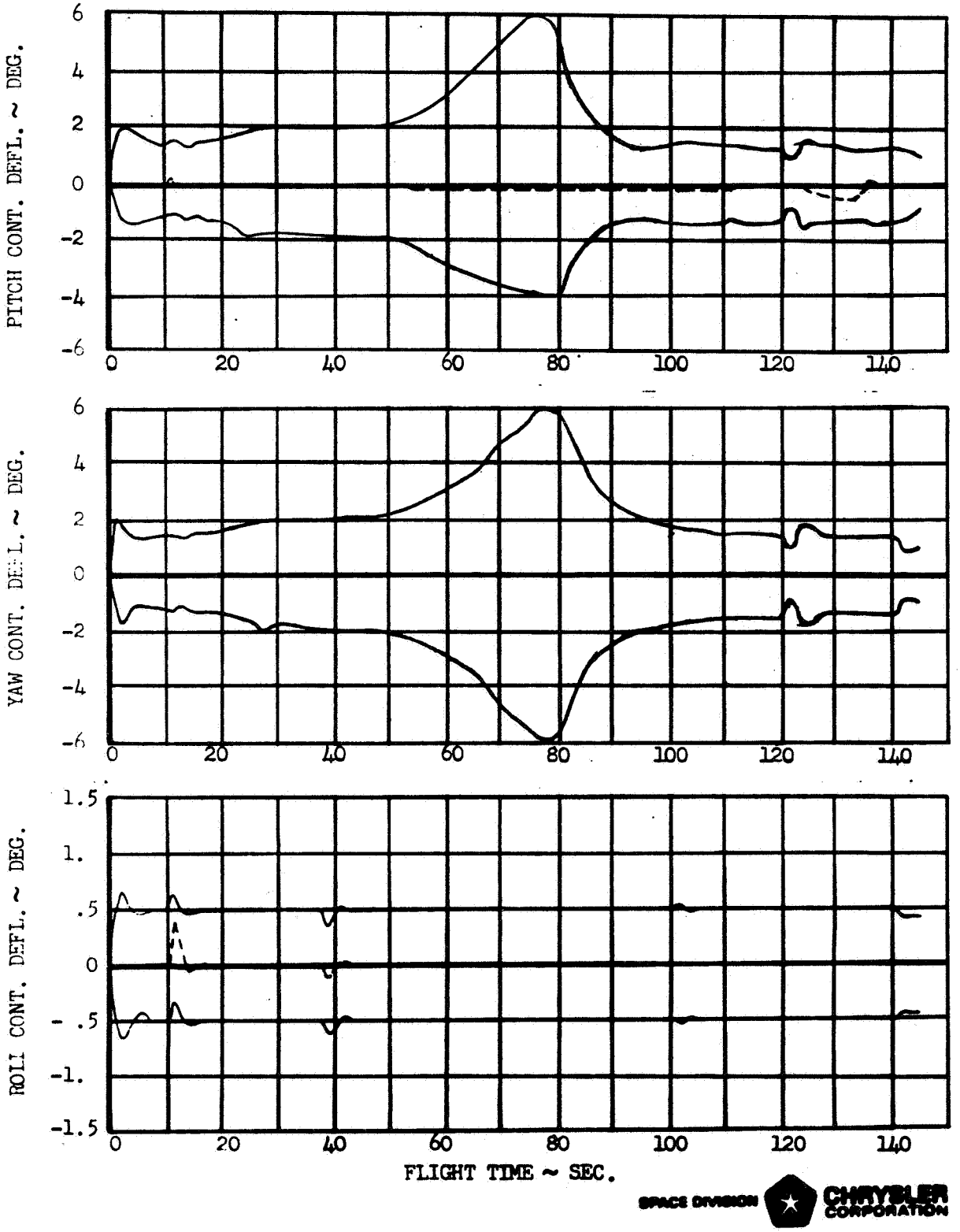

SPACE DIVISION CHRYSLER CORPORATION

FIGURE 28

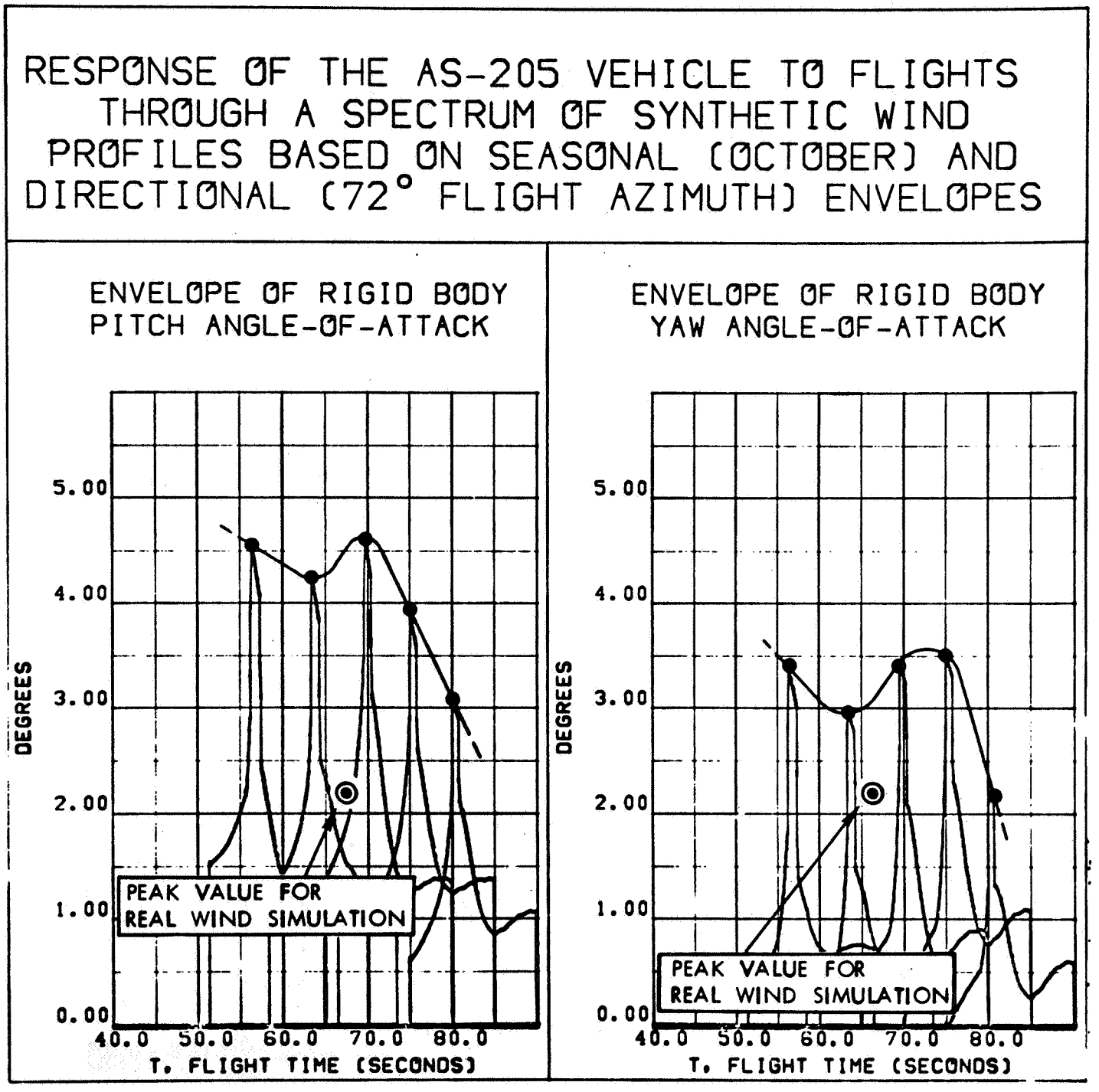
RESPONSE OF THE AS-205 VEHICLE TO FLIGHTS THROUGH A SPECTRUM OF SYNTHETIC WIND PROFILES BASED ON SEASONAL (OCTOBER) AND DIRECTIONAL (72° FLIGHT AZIMUTH) ENVELOPES
ENVELOPE OF RIGID BODY PITCH ANGLE-OF-ATTACK
DEGREES
5.00
4.00
3.00
2.00
1.00
0.00
PEAK VALUE FOR REAL WIND SIMULATION
40.0 50.0 60.0 70.0 80.0
T, FLIGHT TIME (SECONDS)
ENVELOPE OF RIGID BODY YAW ANGLE-OF-ATTACK
DEGREES
5.00
4.00
3.00
2.00
1.00
0.00
PEAK VALUE FOR REAL WIND SIMULATION
40.0 50.0 60.0 70.0 80.0
T, FLIGHT TIME (SECONDS)

FIGURE 29

RESPONSE OF THE AS-205 VEHICLE TO FLIGHTS THROUGH A SPECTRUM OF SYNTHETIC WIND PROFILES BASED ON SEASONAL (OCTOBER) AND DIRECTIONAL (72° FLIGHT AZIMUTH) ENVELOPES

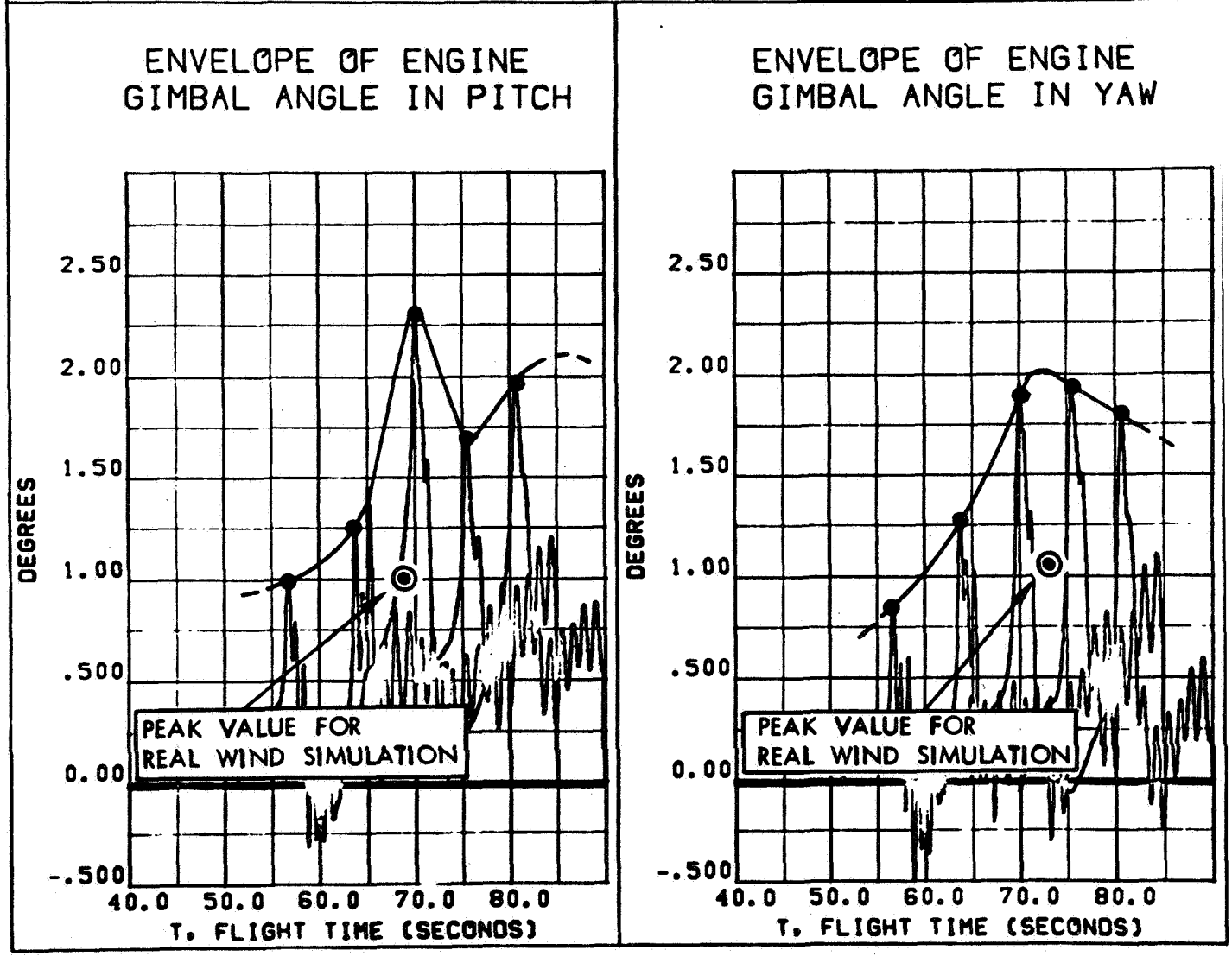

FIGURE 30

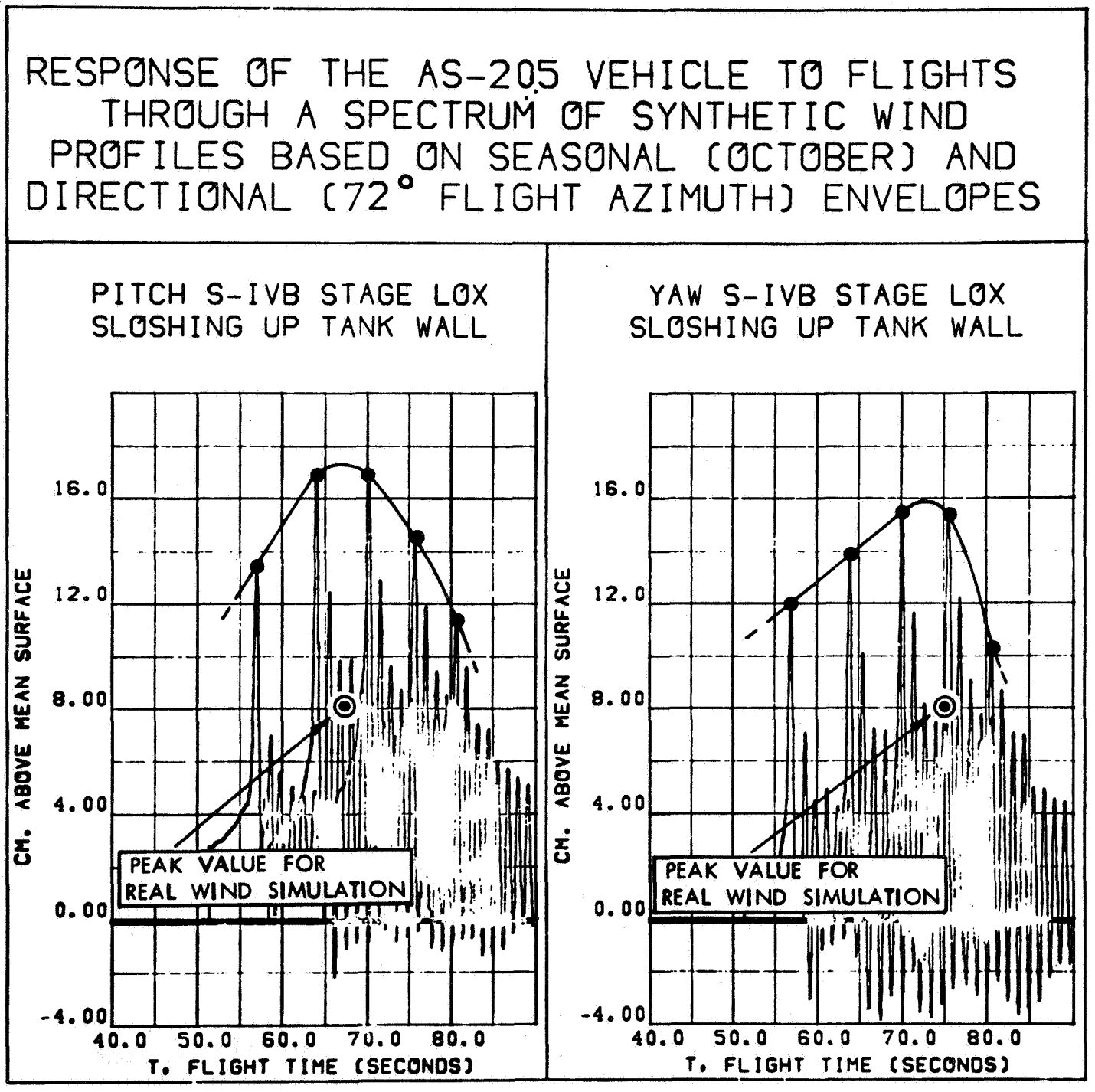
RESPONSE OF THE AS-205 VEHICLE TO FLIGHTS THROUGH A SPECTRUM OF SYNTHETIC WIND PROFILES BASED ON SEASONAL (OCTOBER) AND DIRECTIONAL (72° FLIGHT AZIMUTH) ENVELOPES
PITCH S-IVB STAGE LOX SLOSHING UP TANK WALL
YAW S-IVB STAGE LOX SLOSHING UP TANK WALL
CM. ABOVE MEAN SURFACE
16.0
12.0
8.00
4.00
0.00
-4.00
PEAK VALUE FOR REAL WIND SIMULATION
40.0
50.0
60.0
70.0
80.0
T. FLIGHT TIME (SECONDS)

FIGURE 31

RESPONSE OF THE AS-205 VEHICLE TO FLIGHTS THROUGH A SPECTRUM OF SYNTHETIC WIND PROFILES BASED ON SEASONAL (OCTOBER) AND DIRECTIONAL (72° FLIGHT AZIMUTH) ENVELOPES

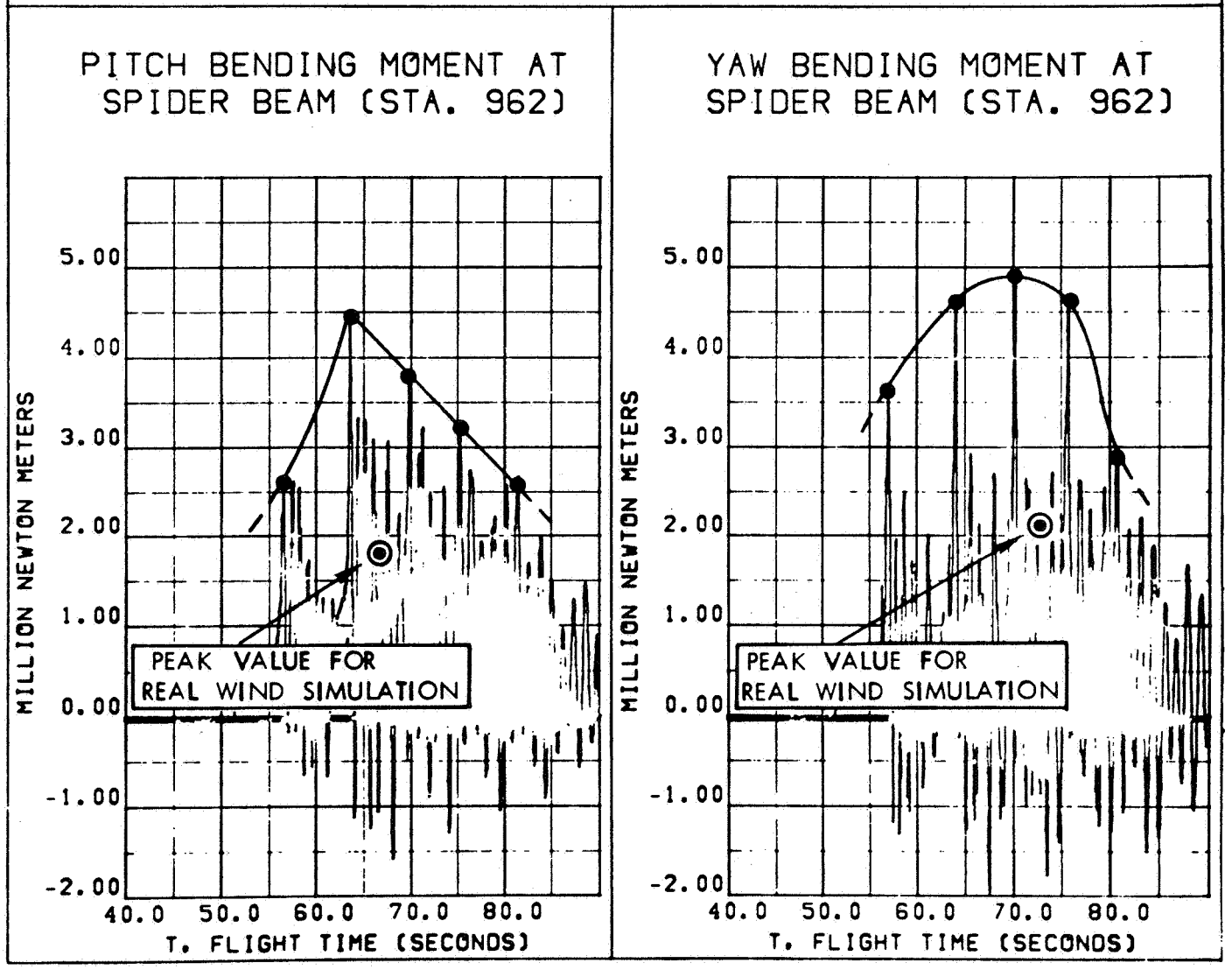

FIGURE 32

RESPONSE OF THE AS-205 VEHICLE TO FLIGHT THROUGH A SAMPLE REAL WIND SIMULATING BETWEEN TWO SIGMA AND THREE SIGMA PEAK WIND SPEEDS IN THE MONTH OF OCTOBER

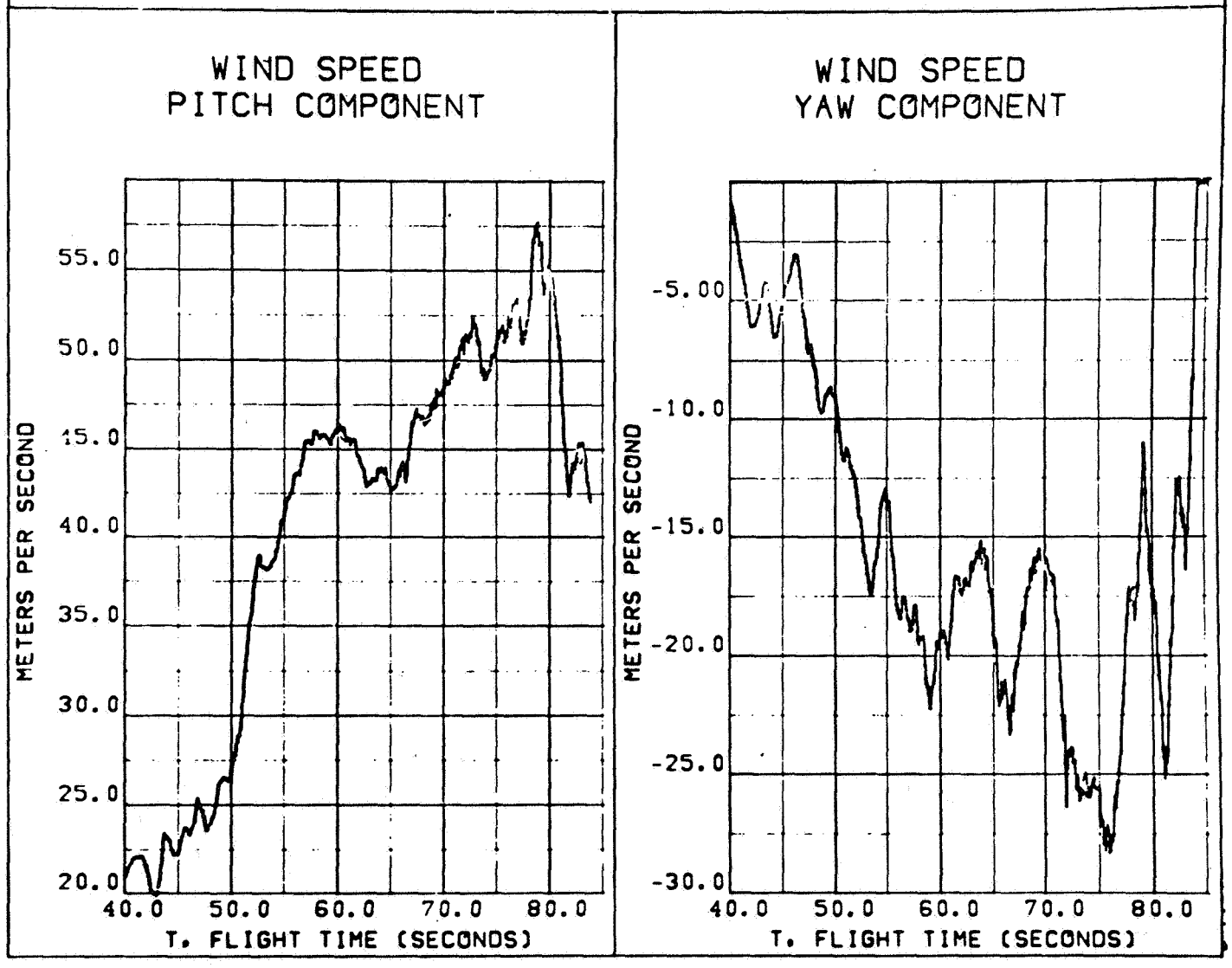

FIGURE 33

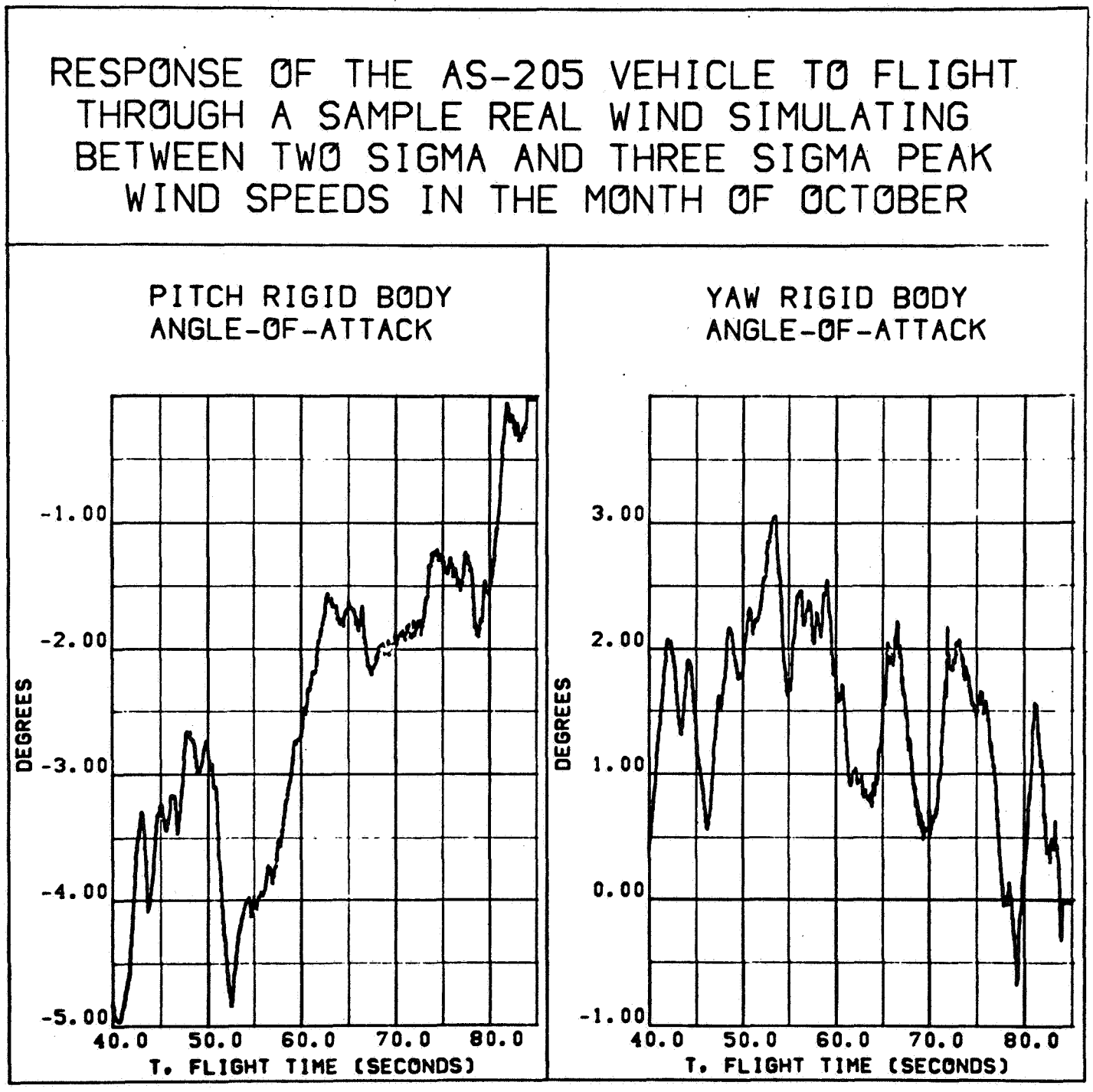
RESPONSE OF THE AS-205 VEHICLE TO FLIGHT THROUGH A SAMPLE REAL WIND SIMULATING BETWEEN TWO SIGMA AND THREE SIGMA PEAK WIND SPEEDS IN THE MONTH OF OCTOBER
PITCH RIGID BODY ANGLE-OF-ATTACK
DEGREES
-1.00
-2.00
-3.00
-4.00
-5.00
40.0
50.0
60.0
70.0
80.0
T, FLIGHT TIME (SECONDS)
YAW RIGID BODY ANGLE-OF-ATTACK
DEGREES
3.00
2.00
1.00
0.00
-1.00
40.0
50.0
60.0
70.0
80.0
T, FLIGHT TIME (SECONDS)

FIGURE 34

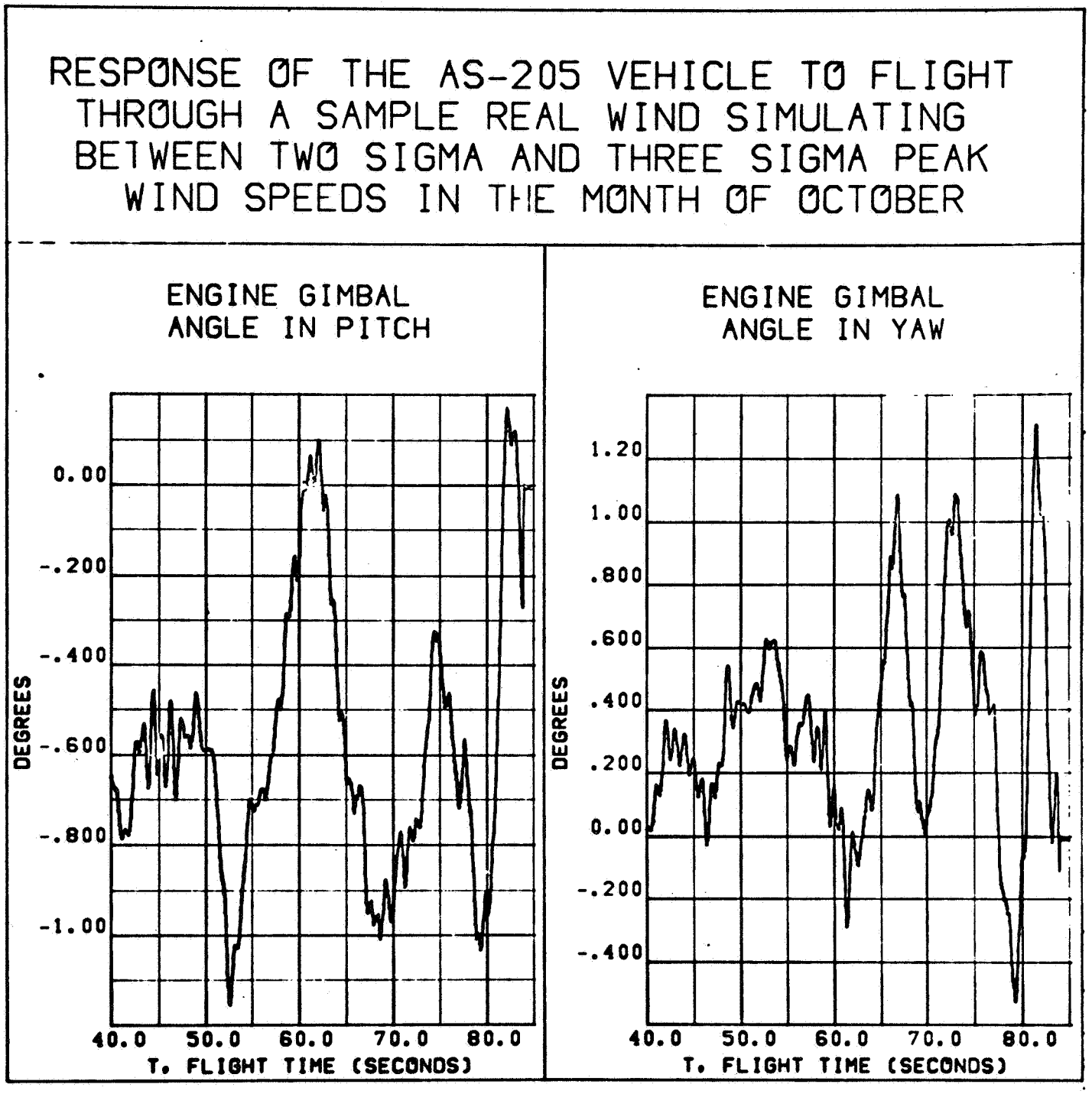
RESPONSE OF THE AS-205 VEHICLE TO FLIGHT THROUGH A SAMPLE REAL WIND SIMULATING BETWEEN TWO SIGMA AND THREE SIGMA PEAK WIND SPEEDS IN THE MONTH OF OCTOBER
ENGINE GIMBAL ANGLE IN PITCH
DEGREES
0.00
-.200
-.400
-.600
-.800
-1.00
40.0
50.0
60.0
70.0
80.0
T, FLIGHT TIME (SECONDS)
ENGINE GIMBAL ANGLE IN YAW
DEGREES
1.20
1.00
.800
.600
.400
.200
0.00
-.200
-.400
40.0
50.0
60.0
70.0
80.0
T, FLIGHT TIME (SECONDS)

FIGURE 35

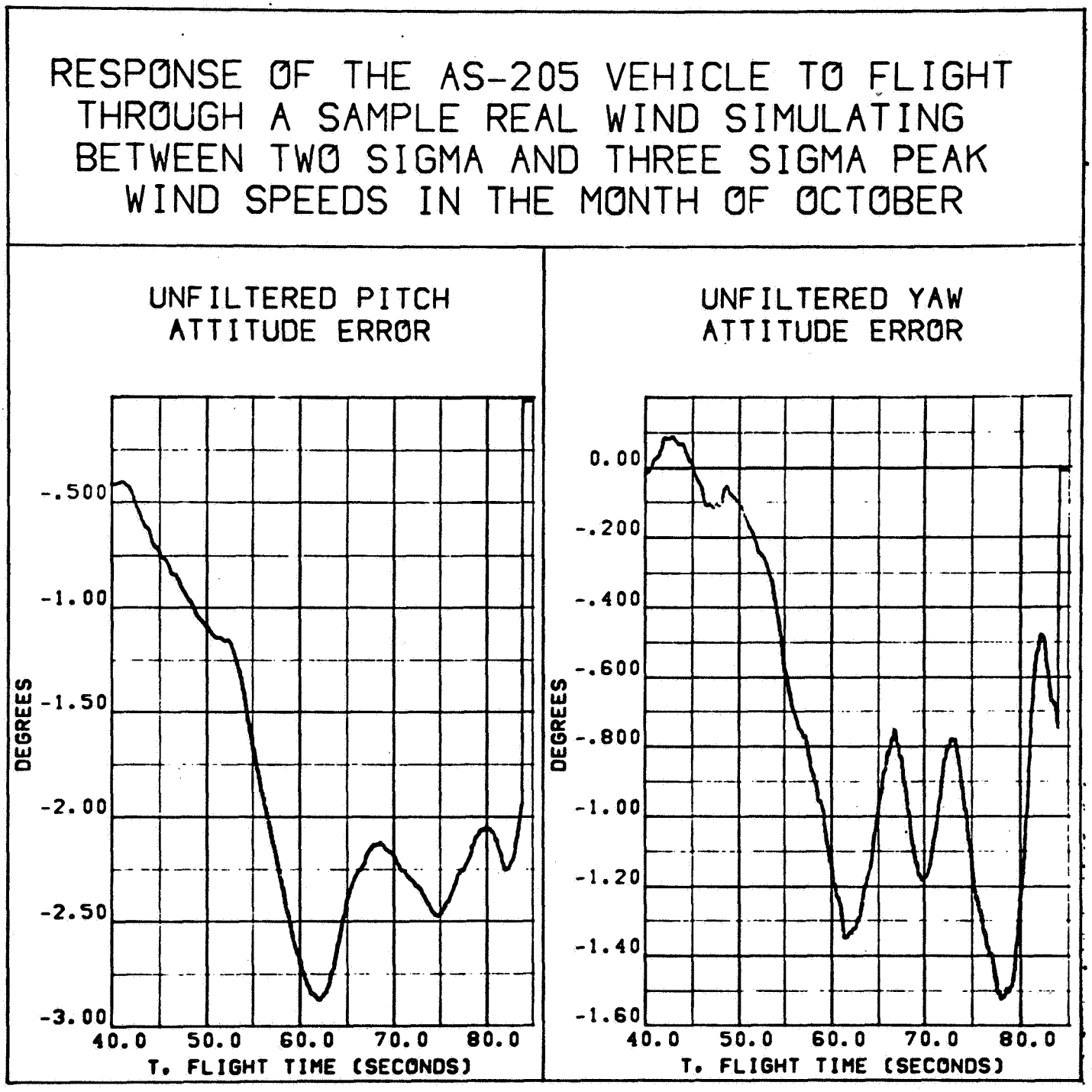
RESPONSE OF THE AS-205 VEHICLE TO FLIGHT THROUGH A SAMPLE REAL WIND SIMULATING BETWEEN TWO SIGMA AND THREE SIGMA PEAK WIND SPEEDS IN THE MONTH OF OCTOBER
UNFILTERED PITCH ATTITUDE ERROR
DEGREES
-.500
-1.00
-1.50
-2.00
-2.50
-3.00
40.0
50.0
60.0
70.0
80.0
T, FLIGHT TIME (SECONDS)
UNFILTERED YAW ATTITUDE ERROR
DEGREES
0.00
-.200
-.400
-.600
-.800
-1.00
-1.20
-1.40
-1.60
40.0
50.0
60.0
70.0
80.0
T, FLIGHT TIME (SECONDS)

FIGURE 36

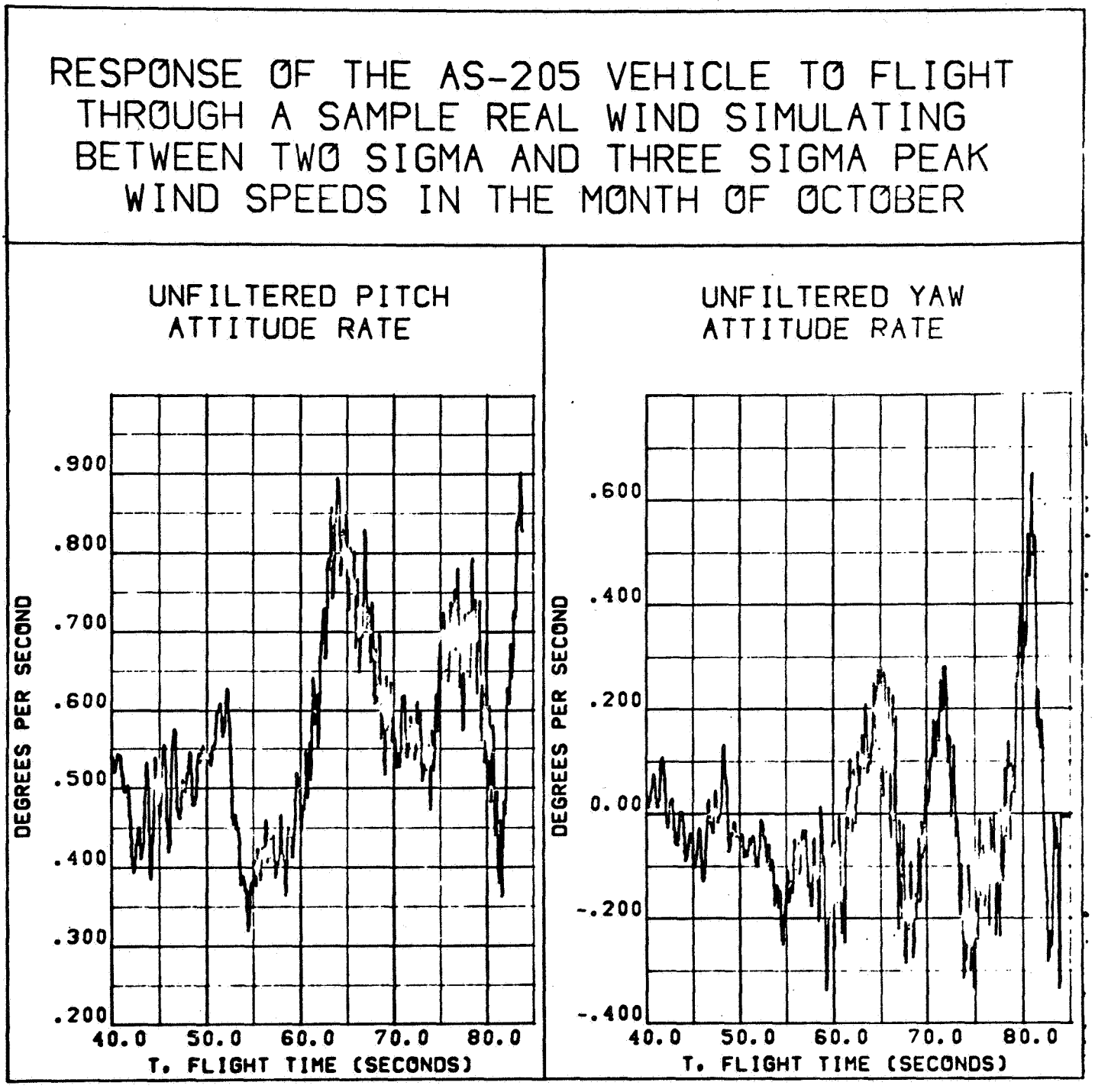
RESPONSE OF THE AS-205 VEHICLE TO FLIGHT THROUGH A SAMPLE REAL WIND SIMULATING BETWEEN TWO SIGMA AND THREE SIGMA PEAK WIND SPEEDS IN THE MONTH OF OCTOBER
UNFILTERED PITCH ATTITUDE RATE
DEGREES PER SECOND
.900
.800
.700
.600
.500
.400
.300
.200
40.0
50.0
60.0
70.0
80.0
T, FLIGHT TIME (SECONDS)
UNFILTERED YAW ATTITUDE RATE
DEGREES PER SECOND
.600
.400
.200
0.00
-.200
-.400
40.0
50.0
60.0
70.0
80.0
T, FLIGHT TIME (SECONDS)

FIGURE 37

RESPONSE OF THE AS-205 VEHICLE TO FLIGHT THROUGH A SAMPLE REAL WIND SIMULATING BETWEEN TWO SIGMA AND THREE SIGMA PEAK WIND SPEEDS IN THE MONTH OF OCTOBER

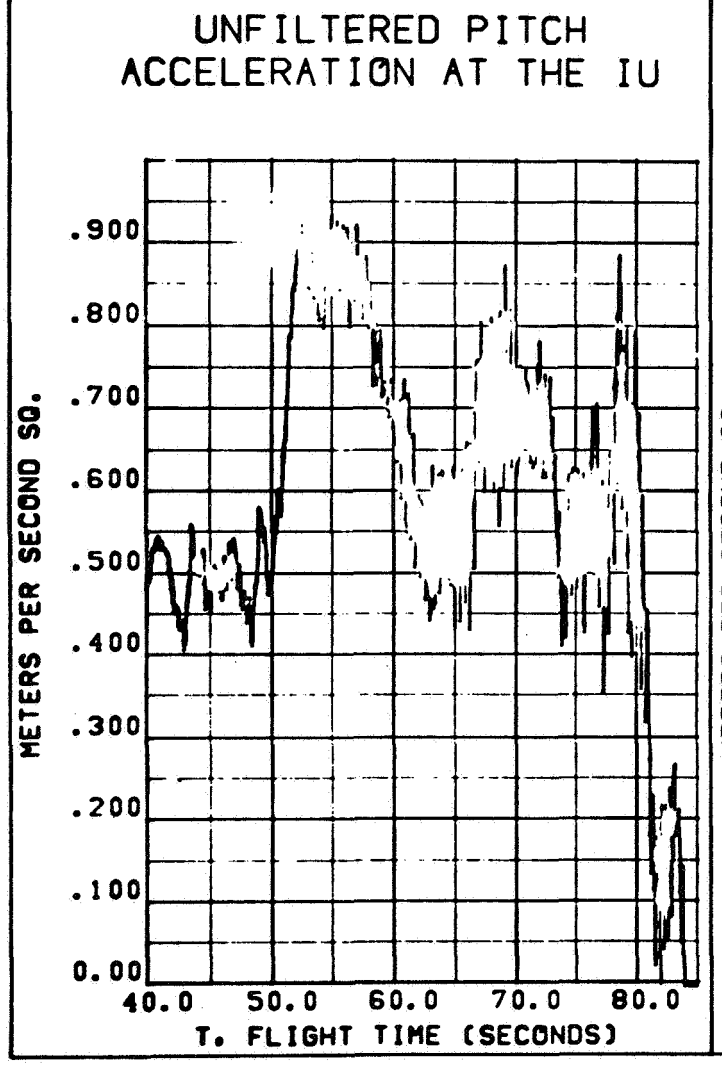

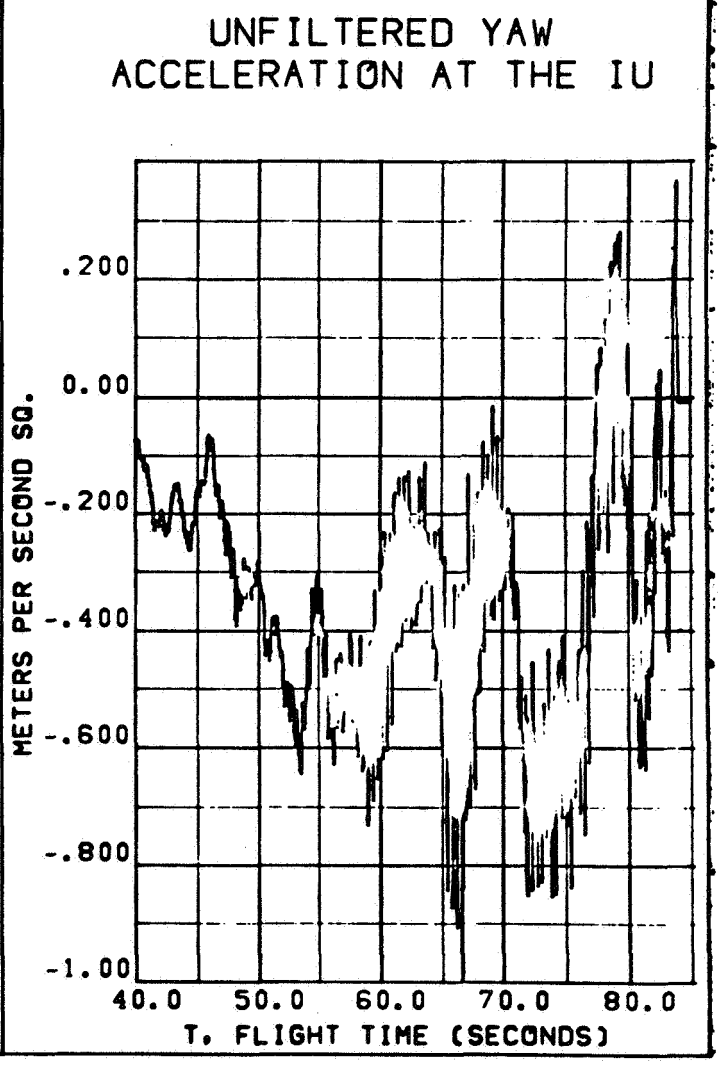

FIGURE 38

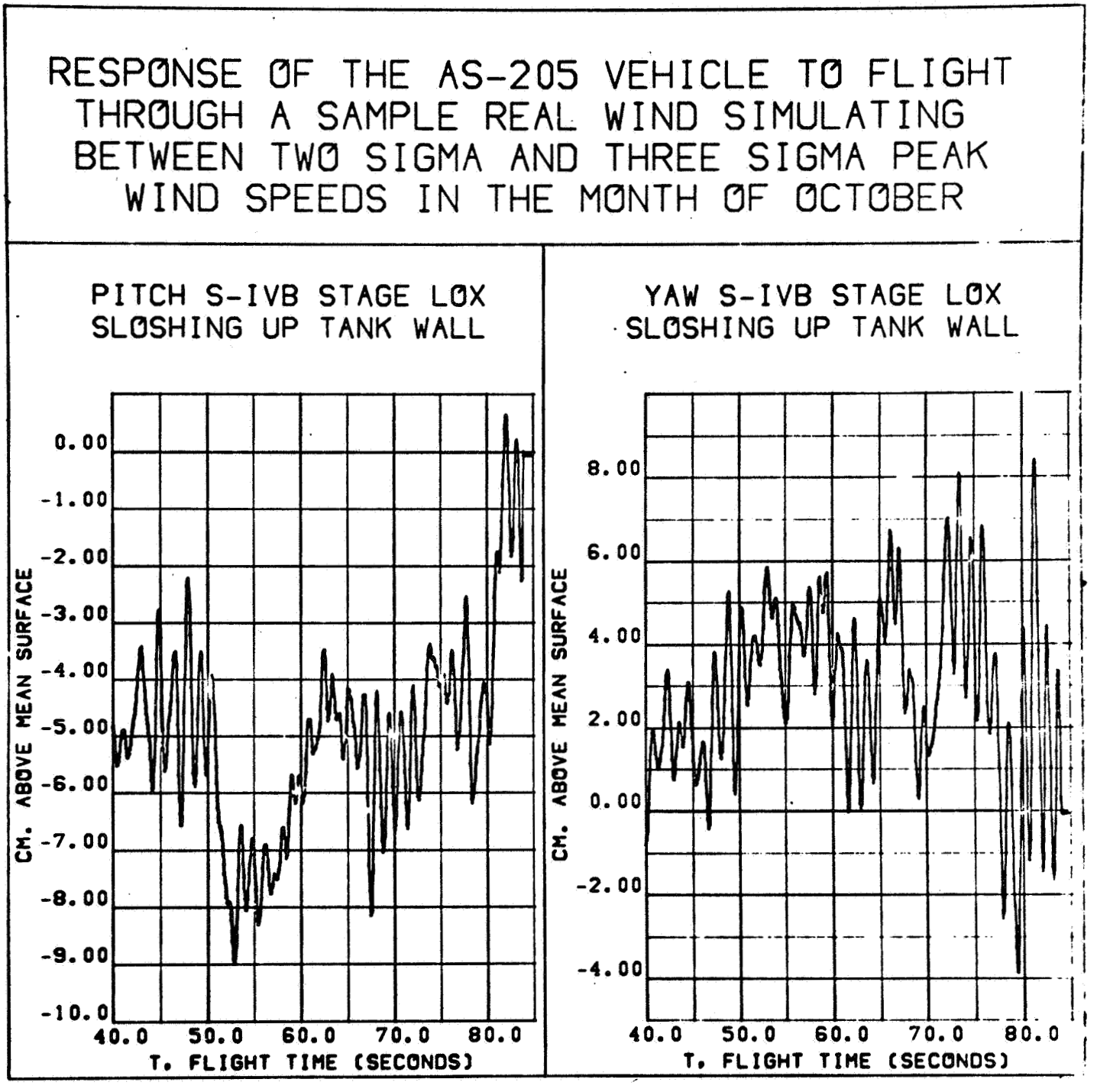
RESPONSE OF THE AS-205 VEHICLE TO FLIGHT THROUGH A SAMPLE REAL WIND SIMULATING BETWEEN TWO SIGMA AND THREE SIGMA PEAK WIND SPEEDS IN THE MONTH OF OCTOBER
PITCH S-IVB STAGE LOX SLOSHING UP TANK WALL
CM. ABOVE MEAN SURFACE
0.00
-1.00
-2.00
-3.00
-4.00
-5.00
-6.00
-7.00
-8.00
-9.00
-10.0
40.0
50.0
60.0
70.0
80.0
T, FLIGHT TIME (SECONDS)
YAW S-IVB STAGE LOX SLOSHING UP TANK WALL
CM. ABOVE MEAN SURFACE
8.00
6.00
4.00
2.00
0.00
-2.00
-4.00
40.0
50.0
60.0
70.0
80.0
T, FLIGHT TIME (SECONDS)

FIGURE 39

RESPONSE OF THE AS-205 VEHICLE TO FLIGHT THROUGH A SAMPLE REAL WIND SIMULATING BETWEEN TWO SIGMA AND THREE SIGMA PEAK WIND SPEEDS IN THE MONTH OF OCTOBER

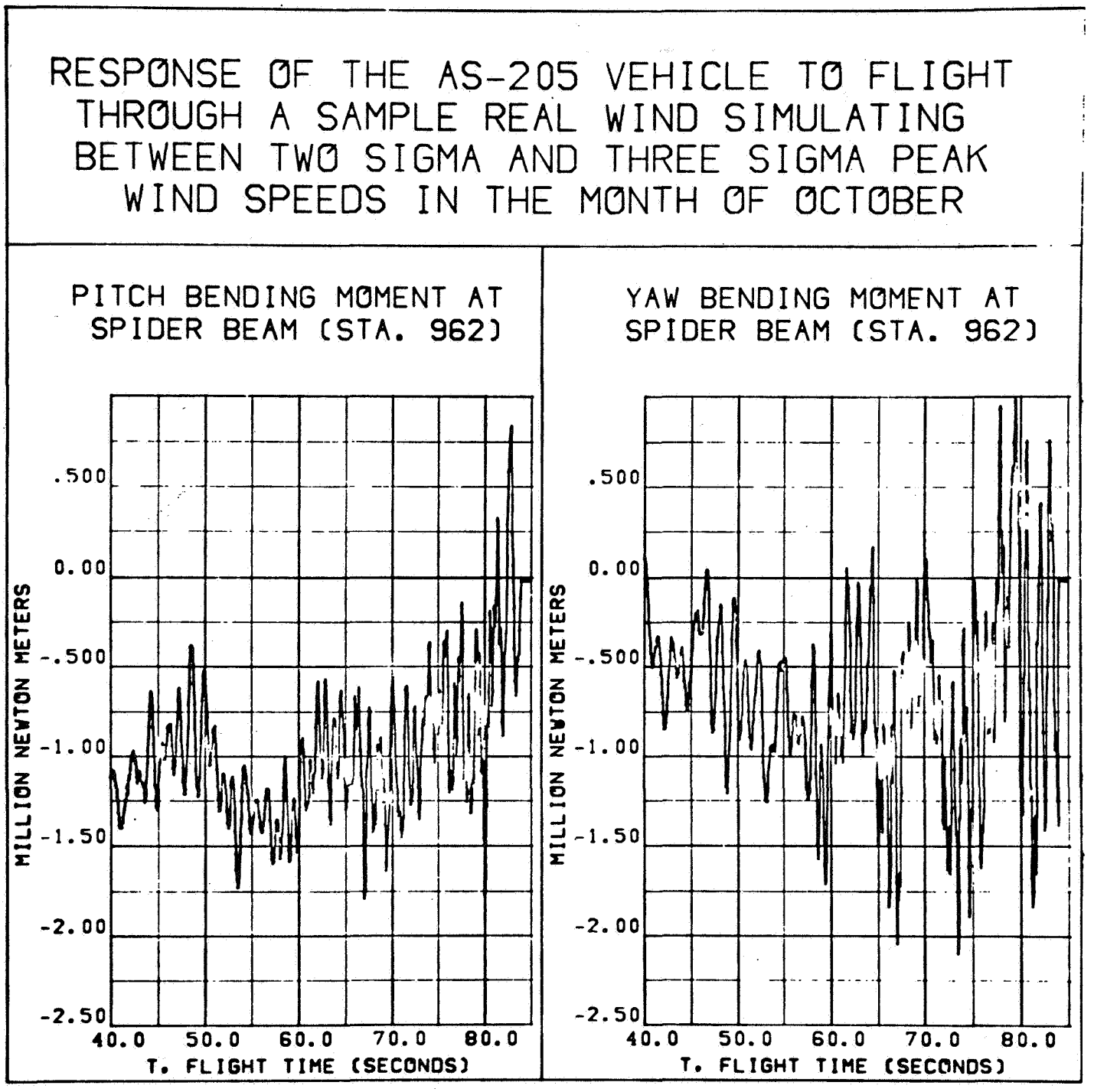

FIGURE 40

AS-204 ENGINE OUT STEERING COMPENSATION

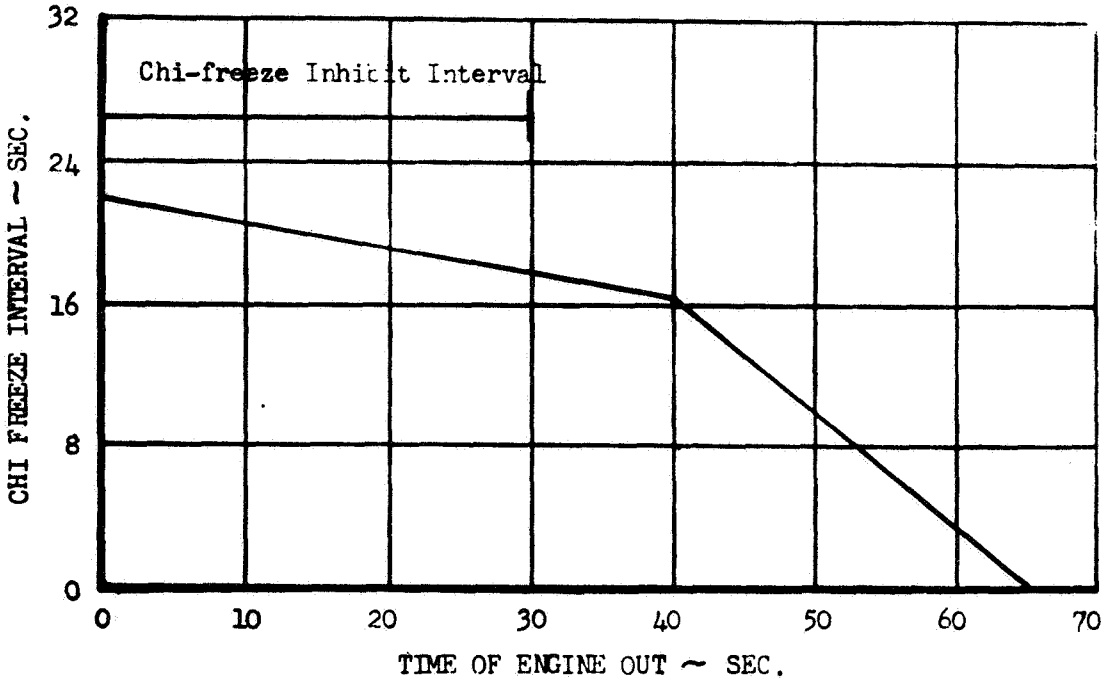

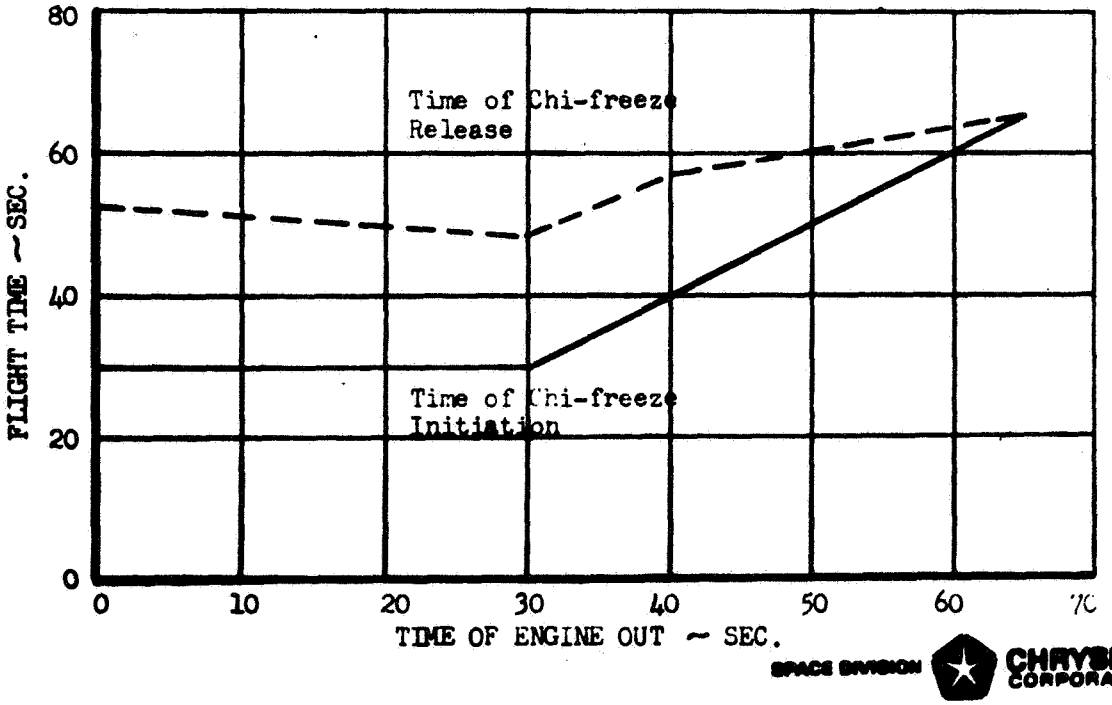

SPACE DIVISION CHRYSLER CORPORATION

FIGURE 41

AS-205/CSM-101 PITCH AND YAW CONTROL SYSTEM GAINS
S-IVB STAGE

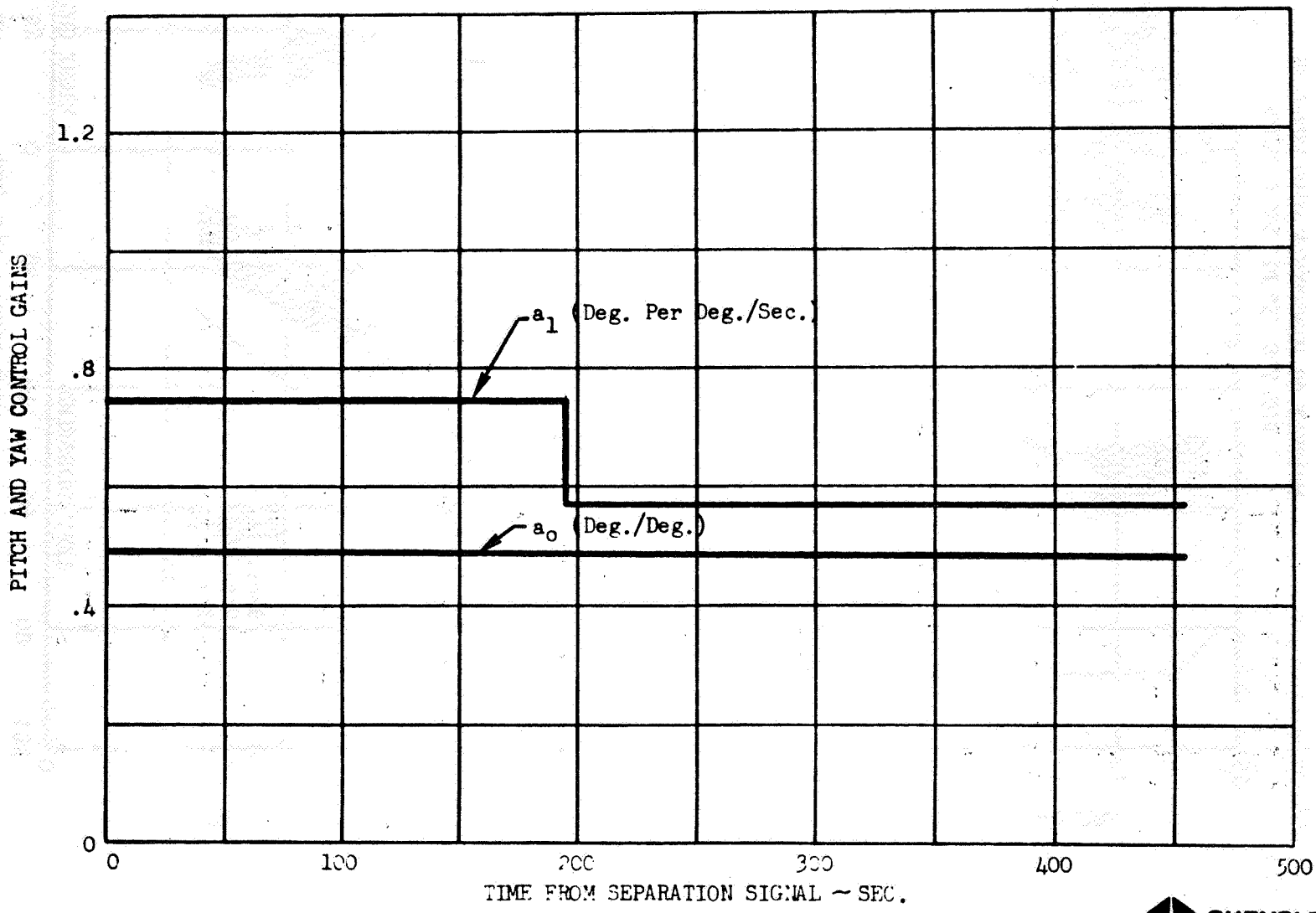

FIGURE 42

MONTHLY 99 PERCENTILE WIND ENVELOPES
FOR THE 75° FLIGHT AZIMUTH

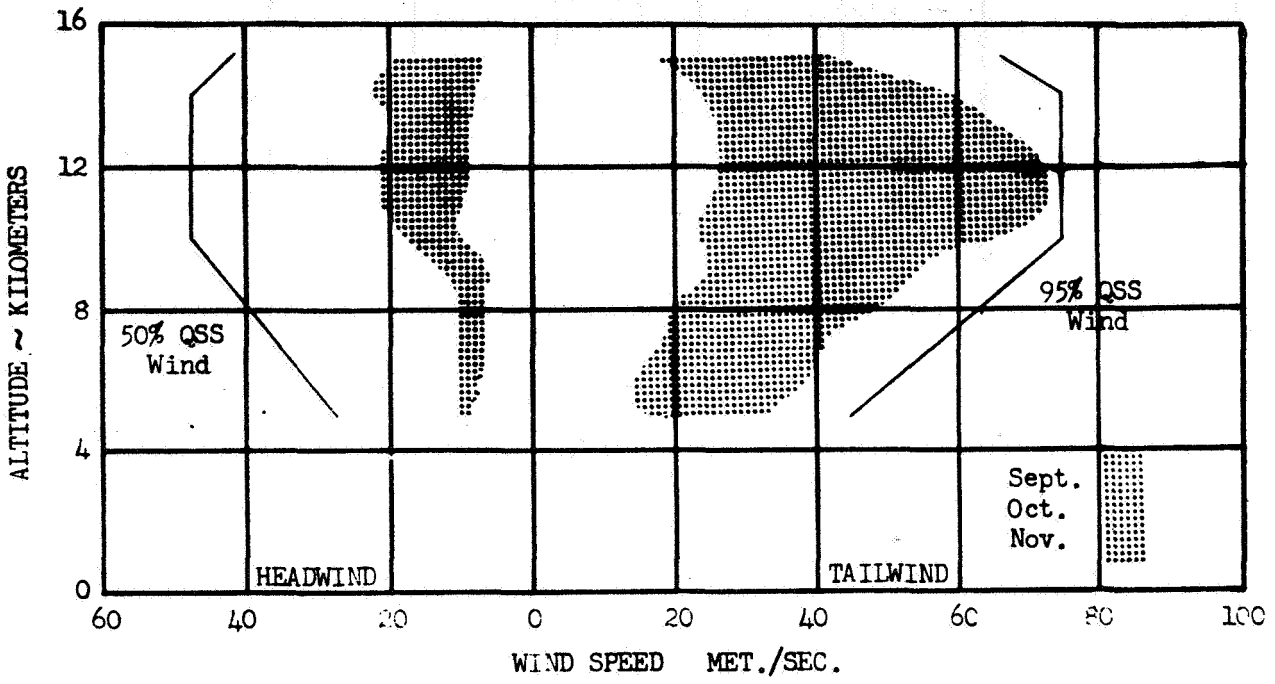

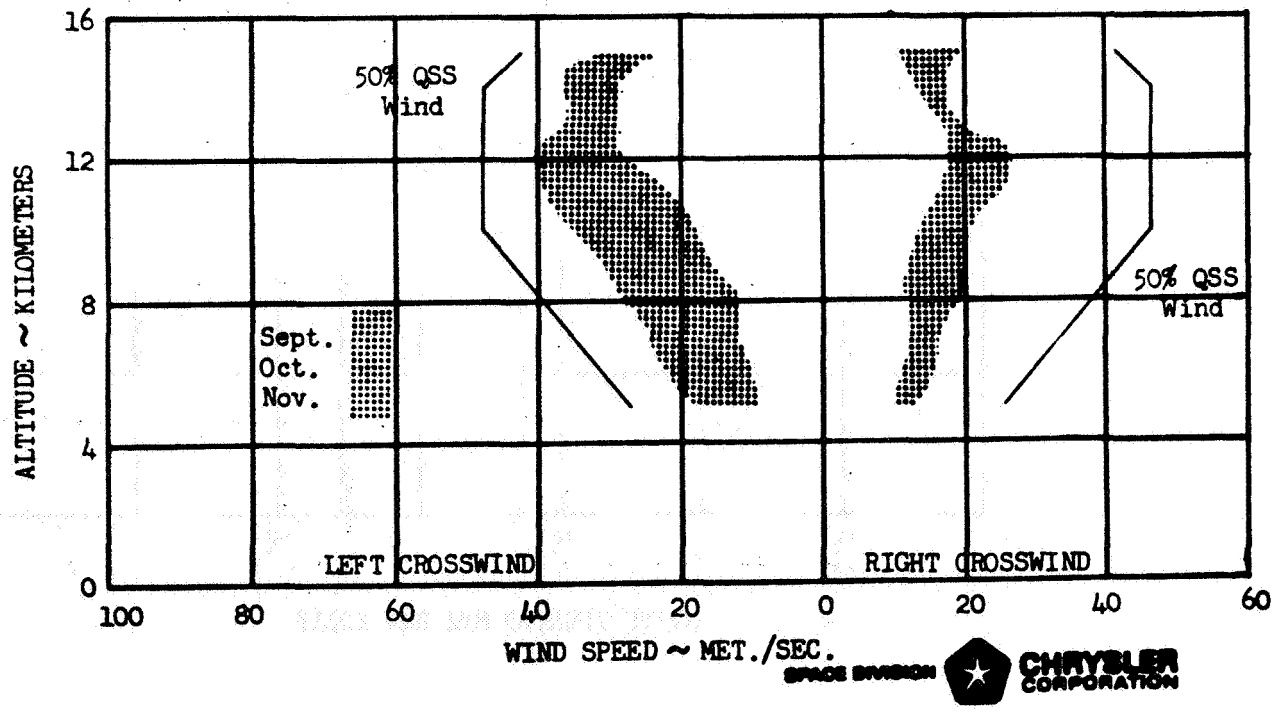

SPACE DIVISION CHRYSLER CORPORATION

FIGURE 43

AS-205/CSM-101 ENVELOPES OF PEAK CONTROL GIMBAL DEFLECTION
NO ENGINE FAILURE

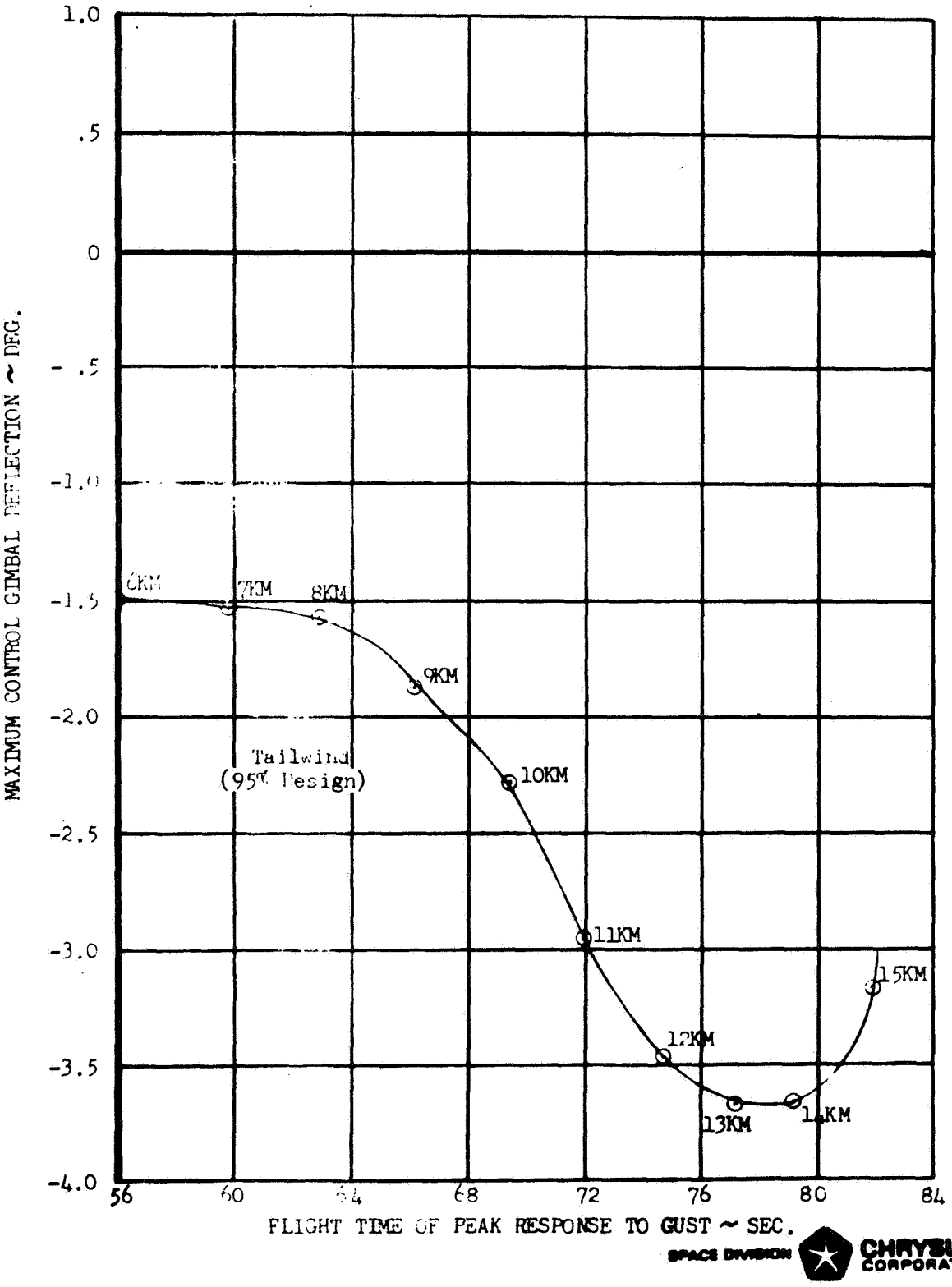

SPACE DIVISION CHRYSLER CORPORATION

FIGURE 44

AS-205/CSM-101 ENVELOPE OF PEAK CONTROL GIMBAL DEFLECTION
NO ENGINE FAILURE

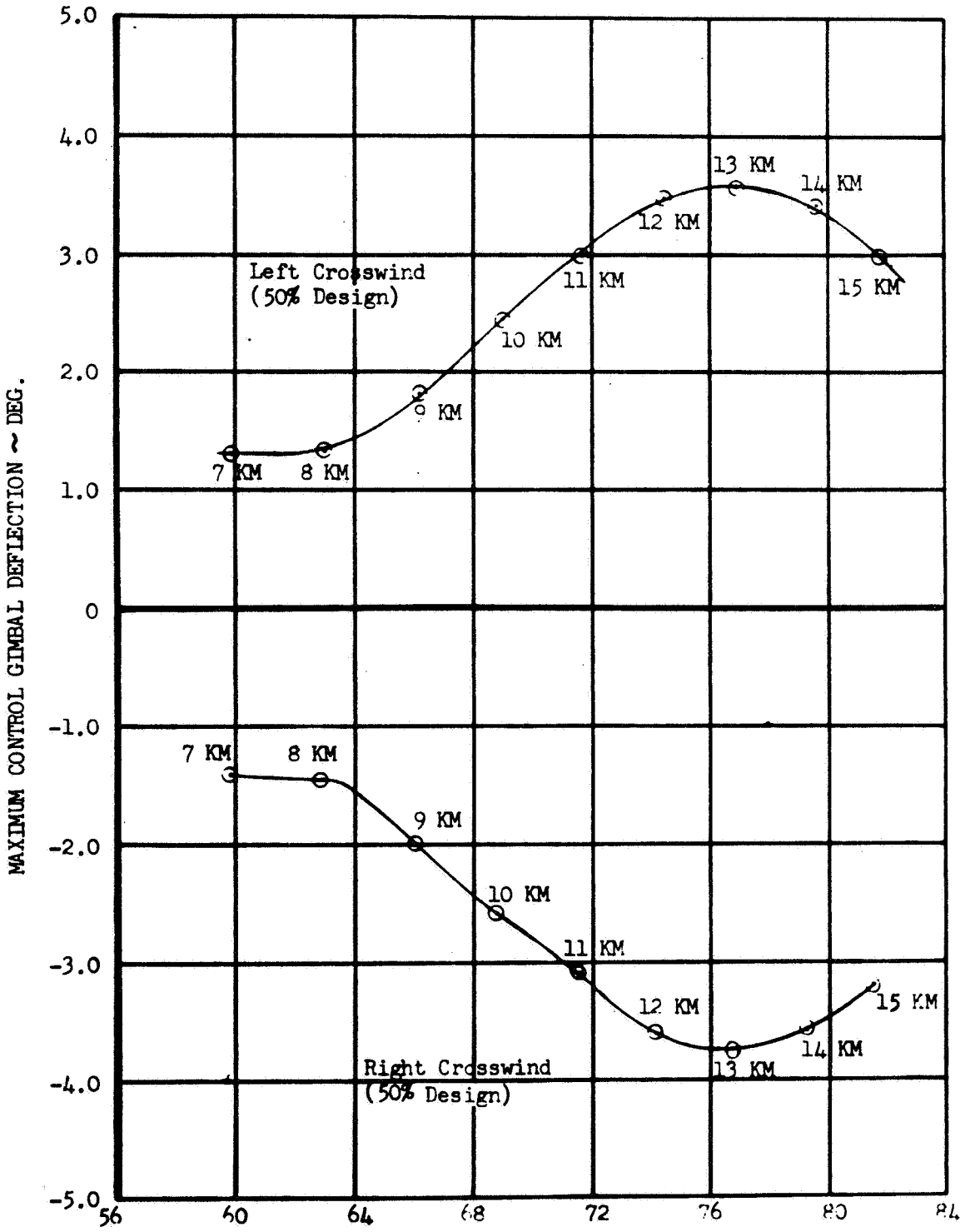

SPACE DIVISION CHRYSLER CORPORATION

FIGURE 45

AS-205/CSM-101 ENVELOPES OF PEAK BENDING MOMENT
CRITICAL RATIOS (S.F. = 1.40)
NO ENGINE FAILURE

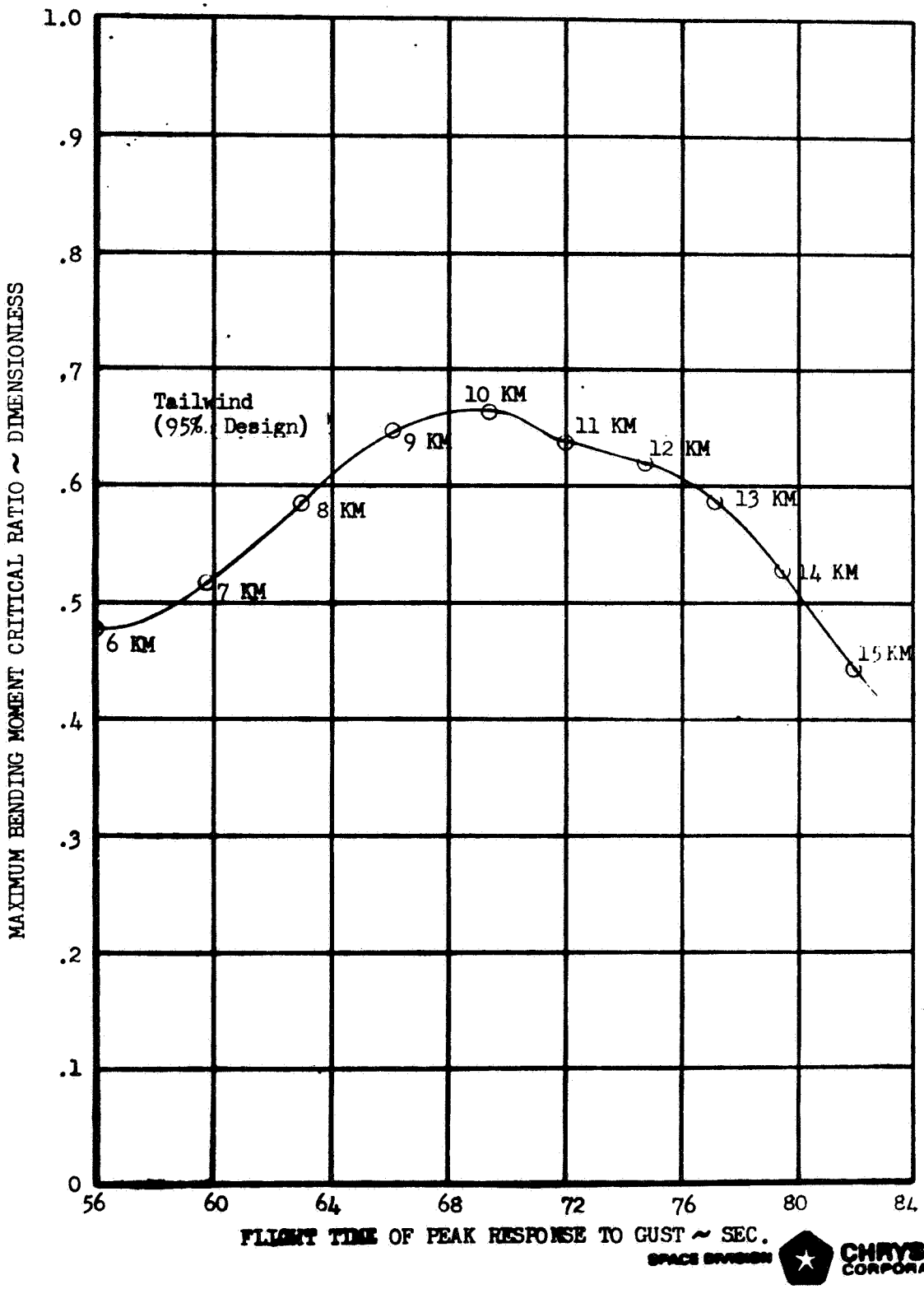

SPACE DIVISION CHRYSLER CORPORATION

FIGURE 46

AS-205/CSM-101 ENVELOPES OF PEAK BENDING MOMENT CRITICAL RATIOS
(S.F. = 1.40)
NO ENGINE FAILURE

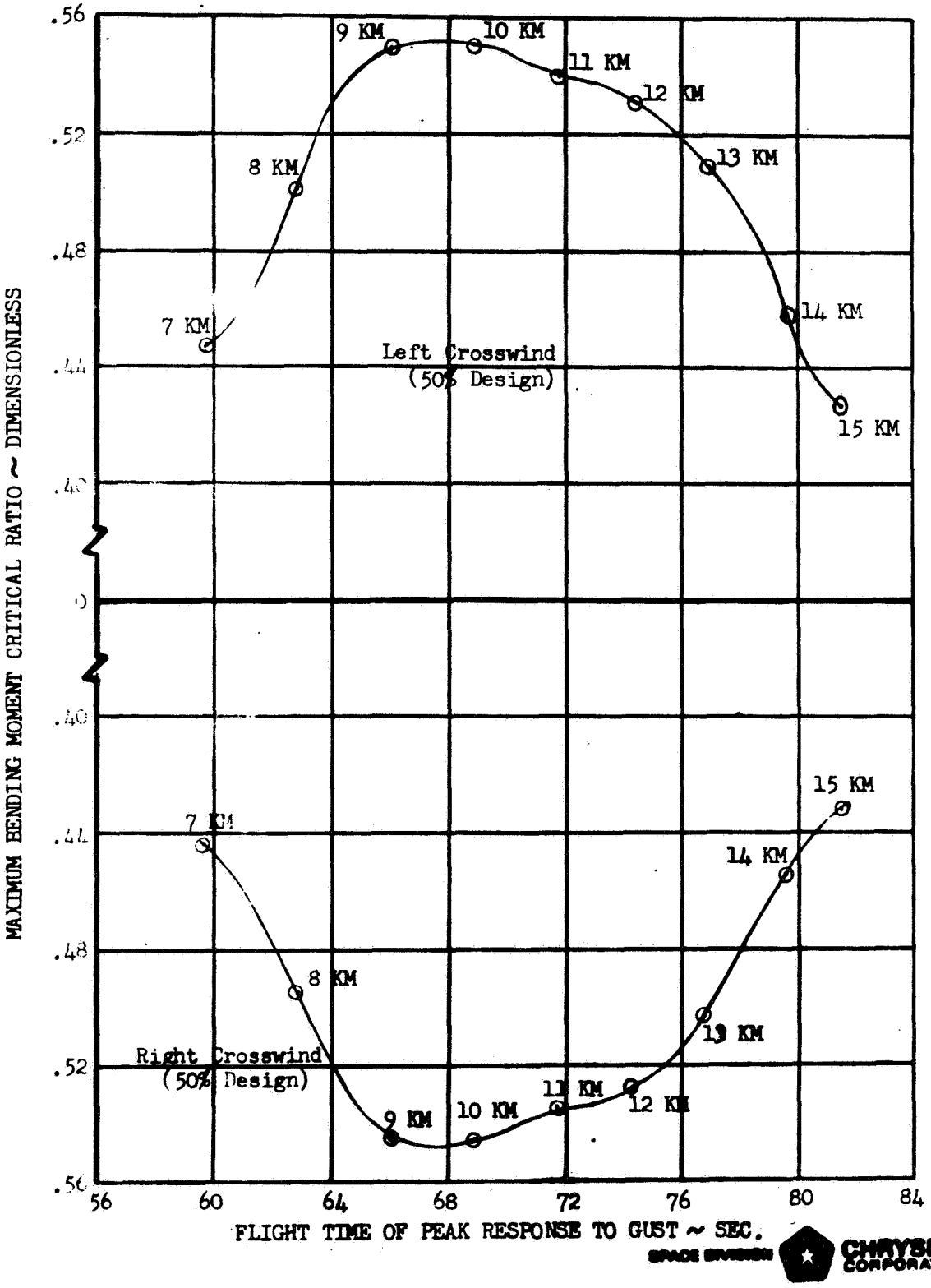

SPACE DIVISION CHRYSLER CORPORATION

FIGURE 47

AS-205/CSM-101 ENVELOPES OF MAXIMUM CONTROL GIMBAL DEFLECTIONS
FOR ENGINE NO. 3 FAILURES WITH NO WINDS

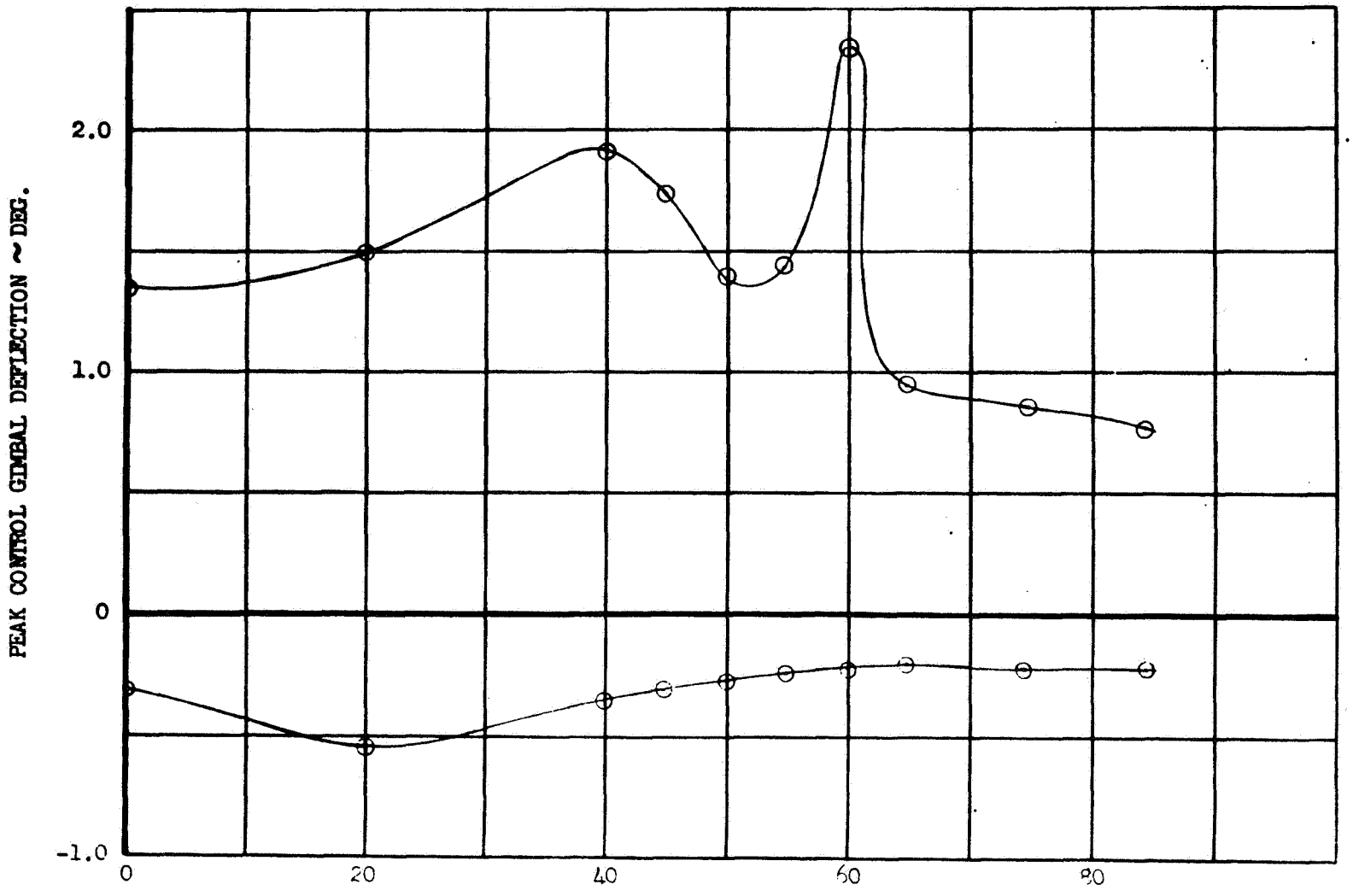

FIGURE 48

AS-205/CSM-101 ENVELOPES OF MAXIMUM CONTROL GIMBAL DEFLECTIONS
FOR ENGINE NO. 4 FAILURES DURING BOOST WITH NO WINDS

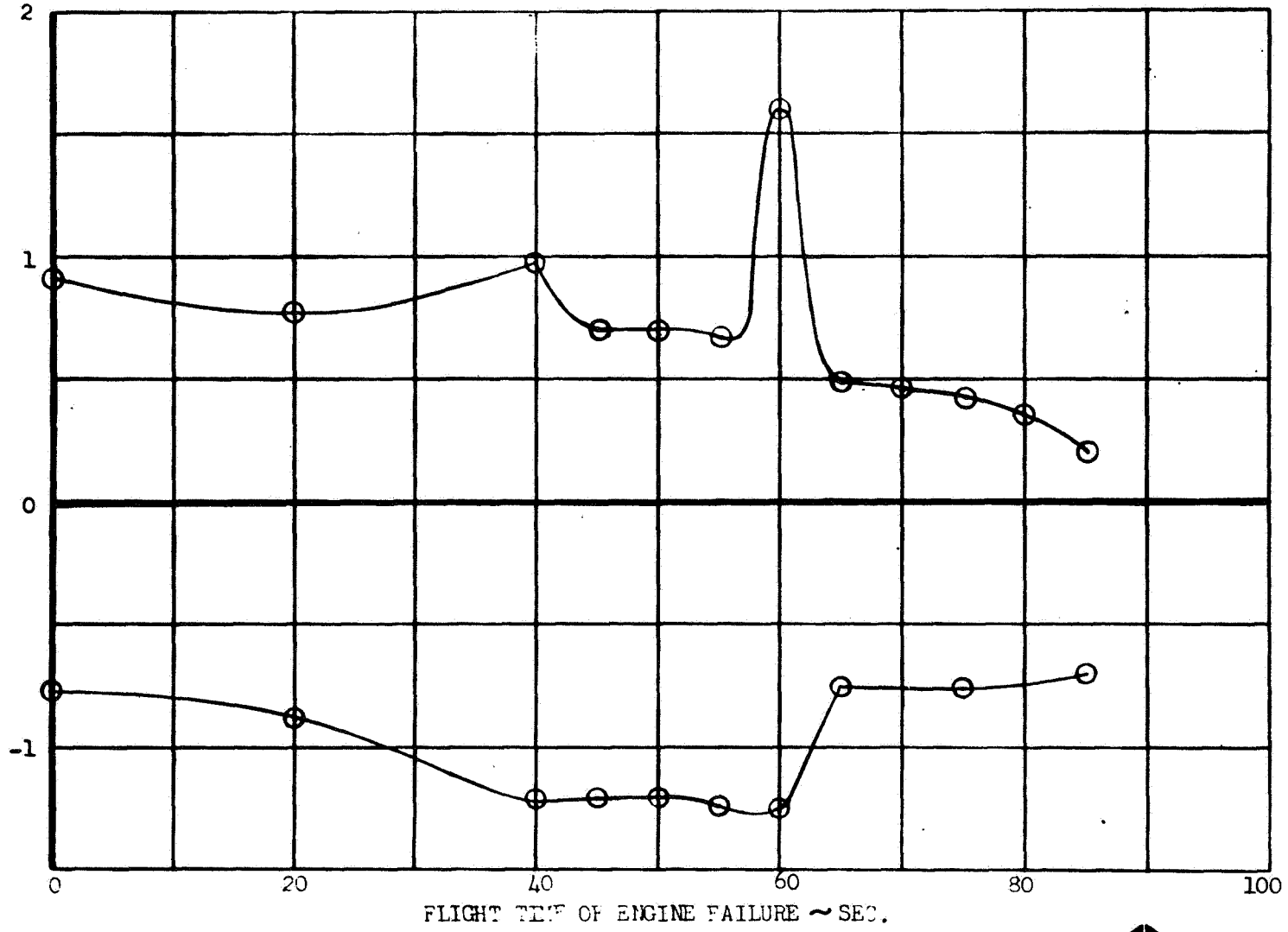

SPACE DIVISION CHRYSLER CORPORATION

FIGURE 49

AS-205/CSM-101 ENVELOPES OF MAXIMUM BENDING MOMENT CRITICAL RATIOS (S.F. = 1.4)
FOR ENGINE NO. 3 FAILURES AND ENGINE NO. 4 FAILURES WITH NO WINDS

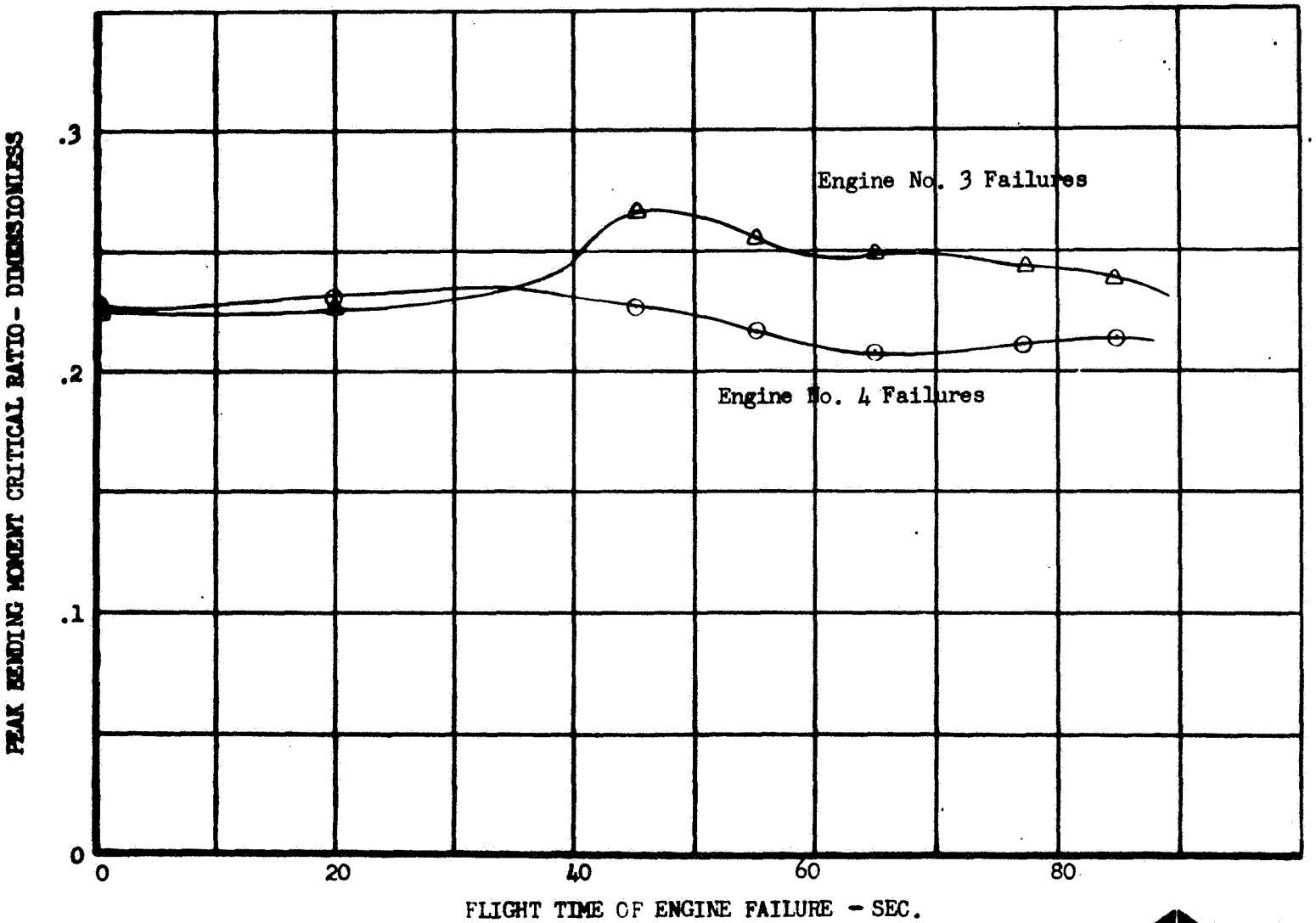

FIGURE 50

AS-205/CSM-101 STAGING AERODYNAMIC MOMENT ON S-IVB STAGE
FOR H-1 ENGINE NO. 3 FAILURES AND H-1 ENGINE NO. 4 FAILURES WITH NO WIND

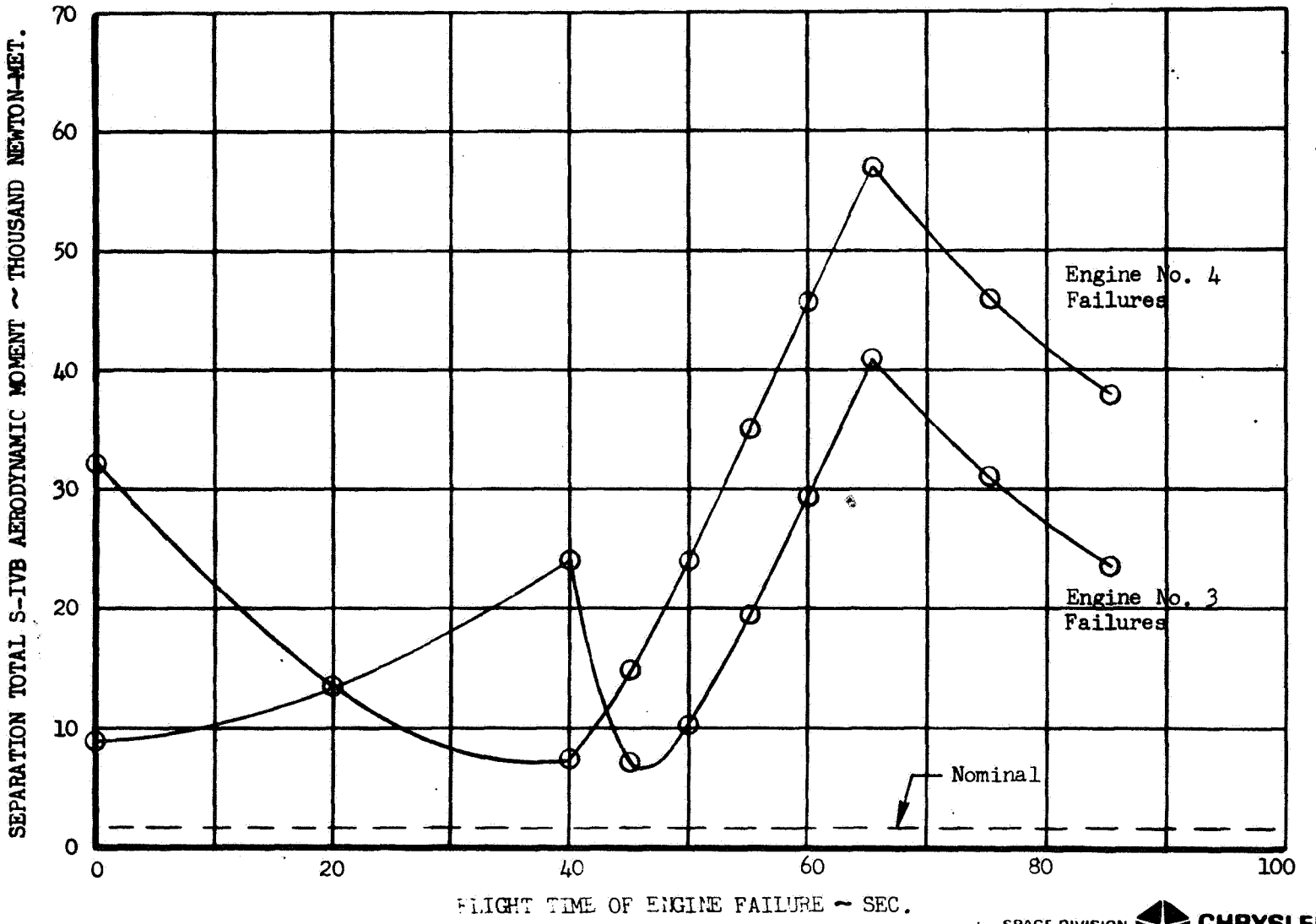

SPACE DIVISION CHRYSLER CORPORATION

FIGURE 51

AS-205/CSM-101 STAGING DYNAMIC PRESSURE TIMES TOTAL ANGLE OF ATTACK
FOR ENGINE NO. 3 FAILURES AND ENGINE NO. 4 FAILURES DURING BOOST WITH NO WINDS

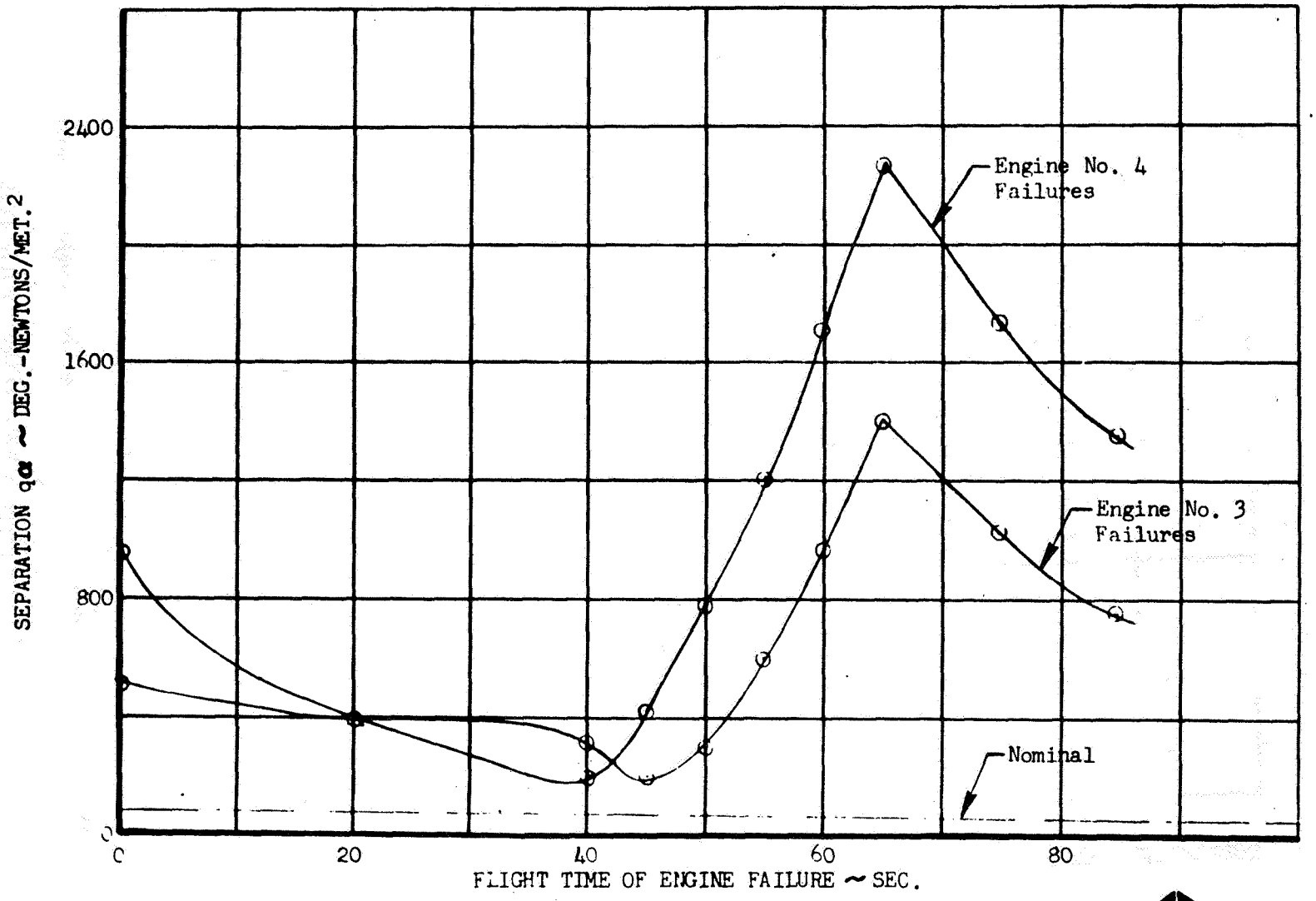

FIGURE 52

AS-205/CSM-101 ENVELOPES OF POST SEPARATION S-IVB MAXIMUM MAGNITUDE OF CONTROL GIMBAL DEFLECTION FOR WORST CASE ENGINE FAILURE DURING BOOST WITH NO WINDS

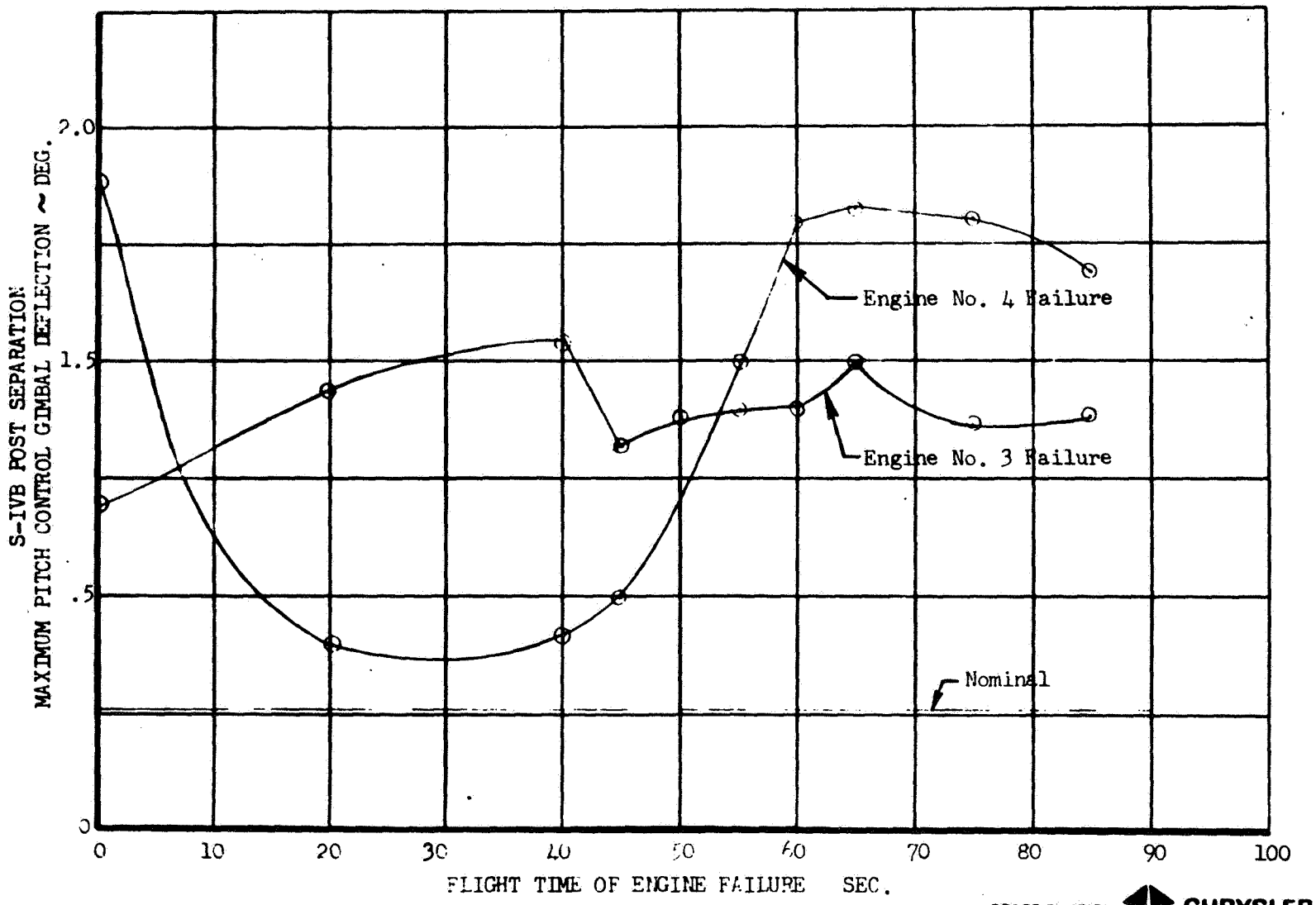

SPACE DIVISION CHRYSLER CORPORATION

FIGURE 53

AS-205/CSM-101 ENVELOPES OF POST SEPARATION S-IVB MAXIMUM MAGNITUDE OF ATTITUDE ERROR FOR WORST CASE ENGINE FAILURES DURING BOOST WITH NO WINDS

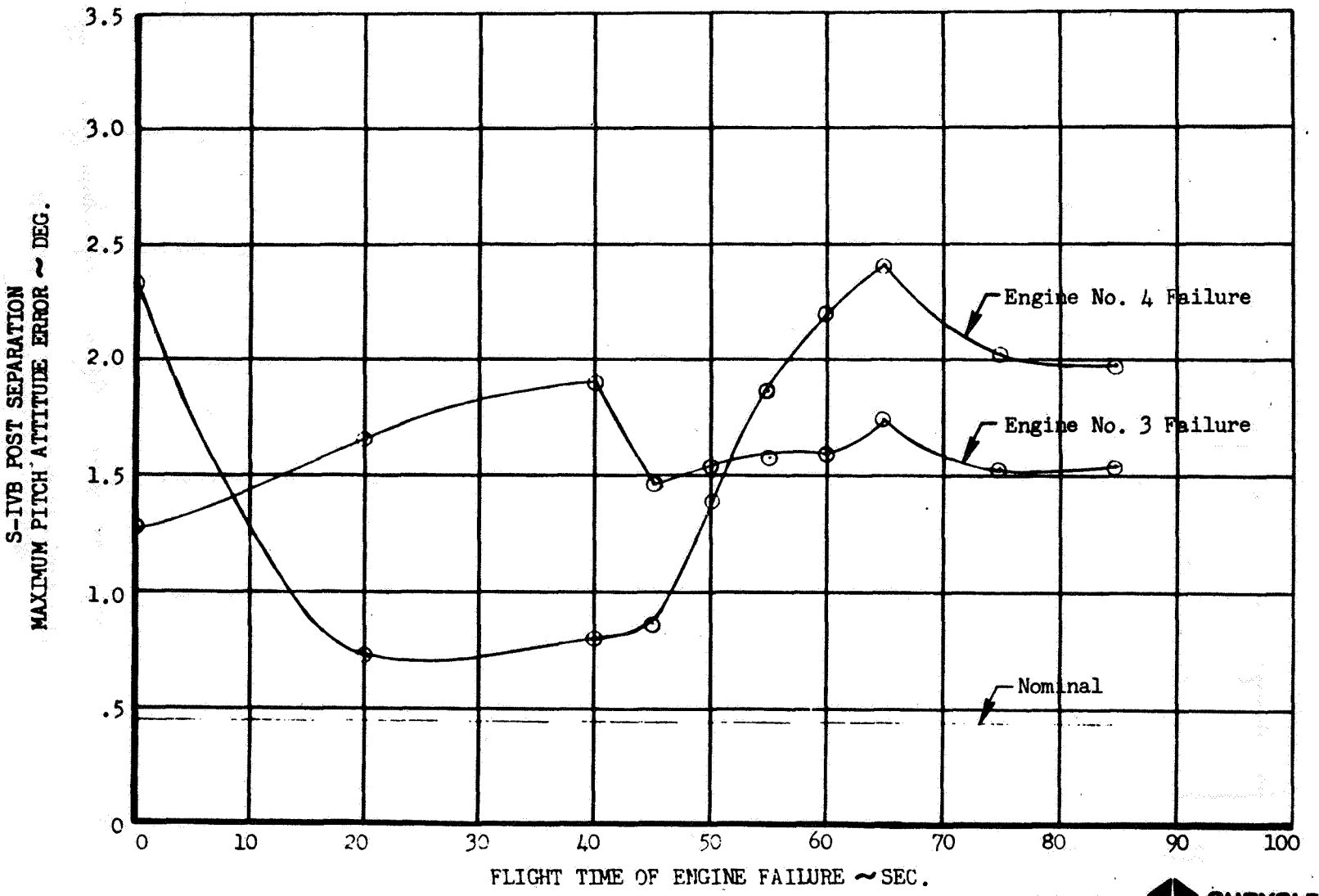

FIGURE 54

AS-205/CSM-101 ENVELOPES OF POST SEPARATION S-IVB MAXIMUM MAGNITUDE OF ATTITUDE RATE
FOR WORST CASE ENGINE FAILURES DURING BOOST WITH NO WINDS

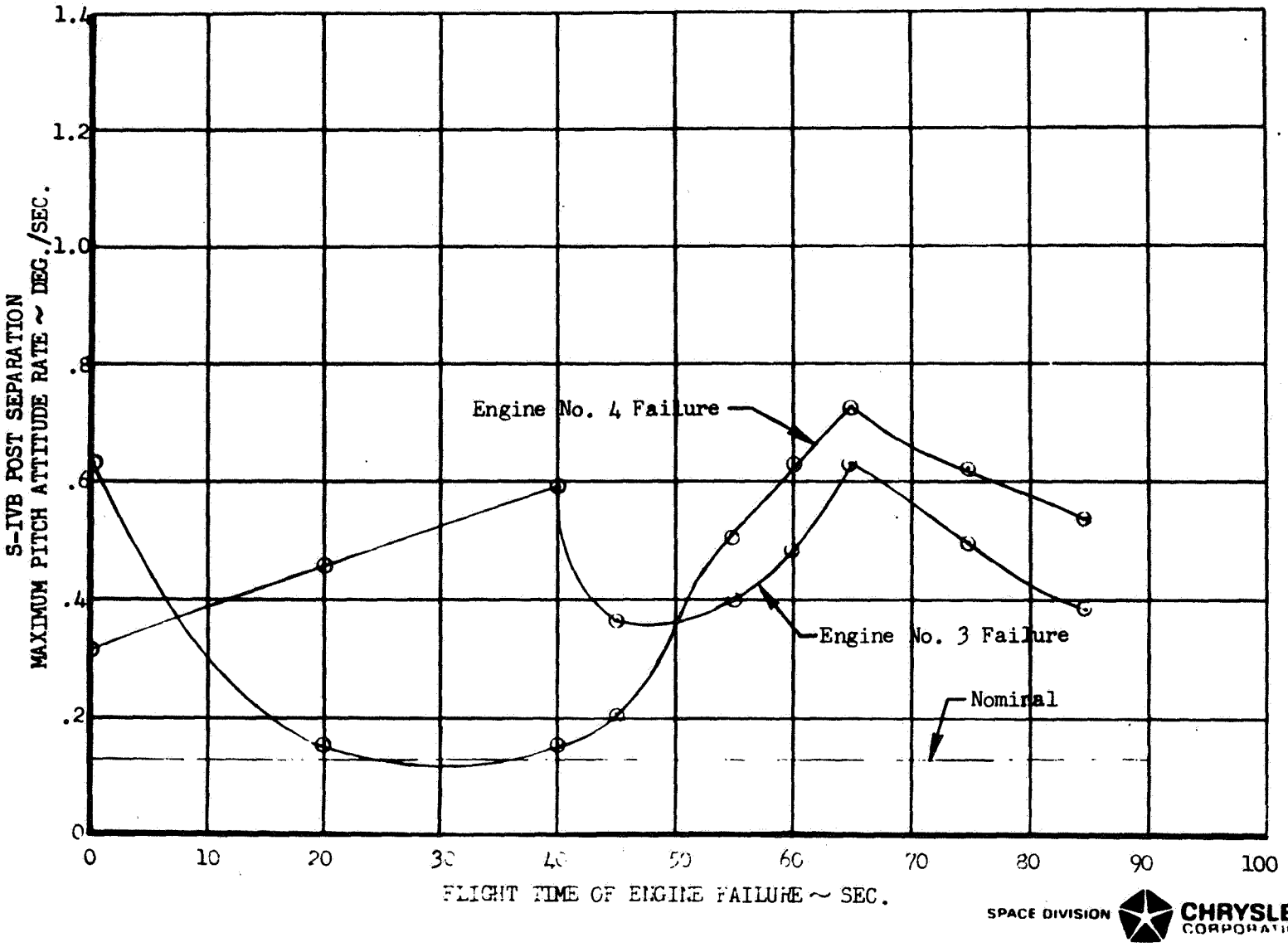

SPACE DIVISION CHRYSLER CORPORATION

FIGURE 55

AS-205/CSM-101 ENVELOPES OF PEAK CONTROL GIMBAL DEFLECTION RESPONSES
TO A SPECTRUM OF 95% DESIGN TAILWINDS AND
50% DESIGN CROSSWINDS FOR ENGINE NO. 4 FAILURES

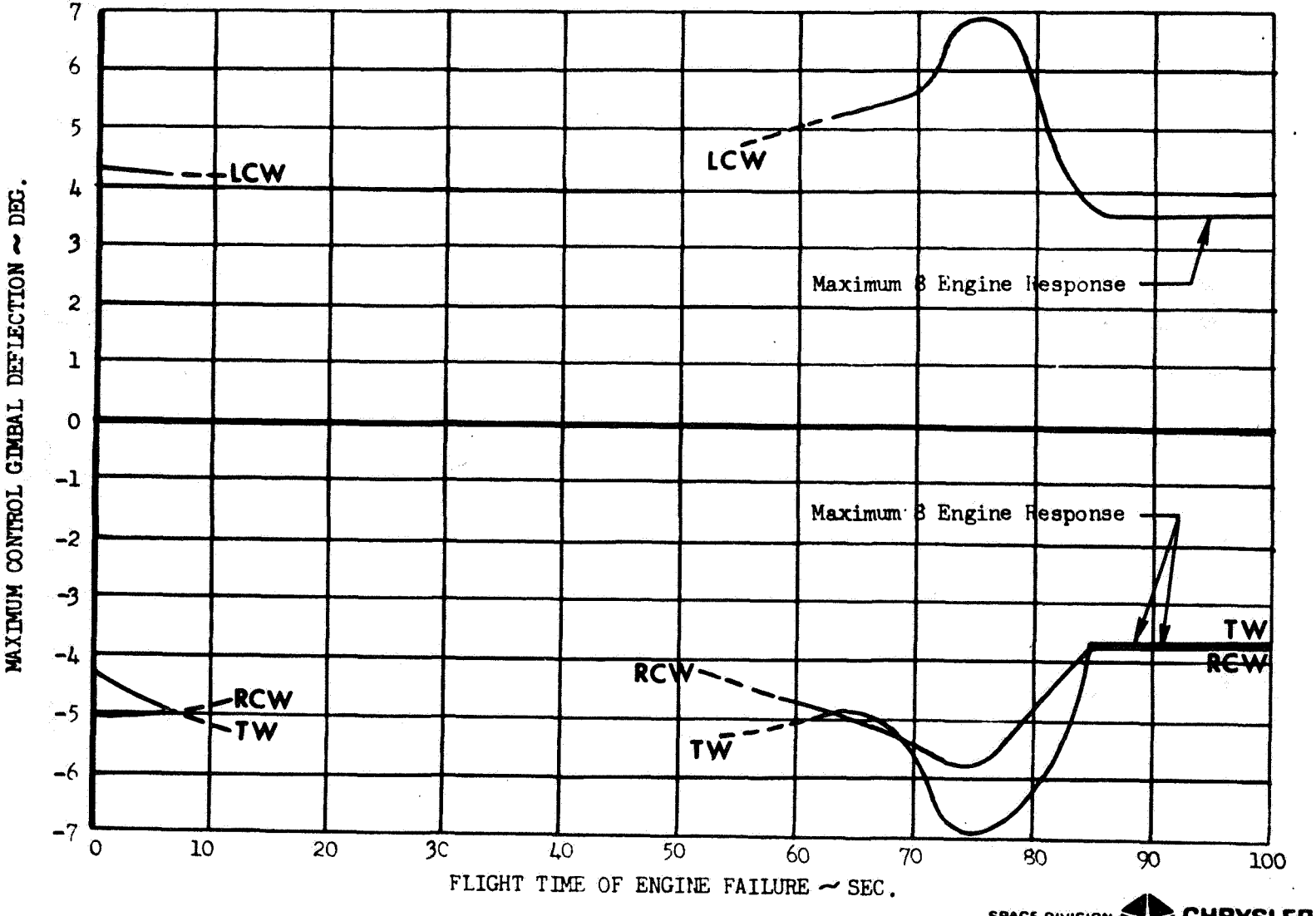

SPACE DIVISION CHRYSLER CORPORATION

FIGURE 56

AS-205/CSM-101 ENVELOPES OF PEAK BENDING MOMENT CRITICAL RATIO RESPONSES (S.F. = 1.40) TO A SPECTRUM OF 95% DESIGN TAILWINDS AND 50% DESIGN CROSSWINDS FOR ENGINE NO. 4 FAILURES

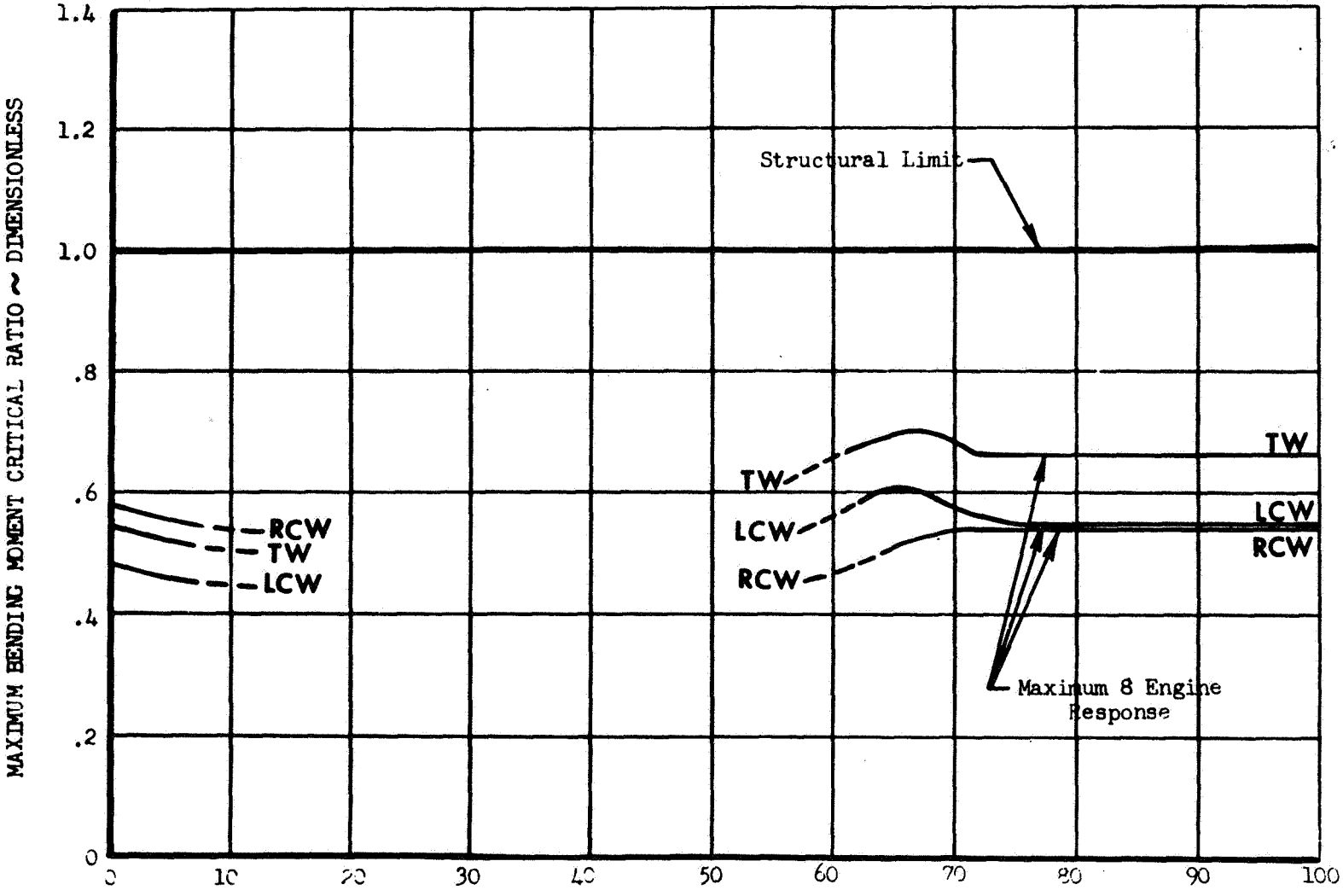

SPACE DIVISION CHRYSLER CORPORATION

FIGURE 57

AS-205/CSM-101 ENVELOPES OF PEAK ROLL ATTITUDE RESPONSES TO A SPECTRUM OF 95% DESIGN TAILWINDS AND 50% DESIGN CROSSWINDS FOR ENGINE NO. 4 FAILURES

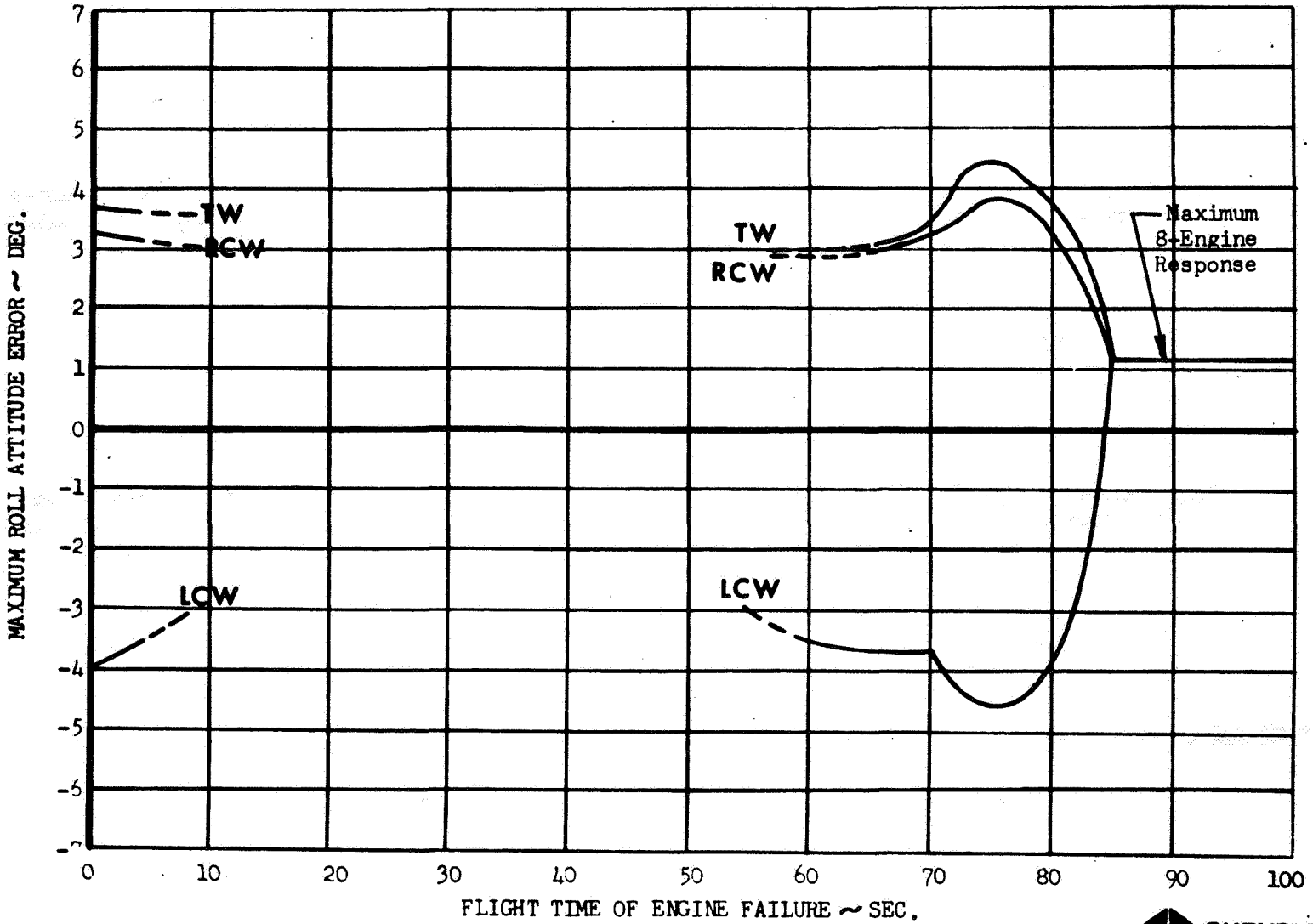

FIGURE 58

AS-205/CSM-101 SEPARATION PLANE CLEARANCE SCHEMATIC

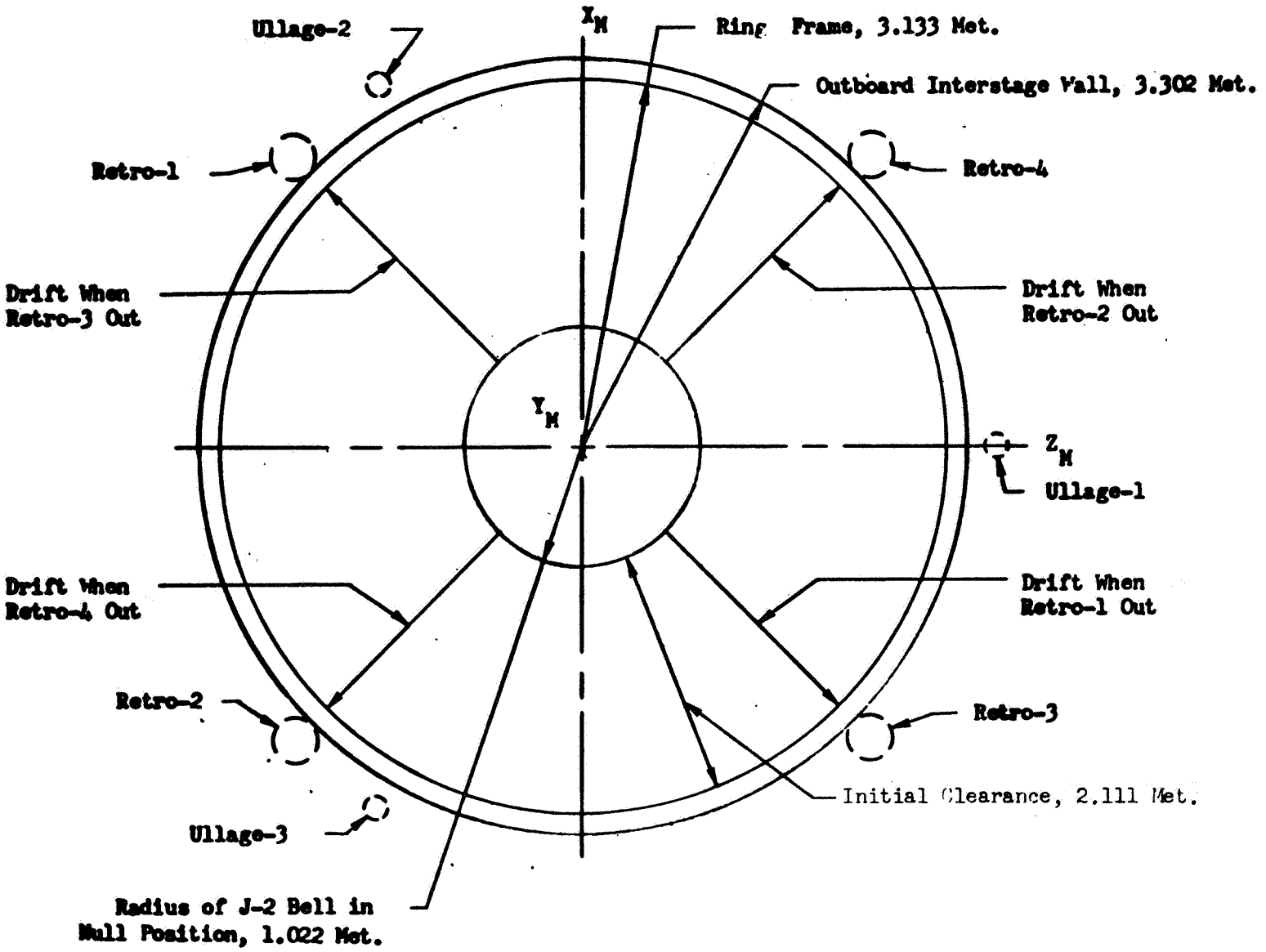

FIGURE 59

AS-205/CSM-101 STAGE SEPARATION SINGLE ENGINE THRUST CURVES

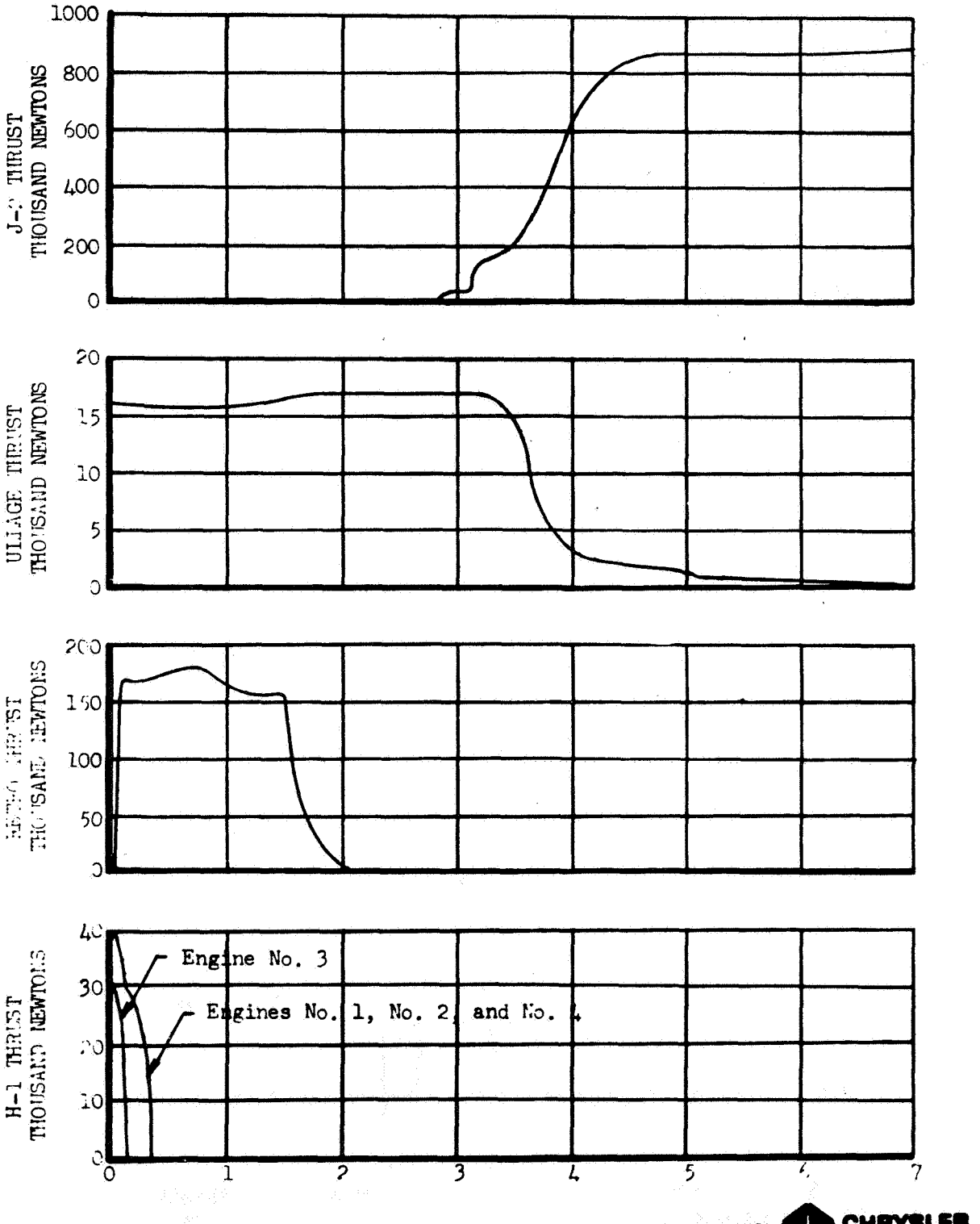

SPACE DIVISION CHRYSLER CORPORATION

TIME FROM SEPARATION STRUCTURE SEVERED ~ SEC.

FIGURE 60

AS-205/CSM-101 STAGE SEPARATION S-IB MOMENT SCHEMATIC

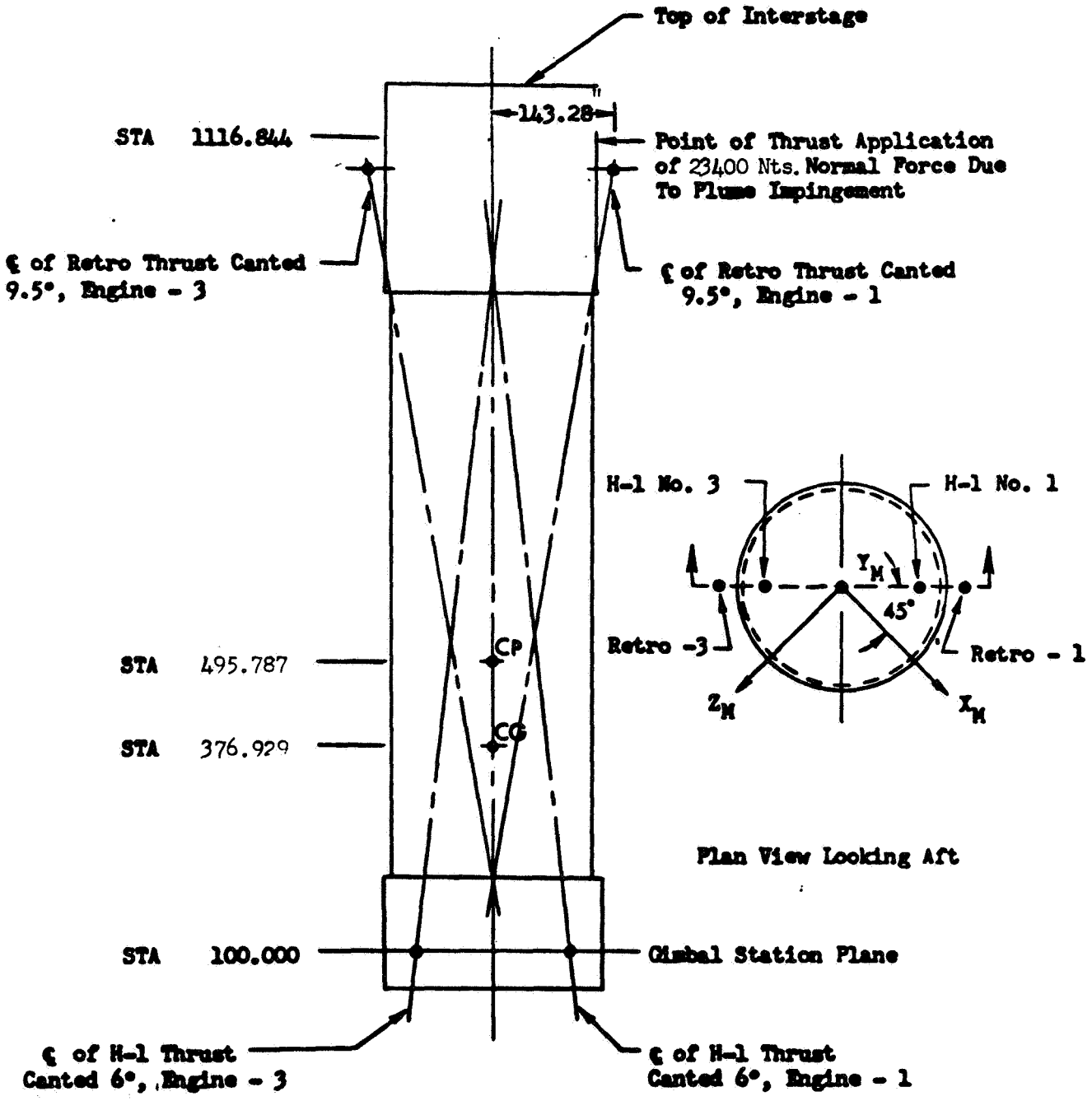

FIGURE 61

AS-205/CSM-101 STAGE SEPARATION S-IVB MOMENT SCHEMATIC

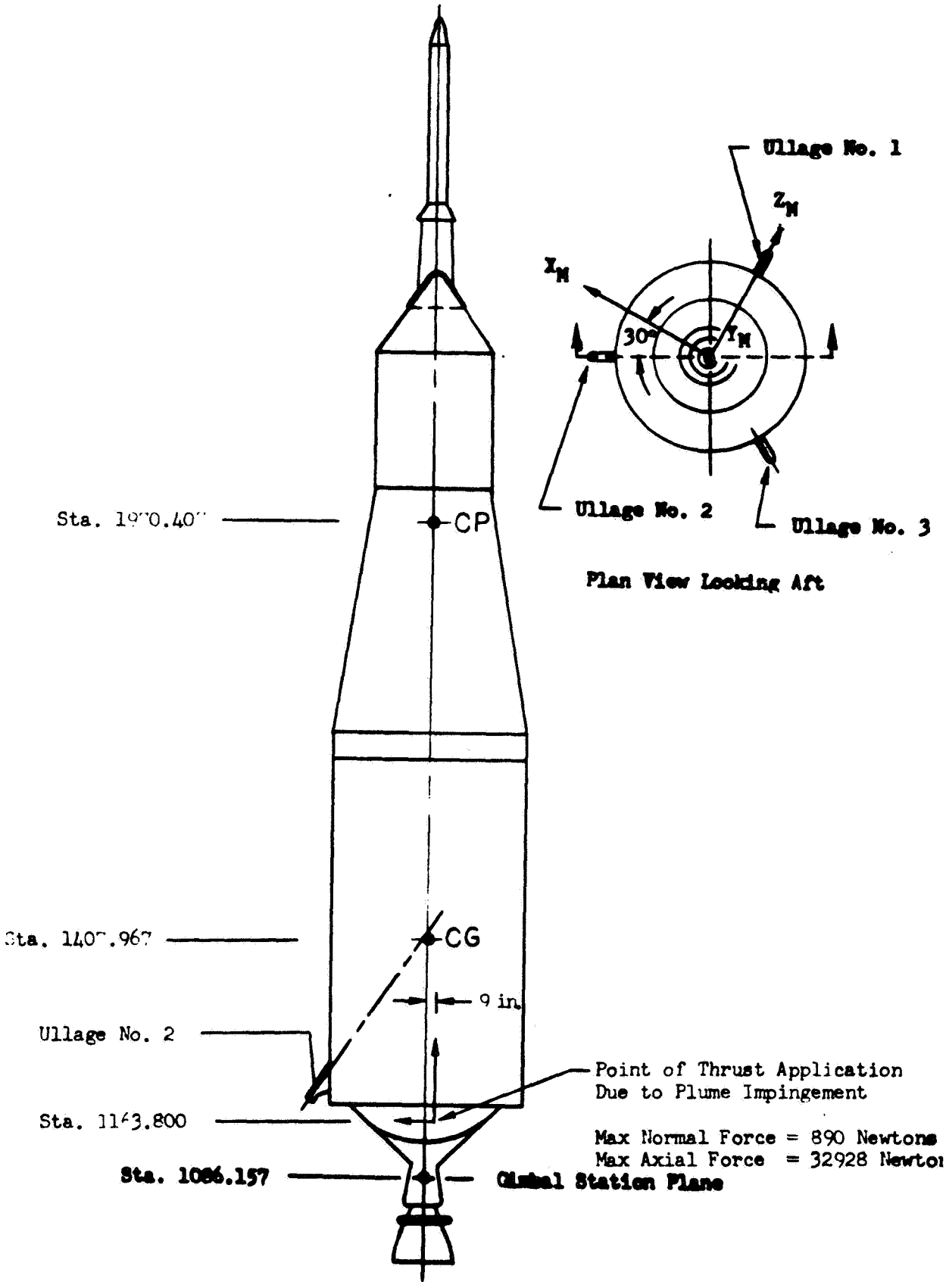

FIGURE 62

AS-205/CSM-101 3σ ENVELOPE OF
S-IVB PITCH ATTITUDE ERROR

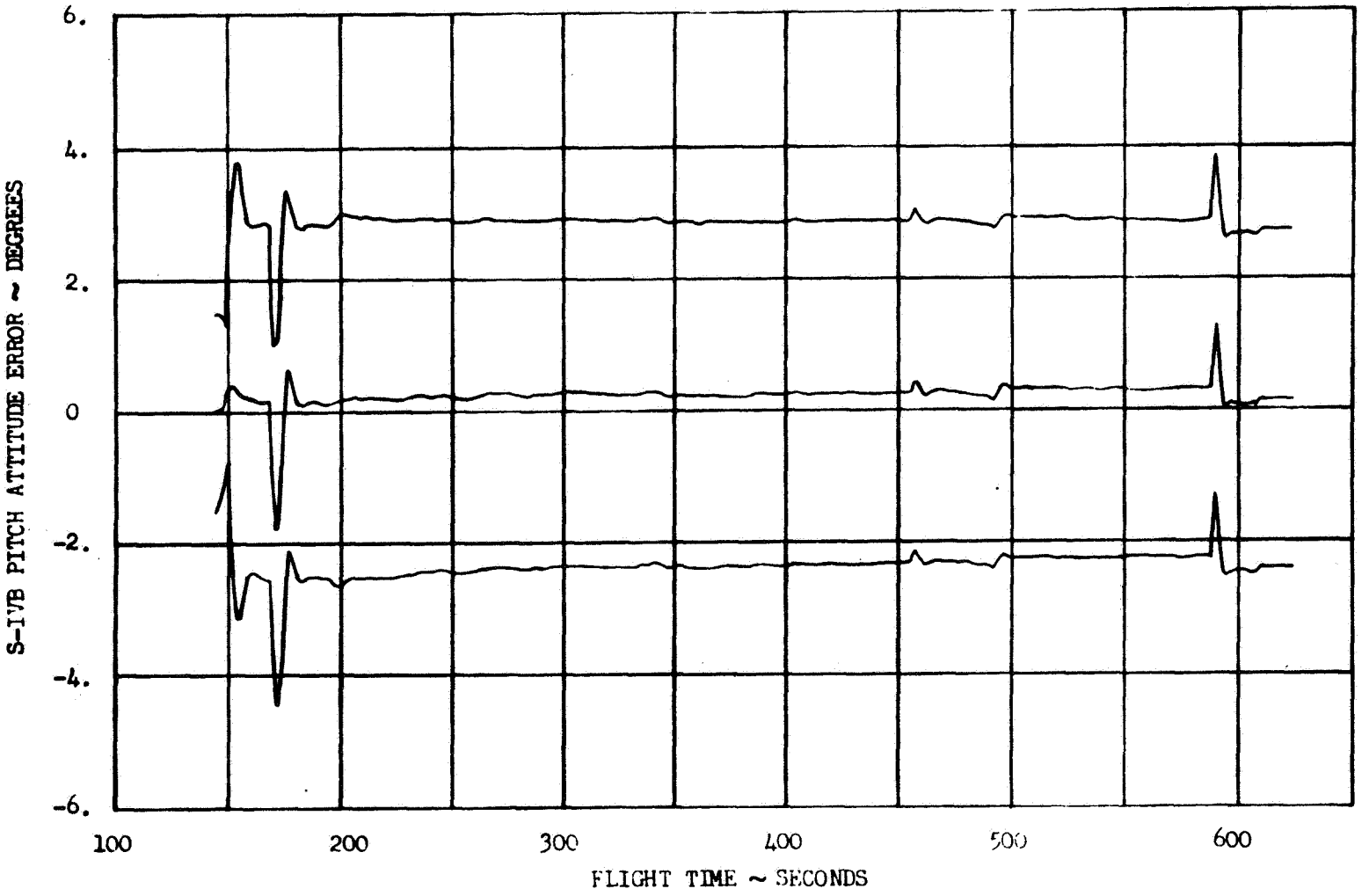

FIGURE 63

AS-205/CSM-101 3σ ENVELOPE OF
S-IVB YAW ATTITUDE ERROR

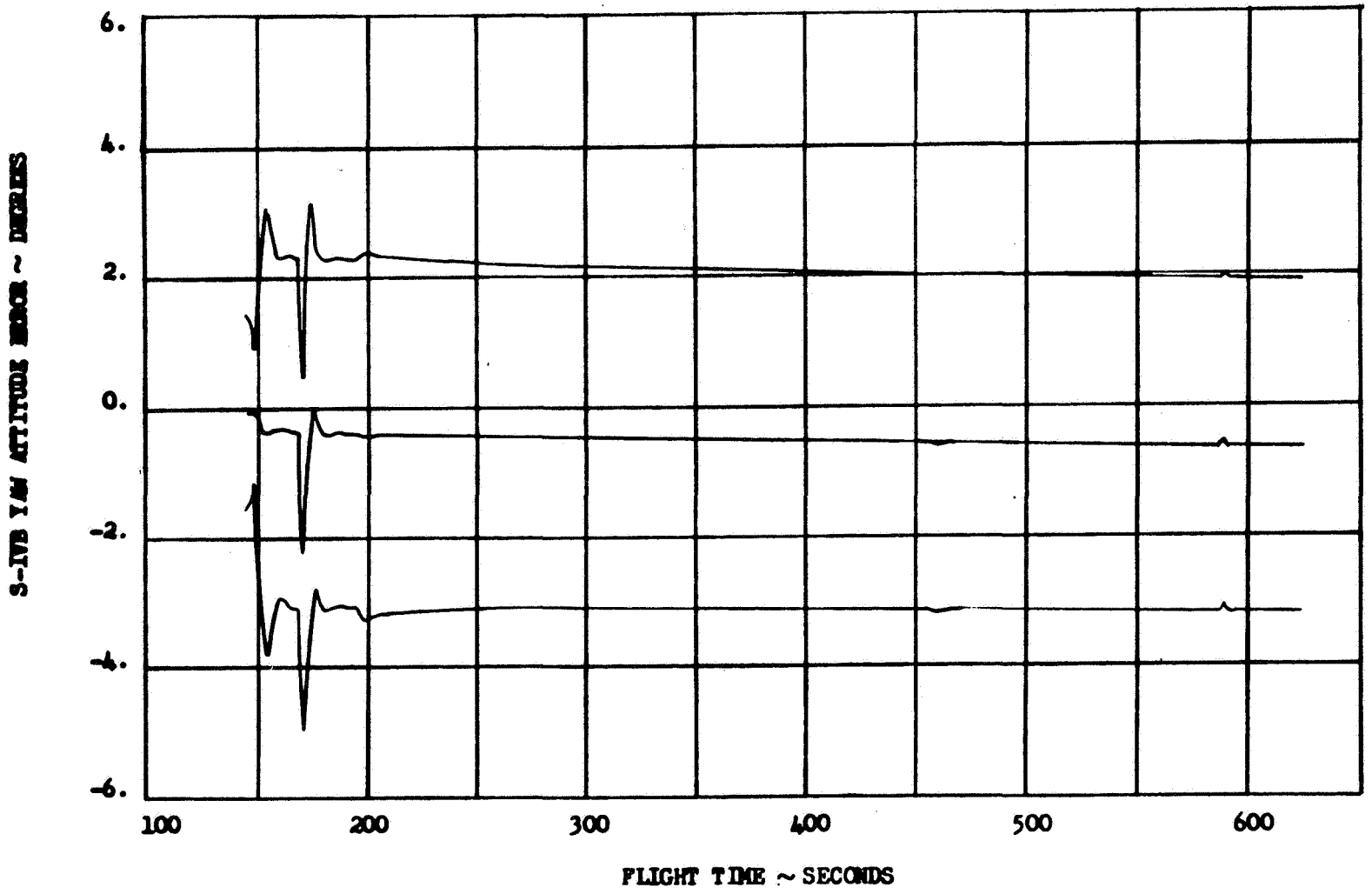

FIGURE 64

AS-205/CSM-101 3σ ENVELOPE OF
S-IVB ROLL ATTITUDE ERROR

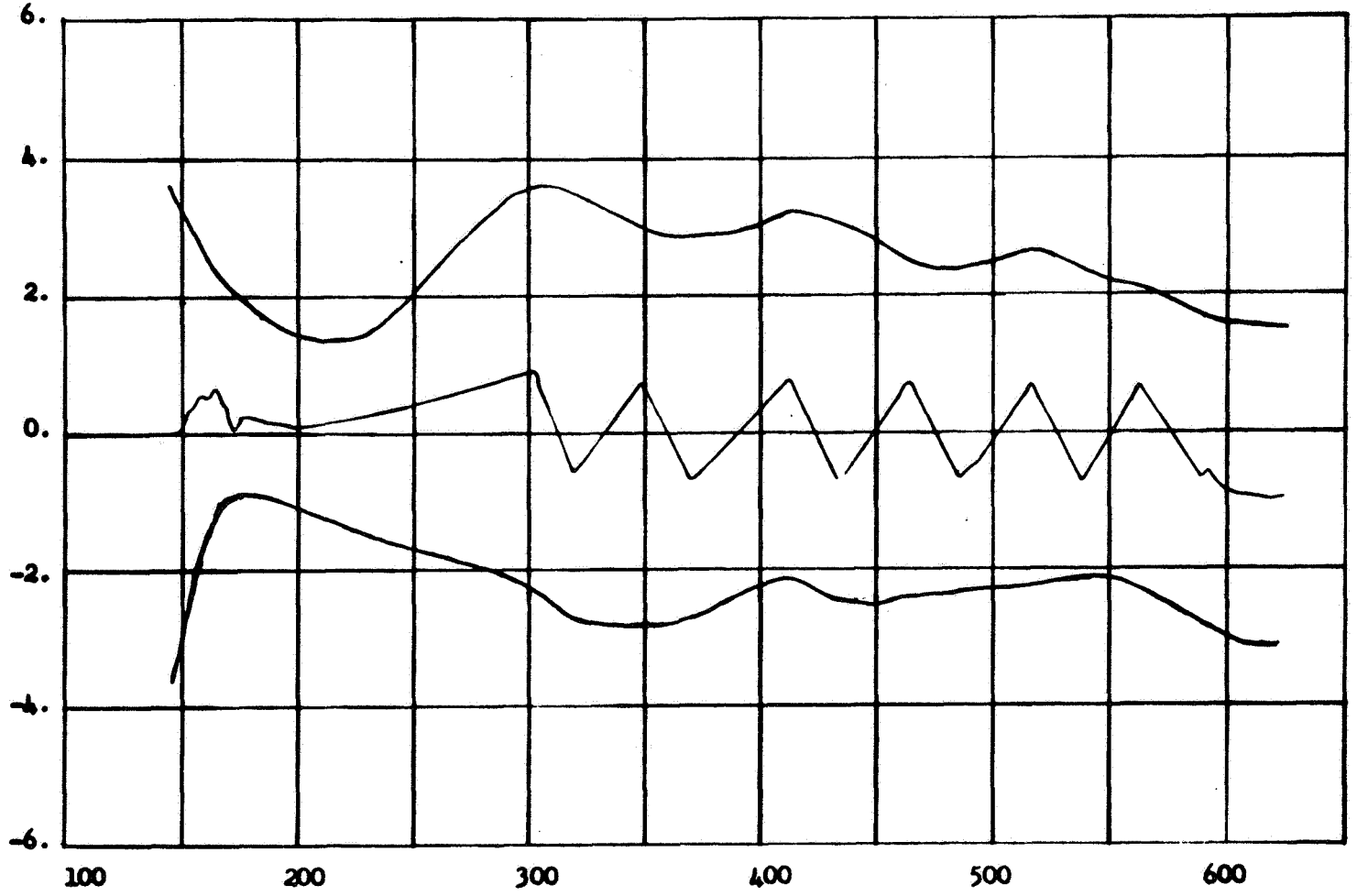

FIGURE 65

AS-205/CSM-101 3σ ENVELOPE OF
S-IVB BODY PITCH RATE

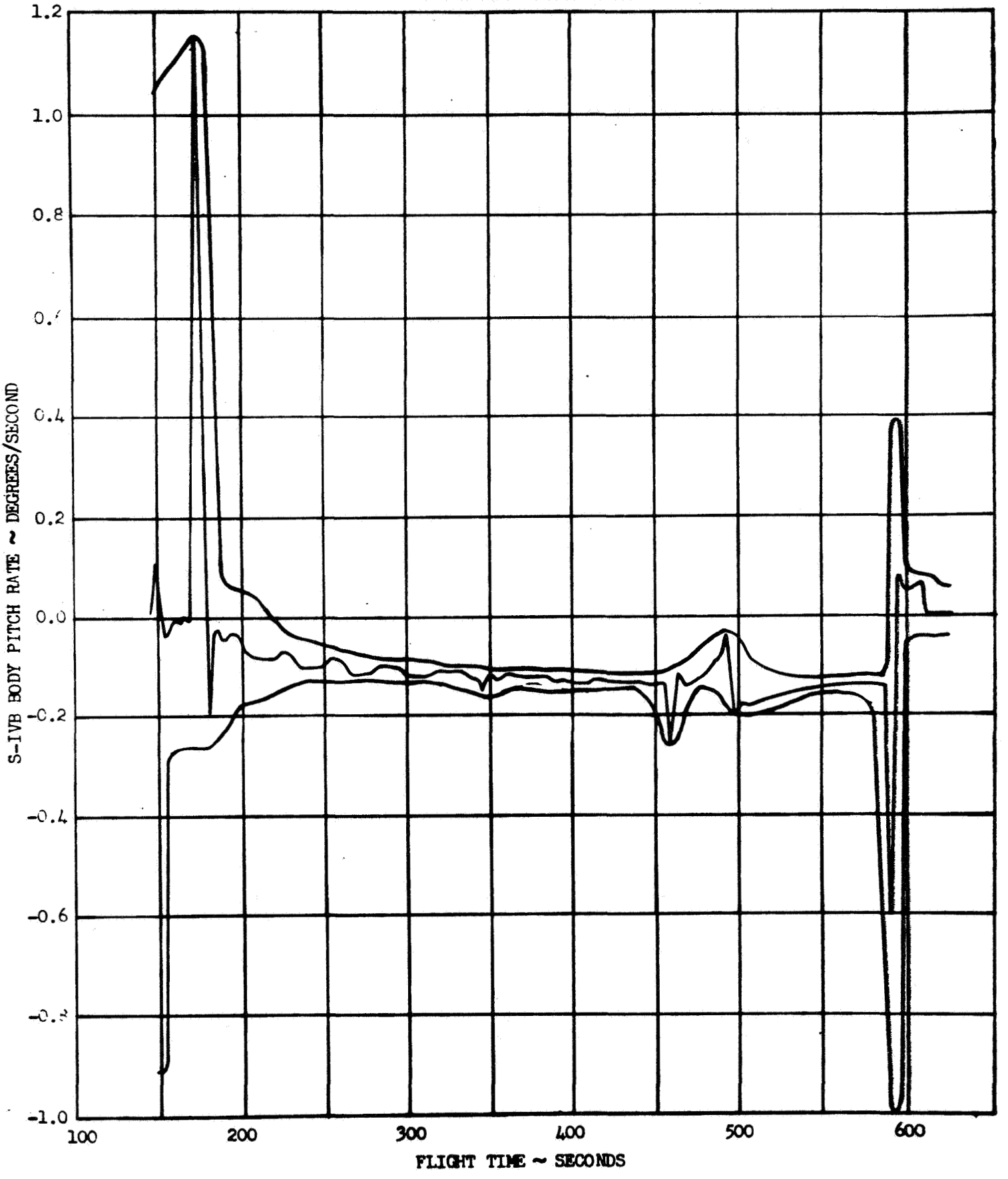

FIGURE 66

AS-205/CSM-101 3σ ENVELOPE OF
S-IVB BODY YAW RATE

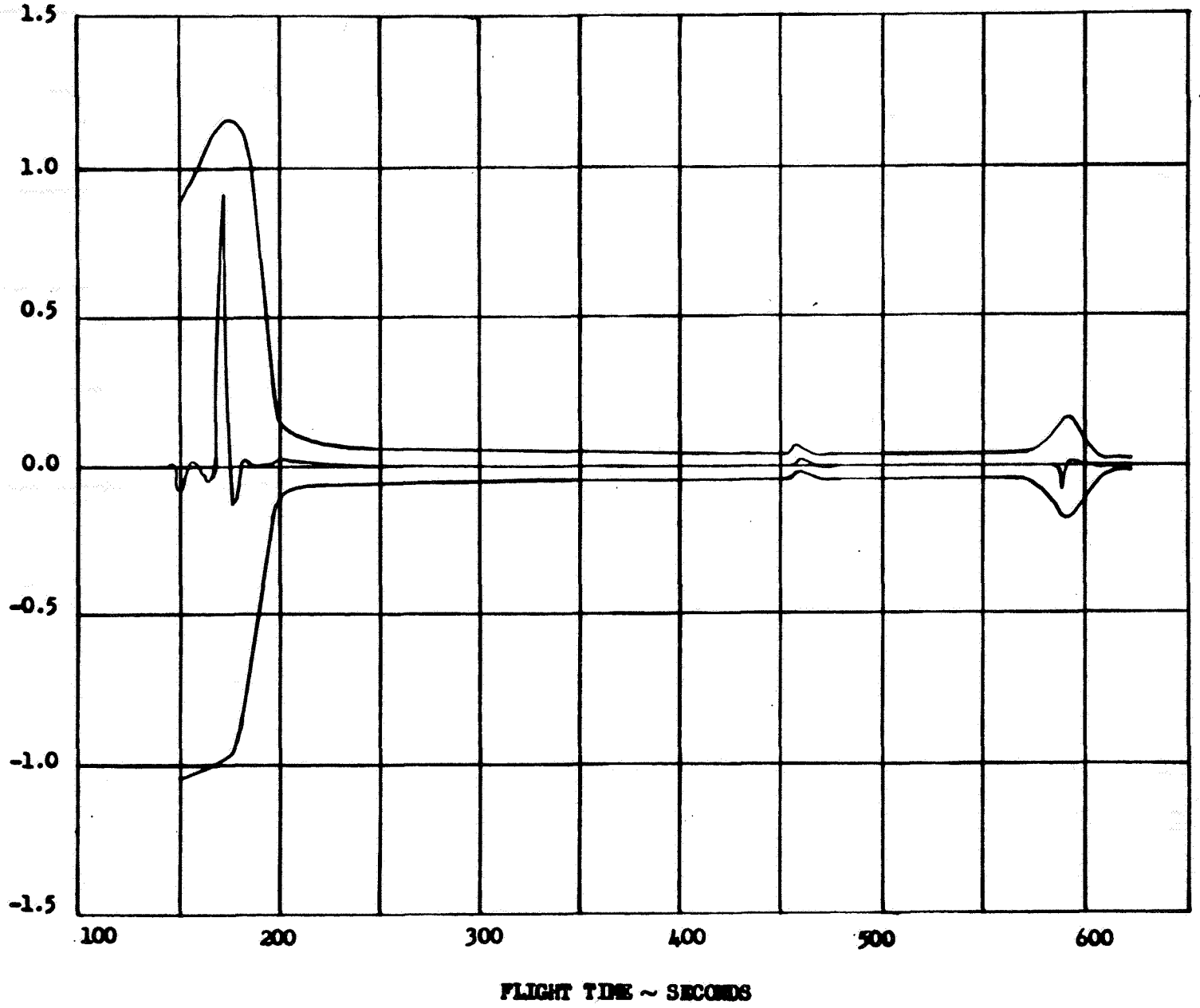

FIGURE 67

AS-205/CSM-101 3σ ENVELOPE OF
S-IVB BODY ROLL RATE

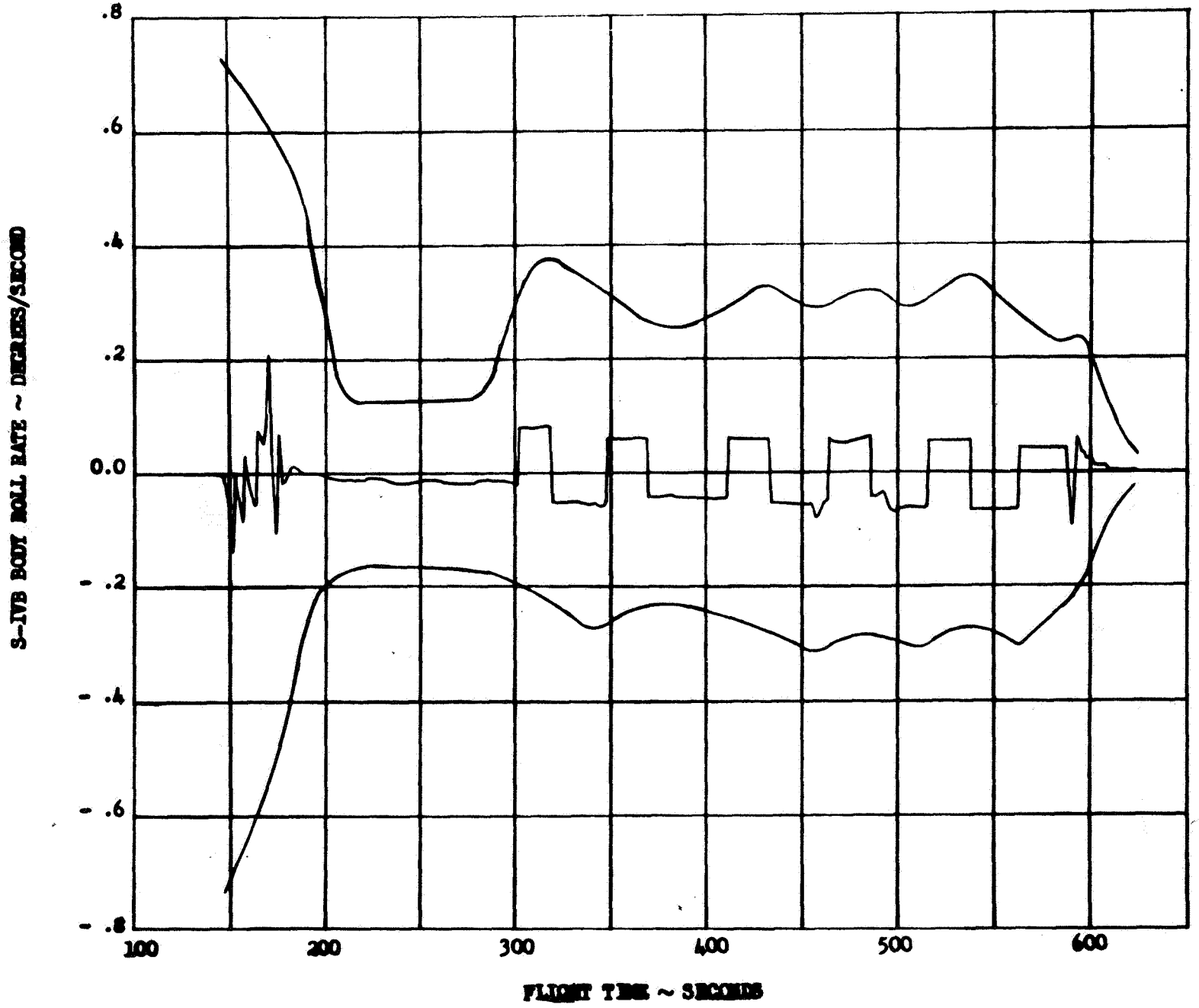

FIGURE 68

AS-205/CSM-101 3σ ENVELOPE OF
J-2 PITCH GIMBAL DEFLECTION

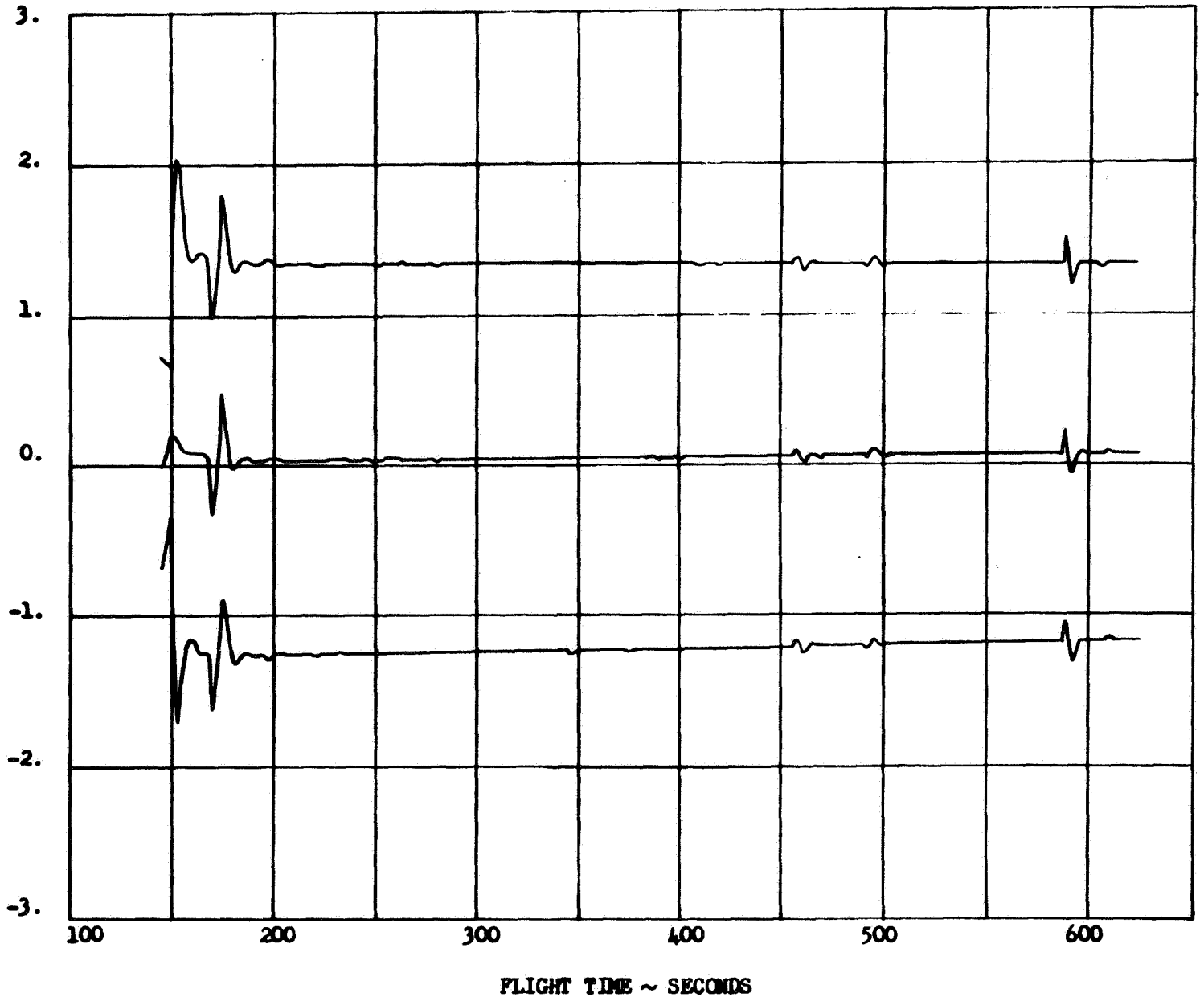

FIGURE 69

AS-205/CSM-101 3σ ENVELOPE OF
J-2 YAW GIMBAL DEFLECTION

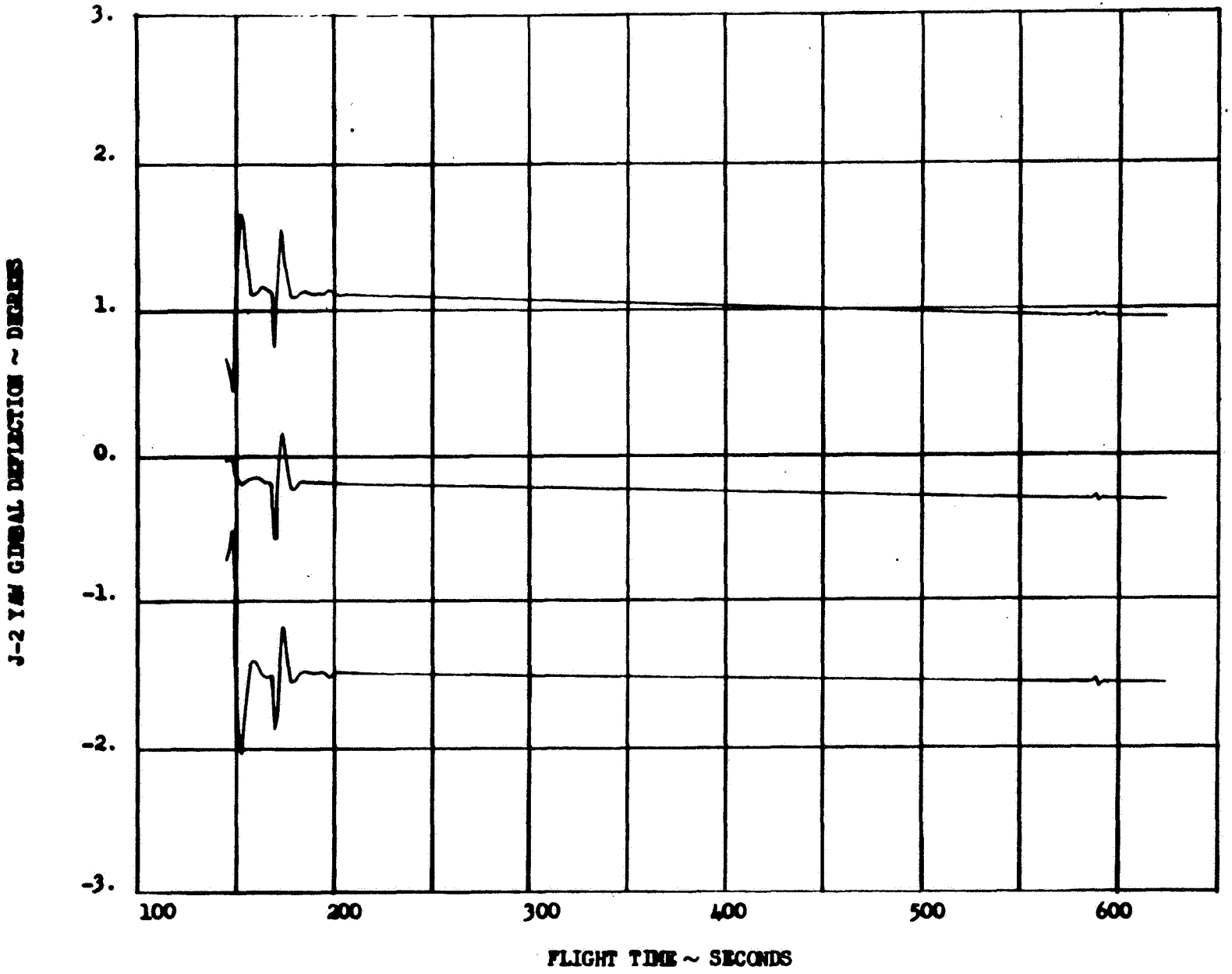

FIGURE 70

AS-205/CSM-101 SEPARATION RELATIVE MOTION
PROFILE VIEW

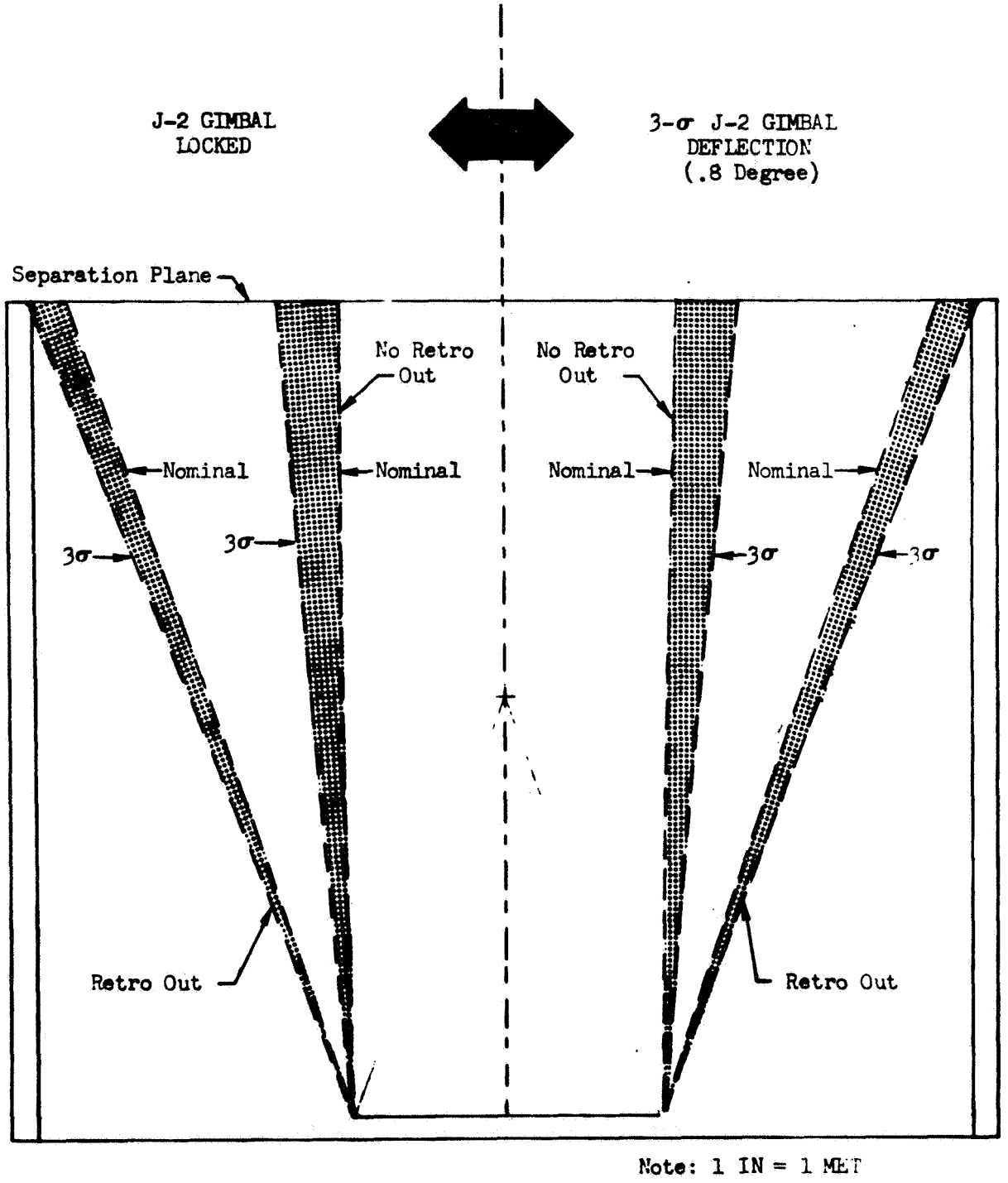

FIGURE 71

S-IVB STAGE ENGINE CONFIGURATION - REAR VIEW

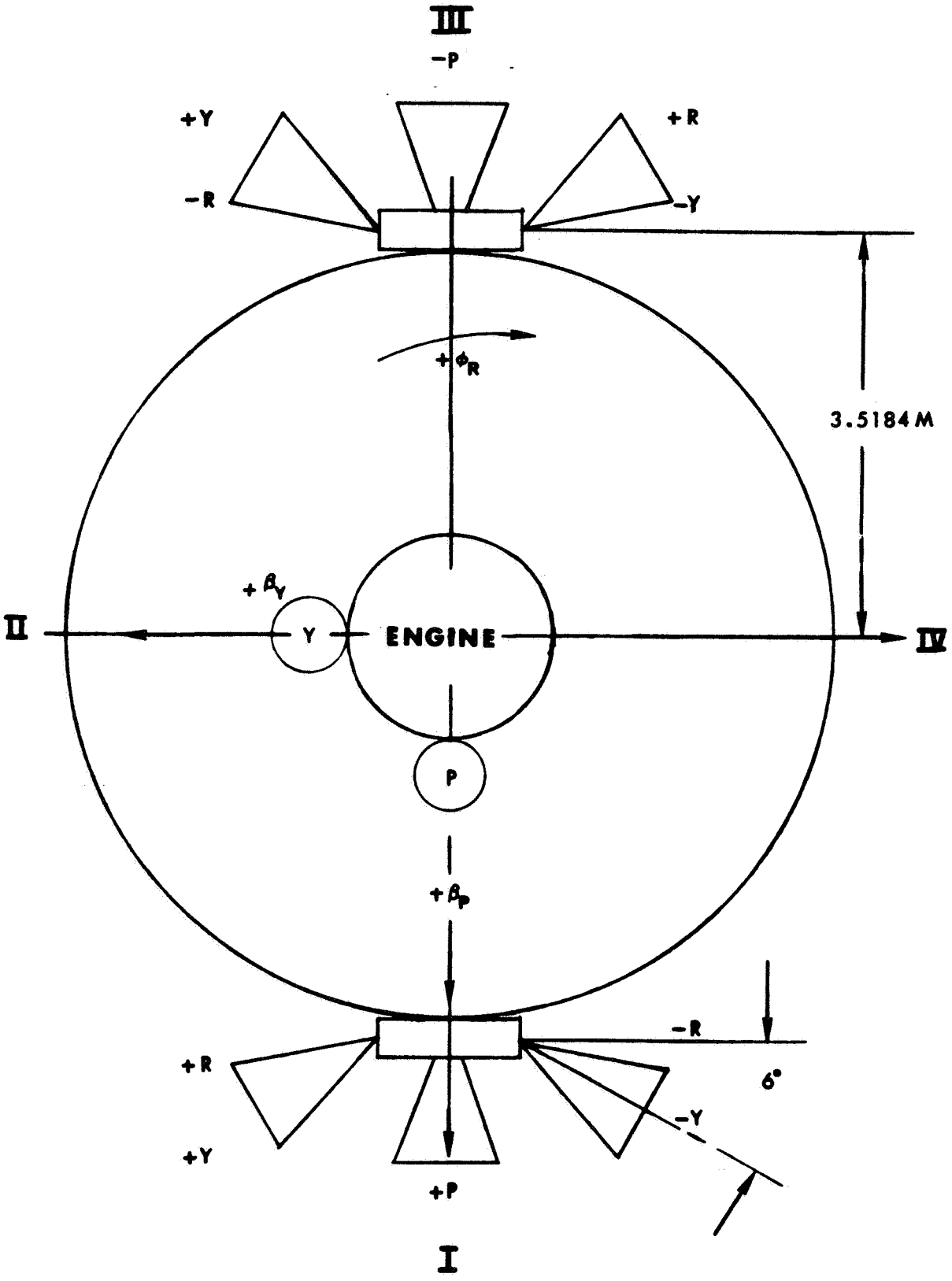

FIGURE 72

AUXILIARY PROPULSION SYSTEM

OPEN LOOP CONTROL SYSTEM BLOCK DIAGRAM

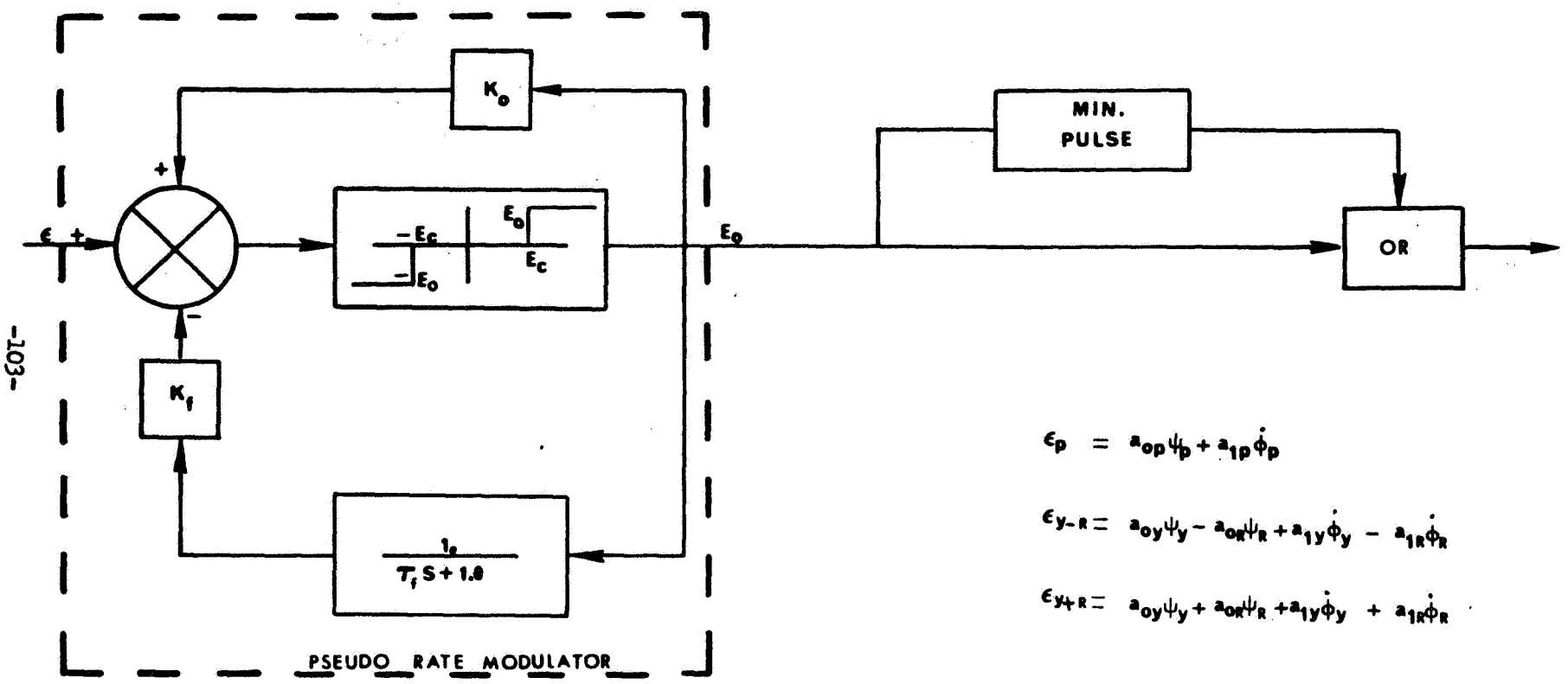

$$\epsilon_p = a_{op}\psi_p + a_{1p}\dot{\phi}_p$$

$$\epsilon_{y-R} = a_{oy}\psi_y - a_{oR}\psi_R + a_{1y}\dot{\phi}_y - a_{1R}\dot{\phi}_R$$

$$\epsilon_{y+R} = a_{oy}\psi_y + a_{oR}\psi_R + a_{1y}\dot{\phi}_y + a_{1R}\dot{\phi}_R$$

SPACE DIVISION CHRYSLER CORPORATION

FIGURE 73

AS-205/CSM-101 ORBITAL ATTITUDE TIMELINES

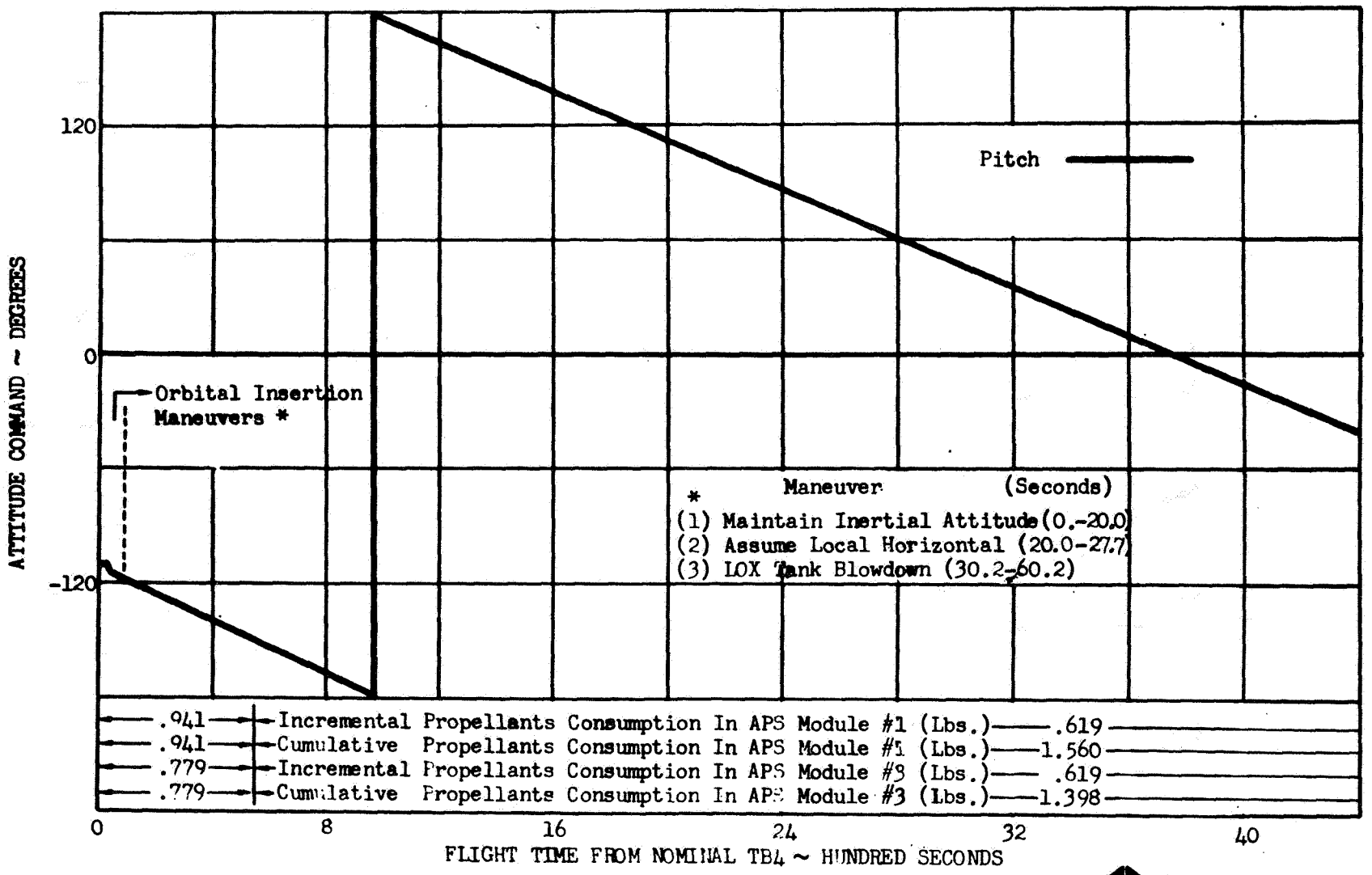

FIGURE 73 (CONT'D.)

AS-205/CSM-101 ORBITAL ATTITUDE TIMELINES

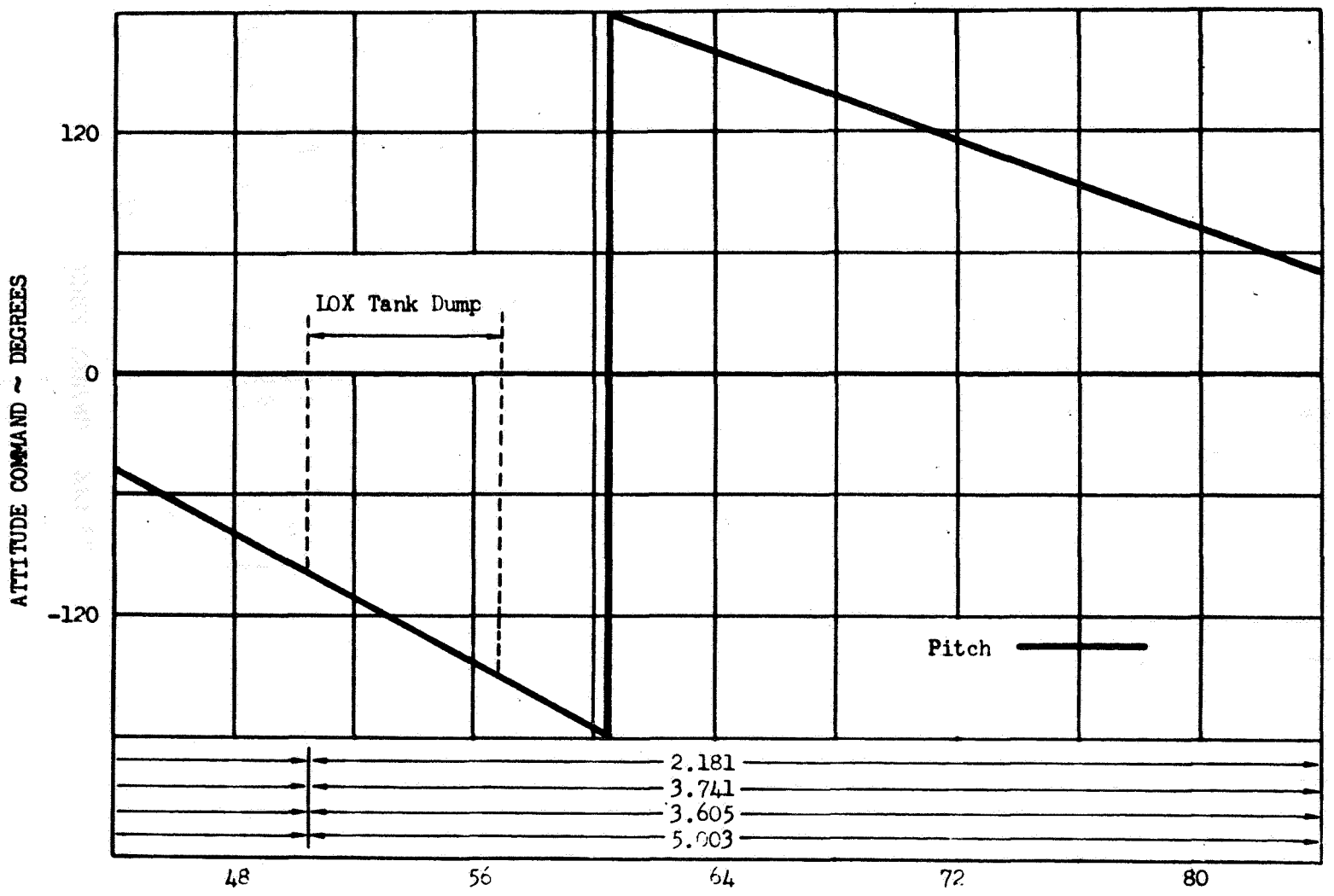

SPACE DIVISION CHRYSLER CORPORATION

FIGURE 73 (CONT'D.)

AS-205/CSM-101 ORBITAL ATTITUDE TIMELINES

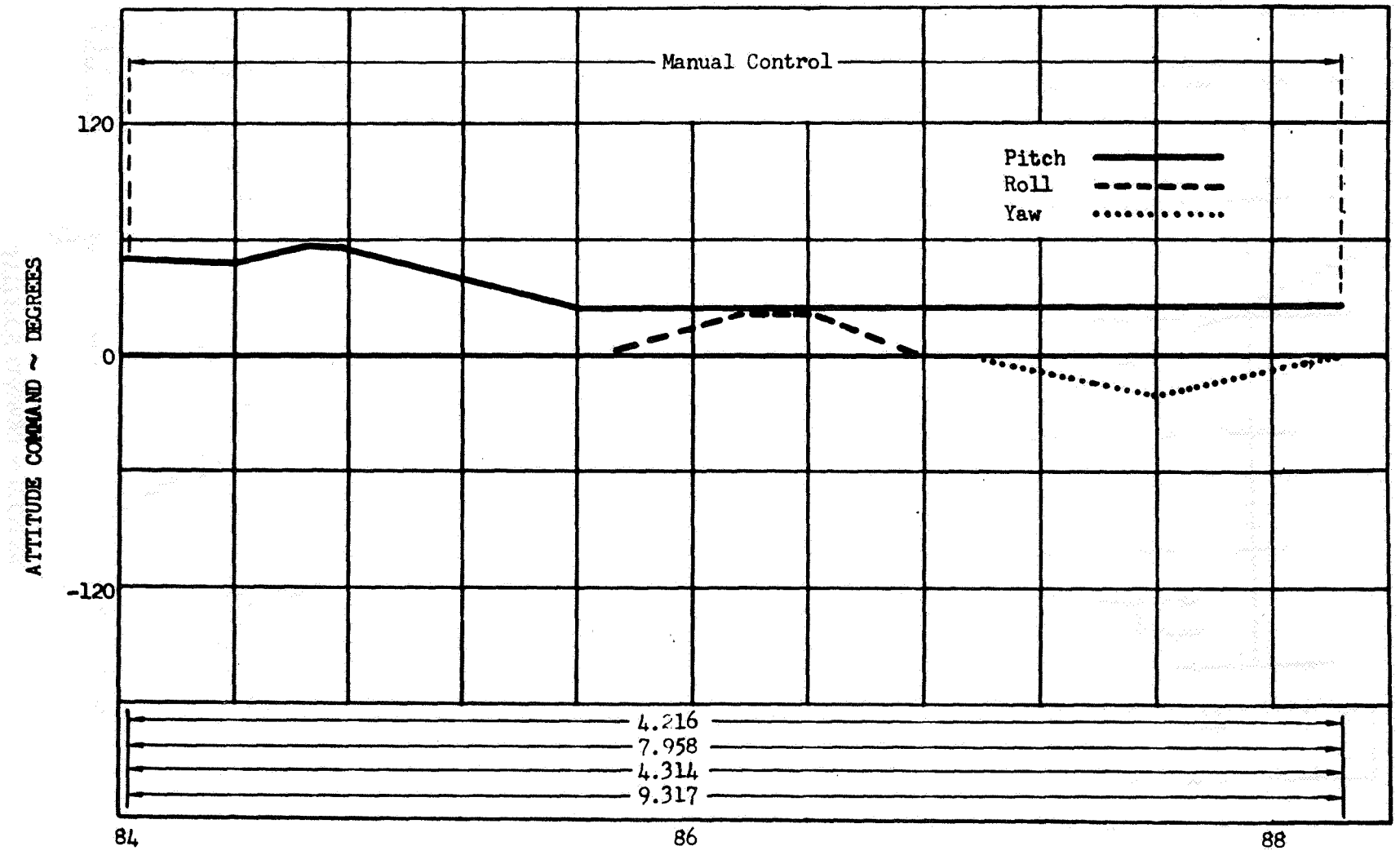

FIGURE 73 (CONT'D.)

AS-205/CSM-101 ORBITAL ATTITUDE TIMELINES

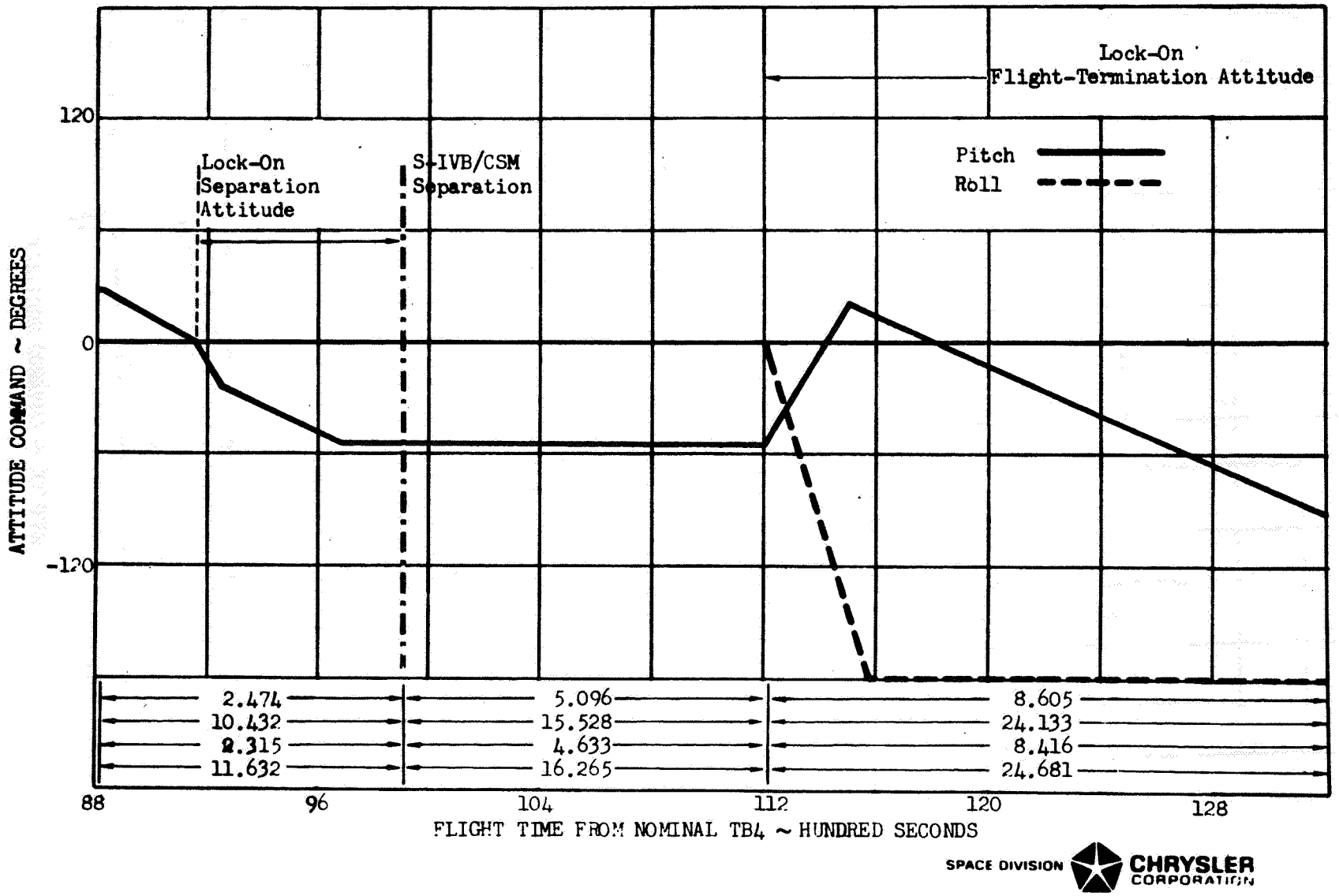

SPACE DIVISION CHRYSLER CORPORATION

FIGURE 74

AS-205/CSM-101 ORBITAL PROPELLANT DUMP J-2 THRUST

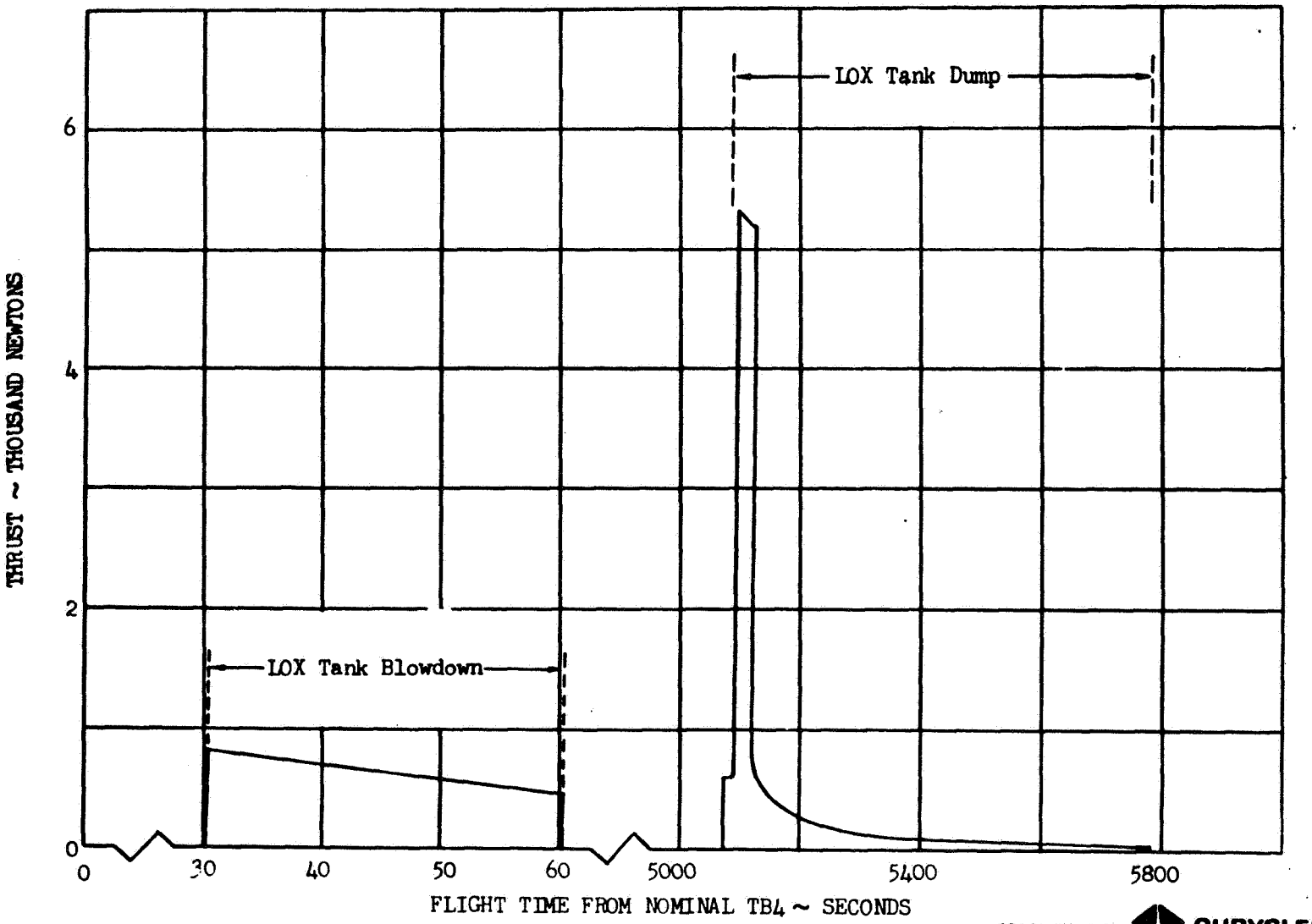

TABLE 1

AS-205/CSM-101 LIFTOFF SUMMARY
UMBILICAL TOWER

OBSTRUCTION	TIME REQUIRED TO CLEAR OBSTRUCTION (SEC)	DRIFT PER UNIT CG OFFSET (MET/MET)	DRIFT PER UNIT COMPOSITE THRUST MISALIGNMENT (MET/DEG)	DRIFT PER UNIT COMPOSITE CONTROL DEFLECTION ERROR (MET/DEG)
Apollo Access Arm Platform	6.80	30.43	4.04	2.023
Tower Top	7.05	33.05	4.47	2.235
Lightning Mast Top	7.95	43.84	6.22	3.108

OBSTRUCTION	INITIAL AVAILABLE CLEARANCE (MET)	FINAL AVAILABLE CLEARANCE (MET)		MINIMUM % OF INITIAL CLEARANCE (%)	
		95% QSS DESIGN WINDS	3σ NOV WINDS	95% QSS DESIGN WINDS	3σ NOV WINDS
Apollo Access Arm Platform	5.40	1.64	1.20	30.60	22.39
Tower Top	6.31	2.17	1.68	34.39	26.62
Lightning Mast Top	9.96	4.43	3.92	44.48	39.36
Apollo Access Arm Platform (With Camera)	5.06	1.33	0.79	26.28	15.61

TABLE 2

AS-205/CSM-101 LIFTOFF SUMMARY
GROUND SUPPORT EQUIPMENT

OBSTRUCTION	TIME REQUIRED TO CLEAR OBSTRUCTION (SEC)	DRIFT PER UNIT CG OFFSET (MET/MET)	DRIFT PER UNIT COMPOSITE THRUST MISALIGNMENT (MET/DEG)	DRIFT PER UNIT COMPOSITE CONTROL DEFLECTION FRROR (MET/DEG)
Fuel Fill Mast	1.15	0.3602	0.2404	0.1203
Lox Fill Mast	1.10	0.3543	0.2270	0.1134
Short Cable Mast II	0.80	0.2697	0.1430	0.0716
Short Cable Mast IV	0.80	0.2697	0.1430	0.0716

OBSTRUCTION	INITIAL AVAILABLE CLEARANCE (CM)	FINAL AVAILABLE CLEARANCE (CM)		MINIMUM % OF INITIAL CLEARANCE (%)	
		95% QSS DESIGN WINDS	3σ NOV WINDS	95% QSS DESIGN WINDS	3σ NOV WINDS
Fuel Fill Mast	130	120.1	119.7	92.38	92.08
Lox Fill Mast	120	111.0	111.0	92.50	92.50
Short Cable Mast II	79	73.7	73.7	93.29	93.29
Short Cable Mast IV	79	73.7	72.5	93.29	91.77

TABLE 3

H-1 ENGINE THRUST MISALIGNMENT
DUE TO VEHICLE ELECTRICAL & MECHANICAL TOLERANCES

	CONTRIBUTOR		(Deg.) CONTROL	FIXED
	Electrical Nulls			
1.	P & Y	.1°	.16	---
2.	Rate Gyro P & Y	.125°/d	.21	---
3.	Servo Amp	.6 MA	.075	---
4.	Servo Valve	.6 MA	.075	---
5.	Actuator Pot	178. MV	.069	---
	Mechanical Misalignment			
6.	Pad to First Ref. Plane P & Y	6'	.16	---
7.	S-IB S-IVB P & Y	6'	.16	---
8.	S-IVB IU P & Y	6'	.1	---
9.	IU Platform P & Y	15'	.3	---
	Undetectable Bias			
10.	Unsymetrical Engine Thrust	45'	.530	.530
11.	Engine to S-IB Ref. Plane	30'	.500	.500
12.	Actuator Tie Points	30'	.500	---

TABLE 4

SEQUENCE OF EVENTS

NOMINAL FLIGHT TIME (SEC.)	PROGRAM TIME (SEC.)	EVENT
- 5.00	---	Guidance Reference Release (GRR).
- 3.10	---	Initiate S-IB Mainstage. Ignition Sequence.
0.00	---	First Motion.
0.20	$(0.0)_1$	Lift-off Signal; Initiate. Time Base 1.
10.20	$(10.0)_1$	Initiate Pitch and Roll Maneuvers.
75.00	---	Maximum Dynamic Pressure.
100.20	$(100.0)_1$	Control Gain Switch Point.
120.20	$(120.0)_1$	Control Gain Switch Point.
133.41	$(133.71)_1$	Enable S-IB Propellant Level Sensors.
134.50	$(134.3)_1$	Tilt Arrest.
136.91	$(0.0)_2$	Level Sensor Activation.
		Initiate Time Base 2.
140.11	$(3.2)_2$	Inboard Engine Cutoff (IECØ).
143.11	$(0.0)_3$	Outboard Engine Cutoff (ØECØ).
		Initiate Time Base 3.
144.21	---	Ullage 90% Buildup.
144.41	$(1.3)_3$	Separation Signal.
144.49	---	S-IB/S-IVB Separation Structure Severed.
144.54	---	Retro 10% Buildup.
		S-IB/S-IVB Separation First Motion.

TABLE 4 (CONT'D.)

SEQUENCE OF EVENTS

NOMINAL FLIGHT TIME (SEC.)	PROGRAM TIME (SEC.)	EVENT
144.57	---	Retro 90% Buildup.
144.61	$(1.5)_3$	S-IVB Roll Control and J-2 Gimbal Activation.
144.87	---	H-1 100% Decayed.
145.42	---	Ungimballed J-2 Bell Clears Top of Interstage (Nominal).
145.56	---	Ungimballed J-2 Bell Clears Top of Interstage (One Retro Out).
145.81	$(2.7)_3$	J-2 Engine Start Command.
148.16	---	Ullage Burnout.
149.41	---	90% J-2 Thrust Level.
151.81	$(8.7)_3$	P.U. Mixture Ratio 5.5 On.
156.41	$(13.3)_3$	Jettison Ullage Rocket Motors.
163.11	---	Jettison Launch Escape Tower.
168.25	$(25.14)_3$	Command [illegible] Initiation.
343.11	$(200.0)_3$	Control Gain Switch Point.
454.41	$(311.3)_3$	P.U. Mixture Ratio 5.5 Off
454.61	$(311.5)_3$	P.U. Mixture Ratio 4.5 On
614.63	---	Guidance Cutoff Signal (GCS).
614.83	$(0.0)_4$	Initiate Time Base 4.
617.03	$(2.2)_4$	P.U. Mixture Ratio 4.5 Off.
		Maintain Cutoff Inertial Attitude for 20 Seconds from TB4.
624.63	$(9.8)_4$	Orbital Insertion.
634.83	$(20.0)_4$	Initiate Maneuver to Align the S-IVB/CSM Along the Local Horizontal (CSM Forward, Position I Down) and Maintain with Respect to Local Reference.

TABLE 4 (CONT'D.)

SEQUENCE OF EVENTS

NOMINAL FLIGHT TIME (SEC.)	PROGRAM TIME (SEC.)	EVENT
645.03	$(30.2)_4$	Initiate LOX Tank Blowdown.
675.03	$(60.2)_4$	End LOX Tank Blowdown.
5666.83	$(5052.0)_4$	Initiate LOX Tank Dump.
6387.83	$(5773.0)_4$	End LOX Tank Dump.
9021.0	$(8406.17)_4$	Begin Manual Control of S-IVB Attitude from the Spacecraft. Maneuver in Roll, Pitch, and Yaw will be based on Maximum Commandable Rates of 0.3°/Second in Pitch and Yaw, and 0.5°/Second in Roll.**
9441.0	$(8826.17)_4$	End Manual Control of S-IVB Attitude from Spacecraft. The I.U. will return to Programmed Timeline whenever the Spacecraft Relinquishes Attitude Control.
9801.0	$(9186.17)_4$	Initiate Maneuver to Pitch Nose Down 20° from the Local Horizontal (Position I Down) and Maintain Orbital Rate.
10296.0	$(9681.17)_4$	Initiate Inertial Attitude Hold Using Platform Gimbal Angles at the Specified Initiation Time. Maintain Inertial Attitude.
10521.0	$(9906.17)_4$	Nominal CSM Physical Separation.
11841.0	$(11226.17)_4$	Initiate Maneuver to Align the S-IVB/IU Along the Local Horizontal, Tail Leading and Roll to Position I up. Maintain Orbital Rate.
16814.83	$(16200.)_4$	End of S-IVB/IU Lifetime.

** Maneuvers which are planned to be exercised during manual control of the S-IVB stage, are defined in Table 10.

TABLE 5
. WIND RESPONSE DISPERSIONS FOR AS-205/CSM-101
NON-WIND BIASED TRAJECTORY

75% DESIGN HEADWIND

TIME (Sec)	ALTITUDE (Km)	WIND SPEED (M/Sec)	α_{ss} (Deg)	ΔSHEAR (Deg)	ΔGUSTS (Deg)	$\Delta C_1, C_2$ (Deg)
56.0	6	37.9	2.92	2.03	1.56	.05
63.0	8	47.4	2.69	1.93	1.23	.03
69.2	10	57.0	2.42	2.08	1.02	.02
72.0	11	57.0	1.83	2.39	.97	-.04
75.2	12	57.0	1.71	2.19	.98	.10
77.7	13	57.0	1.62	2.13	.88	.09
79.7	14	57.0	1.46	2.19	.78	.02

TIME (Sec)	ALTITUDE (Km)	WIND SPEED (M/Sec)	β_{ss} (Deg)	ΔSHEAR (Deg)	ΔGUSTS (Deg)	$\Delta C_1, C_2$ (Deg)
56.8	6	37.9	.24	.21	.38	1.52
64.0	8	47.4	1.11	.43	.71	1.56
70.0	10	57.0	1.20	1.52	1.08	1.42
72.9	11	57.0	0.98	2.21	1.17	1.35
75.5	12	57.0	1.19	2.39	1.19	1.29
78.0	13	57.0	1.30	2.32	1.08	1.15
80.3	14	57.0	1.14	2.26	.88	.98

95% DESIGN HEADWIND

TIME (Sec)	ALTITUDE (Km)	WIND SPEED (M/Sec)	α_{ss} (Deg)	ΔSHEAR (Deg)	ΔGUSTS (Deg)	$\Delta C_1, C_2$ (Deg)
55.9	6	51.0	3.66	2.48	1.51	.05
63.3	8	63.0	3.32	2.51	1.22	.22
69.3	10	75.0	3.02	2.81	.92	.09
72.6	11	75.0	2.22	3.19	.94	.10
75.2	12	75.0	2.11	2.98	1.01	.22
77.7	13	75.0	2.02	2.87	.83	.18
79.6	14	75.0	1.86	2.85	.62	.10

TIME (Sec)	ALTITUDE (Km)	WIND SPEED (M/Sec)	β_{ss} (Deg)	ΔSHEAR (Deg)	ΔGUSTS (Deg)	$\Delta C_1, C_2$ (Deg)
56.8	6	51.0	.20	.27	.48	1.88
63.8	8	63.0	1.22	.93	.97	1.99
70.4	10	75.0	1.50	2.55	1.31	1.87
72.8	11	75.0	1.33	3.32	1.40	1.86
75.6	12	75.0	1.53	3.74	1.28	1.55
77.8	13	75.0	1.68	3.45	1.27	1.61
80.5	14	75.0	1.40	3.20	1.00	1.25

TABLE 5
(Continued)

75% DESIGN TAILWIND

TIME (Sec)	ALTITUDE (Km)	WIND SPEED (M/Sec)	α_{ss} (Deg)	ΔSHEAR (Deg)	ΔGUSTS (Deg)	$\Delta C_1, C_2$ (Deg)
56.0	6	37.9	-3.00	-2.23	-1.87	-.01
63.1	8	47.4	-2.65	-2.25	-1.53	-.01
69.3	10	57.0	-2.73	-2.20	-1.32	-.03
72.0	11	57.0	-2.11	-2.57	-1.14	-.06
74.8	12	57.0	-1.84	-2.55	-1.11	-.01
77.2	13	57.0	-1.25	-2.93	-1.03	-.01
79.7	14	57.0	-1.13	-2.80	- .98	-.01

TIME (Sec)	ALTITUDE (Km)	WIND SPEED (M/Sec)	β_{ss} (Deg)	ΔSHEAR (Deg)	ΔGUSTS (Deg)	$\Delta C_1, C_2$ (Deg)
57.0	6	37.9	- .38	- .45	- .54	-1.28
64.0	8	47.4	- .53	- .03	- .44	-1.42
70.2	10	57.0	-1.49	- .14	- .45	-1.30
72.9	11	57.0	- .83	-1.19	- .60	-1.20
75.6	12	57.0	- .87	-1.49	- .69	-1.08
78.1	13	57.0	- .97	-1.14	-1.21	- .99
80.5	14	57.0	- .95	-1.58	- .71	- .87

95% DESIGN TAILWIND

TIME (Sec)	ALTITUDE (Km)	WIND SPEED (M/Sec)	α_{ss} (Deg)	ΔSHEAR (Deg)	ΔGUSTS (Deg)	$\Delta C_1, C_2$ (Deg)
56.1	6	51.0	-3.96	-2.82	-1.92	- .03
63.1	8	63.0	-3.43	-3.00	-1.57	- .06
69.4	10	75.0	-3.62	-3.06	-1.34	.01
72.0	11	75.0	-2.91	-3.39	-1.20	.01
75.0	12	75.0	-2.50	-3.44	-1.14	.01
77.4	13	75.0	-2.34	-3.34	-1.04	.01
79.8	14	75.0	-2.19	-3.11	-1.16	.01

TIME (Sec)	ALTITUDE (Km)	WIND SPEED (M/Sec)	β_{ss} (Deg)	ΔSHEAR (Deg)	ΔGUSTS (Deg)	$\Delta C_1, C_2$ (Deg)
57.0	6	51.0	- .47	- .61	- .69	-1.51
64.0	8	63.0	- .38	- .33	- .36	-1.75
70.1	10	75.0	-1.18	- .94	- .67	-1.64
73.0	11	75.0	-1.11	-1.53	- .68	-1.52
75.6	12	75.0	-1.12	-1.98	- .70	-1.40
78.1	13	75.0	-1.23	-2.22	- .70	-1.27
80.2	14	75.0	-1.26	-2.19	- .68	-1.09

TABLE 5
(Continued)

75% DESIGN LEFT CROSSWIND

TIME (Sec)	ALTITUDE (Km)	WINDSPEED (M/Sec)	α_{ss} (Deg)	ΔSHEAR (Deg)	ΔGUSTS (Deg)	$\Delta C_1, C_2$ (Deg)
56.0	6	37.9	-3.13	-2.24	-1.77	-.04
63.0	8	47.4	-2.90	-2.18	-1.49	-.01
69.2	10	57.0	-2.89	-2.29	-1.33	-.02
72.0	11	57.0	-2.28	-2.74	-1.18	-.02
74.8	12	57.0	-2.07	-2.75	-1.18	+.05
77.2	13	57.0	-2.00	-2.68	-1.07	-.04
79.7	14	57.0	-1.85	-2.65	-1.02	-.01

TIME (Sec)	ALTITUDE (Km)	WINDSPEED (M/Sec)	β_{ss} (Deg)	ΔSHEAR (Deg)	ΔGUSTS (Deg)	$\Delta C_1, C_2$ (Deg)
56.9	6	37.9	- .36	- .36	- .54	-1.49
64.0	8	47.4	- .92	- .27	- .65	-1.63
70.1	10	57.0	-1.29	-1.19	- .90	-1.55
72.9	11	57.0	-1.05	-1.98	-1.04	-1.44
75.5	12	57.0	-1.25	-2.31	-1.09	-1.38
78.0	13	57.0	-1.36	-2.44	-1.10	-1.30
80.4	14	57.0	-1.32	-2.26	-1.05	-1.17

95% DESIGN LEFT CROSSWIND

TIME (Sec)	ALTITUDE (Km)	WINDSPEED (M/Sec)	α_{ss} (Deg)	ΔSHEAR (Deg)	ΔGUSTS (Deg)	$\Delta C_1, C_2$ (Deg)
56.0	6	51.0	-4.20	-2.55	-1.85	.01
63.0	8	63.0	-3.65	-3.00	-1.45	.01
69.2	10	75.0	-3.74	-3.26	-1.16	.01
72.1	11	75.0	-3.00	-3.65	-1.20	.01
74.8	12	75.0	-2.70	-3.70	- .80	.01
77.2	13	75.0	-2.59	-3.91	-1.20	.01
79.6	14	75.0	-2.50	-3.45	-1.03	.01

TIME (Sec)	ALTITUDE (Km)	WINDSPEED (M/Sec)	β_{ss} (Deg)	ΔSHEAR (Deg)	ΔGUSTS (Deg)	$\Delta C_1, C_2$ (Deg)
57.1	6	51.0	- .40	- .57	- .62	-1.76
64.0	8	63.0	- .99	- .73	- .79	-2.04
70.1	10	75.0	-1.59	-2.00	-1.22	-2.11
72.9	11	75.0	-1.83	-2.90	- .34	-2.76
75.5	12	75.0	-1.65	-3.38	-1.20	-1.80
78.1	13	75.0	-1.79	-3.59	-1.10	-1.73
80.5	14	75.0	-1.70	-3.42	-1.03	-1.49

TABLE 6

WIND RESPONSE DISPERSIONS FOR AS-205/CSM-101
WIND BIASED TRAJECTORY

50% DESIGN HEADWIND

TIME (Sec)	ALTITUDE (Km)	WIND SPEED (M/Sec)	α_{ss} (Deg)	ΔSHEAR (Deg)	ΔGUSTS (Deg)	$\Delta C_1, C_2$ (Deg)
56.0	6	32.2	2.49	1.71	1.69	.01
63.2	8	39.6	2.32	1.57	1.31	.01
69.2	10	47.0	2.08	1.77	1.06	.01
72.0	11	47.0	1.57	2.03	.95	.05
75.1	12	47.0	1.48	1.87	.98	.07
77.8	13	47.0	1.40	1.80	.89	.10
79.9	14	47.0	1.20	1.91	.82	.05

TIME (Sec)	ALTITUDE (Km)	WIND SPEED (M/Sec)	β_{ss} (Deg)	ΔSHEAR (Deg)	ΔGUSTS (Deg)	$\Delta C_1, C_2$ (Deg)
56.8	6	32.2	.26	.25	.31	1.29
64.0	8	39.6	1.01	.30	.62	1.40
70.0	10	47.0	1.10	1.15	.94	1.29
72.8	11	47.0	.78	1.80	1.02	1.20
75.5	12	47.0	1.00	1.92	1.10	1.16
78.0	13	47.0	1.10	2.00	.90	1.00
80.2	14	47.0	1.05	1.99	.68	.90

75% DESIGN HEADWIND

TIME (Sec)	ALTITUDE (Km)	WIND SPEED (M/Sec)	α_{ss} (Deg)	ΔSHEAR (Deg)	ΔGUSTS (Deg)	$\Delta C_1, C_2$ (Deg)
56.0	6	37.9	4.19	2.01	1.44	.01
63.1	8	47.4	3.93	1.91	1.20	.01
69.4	10	57.0	3.86	2.02	.98	.01
72.8	11	57.0	3.38	2.28	1.05	.01
74.8	12	57.0	3.27	2.39	.84	.01
77.2	13	57.0	2.86	2.19	.90	.01
79.8	14	57.0	2.29	2.14	.81	.01

TIME (Sec)	ALTITUDE (Km)	WIND SPEED (M/Sec)	β_{ss} (Deg)	ΔSHEAR (Deg)	ΔGUSTS (Deg)	$\Delta C_1, C_2$ (Deg)
57.0	6	37.9	.15	.36	.49	1.81
64.1	8	47.4	1.27	.86	.98	1.84
70.3	10	57.0	2.00	1.96	1.33	1.67
73.0	11	57.0	2.21	2.70	1.38	1.52
75.6	12	57.0	2.40	2.89	1.30	1.62
78.2	13	57.0	2.18	2.57	1.23	1.14
80.5	14	57.0	1.81	2.21	.99	1.05

TABLE 6
(Continued)

75% DESIGN TAILWIND

TIME (Sec)	ALTITUDE (Km)	WIND SPEED (M/Sec)	α_{ss} (Deg)	ΔSHEAR (Deg)	ΔGUSTS (Deg)	$\Delta C_1, C_2$ (Deg)
56.1	6	37.9	-1.29	-1.19	-1.92	- .01
63.8	8	47.4	-1.06	-2.22	-1.59	- .01
69.5	10	57.0	-1.30	-2.02	-1.48	- .01
72.3	11	57.0	- .30	-2.68	-1.27	- .01
75.0	12	57.0	- .09	-2.50	-1.28	- .01
77.4	13	57.0	- .30	-2.40	-1.02	- .20
80.0	14	57.0	- .50	-2.35	- .95	- .20

TIME (Sec)	ALTITUDE (Km)	WIND SPEED (M/Sec)	β_{ss} (Deg)	ΔSHEAR (Deg)	ΔGUSTS (Deg)	$\Delta C_1, C_2$ (Deg)
57.2	6	37.9	- .19	- .47	- .45	-1.02
64.2	8	47.4	- .33	- .44	- .03	-1.12
70.3	10	57.0	- .42	-1.06	- .41	-1.06
73.0	11	57.0	- .08	-1.35	- .59	- .84
75.8	12	57.0	- .40	-1.37	- .69	-1.00
78.2	13	57.0	- .26	-1.63	- .73	- .90
80.6	14	57.0	- .33	-1.80	- .60	- .85

95% DESIGN TAILWIND

TIME (Sec)	ALTITUDE (Km)	WIND SPEED (M/Sec)	α_{ss} (Deg)	ΔSHEAR (Deg)	ΔGUSTS (Deg)	$\Delta C_1, C_2$ (Deg)
56.2	6	51.0	-2.21	-3.78	- .94	.01
63.3	8	63.0	-1.85	-2.92	-1.73	.01
69.5	10	75.0	-1.86	-3.25	-1.45	.01
72.2	11	75.0	- .98	-3.54	-1.36	.01
75.0	12	75.0	- .63	-3.51	-1.28	.01
77.5	13	75.0	- .80	-3.40	-1.02	.01
80.0	14	75.0	-1.00	-3.15	-1.20	.01

TIME (Sec)	ALTITUDE (Km)	WIND SPEED (M/Sec)	β_{ss} (Deg)	ΔSHEAR (Deg)	ΔGUSTS (Deg)	$\Delta C_1, C_2$ (Deg)
57.1	6	51.0	- .31	- .58	- .36	-1.35
64.1	8	63.0	- .41	- .12	- .32	-1.47
70.2	10	75.0	- .75	- .95	- .45	-1.41
73.0	11	75.0	- .16	-1.84	- .55	-1.25
75.7	12	75.0	- .29	-2.05	- .68	-1.19
78.1	13	75.0	- .50	-2.29	- .71	-1.18
80.7	14	75.0	- .62	-2.29	- .68	-1.11

TABLE 6
(Continued)

75% DESIGN LEFT CROSSWIND

TIME (Sec)	ALTITUDE (Km)	WIND SPEED (M/Sec)	α_{ss} (Deg)	ΔSHEAR (Deg)	ΔGUSTS (Deg)	$\Delta C_1, C_2$ (Deg)
56.0	6	37.9	-3.00	-2.21	-1.91	- .01
63.3	8	47.4	-3.85	-1.07	-1.58	- .01
69.5	10	57.0	-2.79	-2.23	-1.56	- .01
72.1	11	57.0	-2.14	-2.71	-1.33	- .01
75.2	12	57.0	-2.01	-2.77	-1.15	- .01
77.2	13	57.0	-1.98	-2.70	-1.04	- .01
79.9	14	57.0	-1.78	-2.62	-1.03	- .01

TIME (Sec)	ALTITUDE (Km)	WIND SPEED (M/Sec)	β_{ss} (Deg)	ΔSHEAR (Deg)	ΔGUSTS (Deg)	$\Delta C_1, C_2$ (Deg)
57.0	6	37.9	- .30	- .41	- .48	-1.50
64.0	8	47.4	- .85	- .49	- .68	-1.78
70.2	10	57.0	-1.30	-1.35	- .98	-1.41
73.0	11	57.0	-1.12	-2.06	-1.11	-1.42
75.8	12	57.0	-1.31	-2.41	-1.16	-1.35
78.1	13	57.0	-1.41	-2.48	-1.12	-1.30
80.5	14	57.0	-1.39	-2.26	-1.10	-1.11

95% DESIGN LEFT CROSSWIND

TIME (Sec)	ALTITUDE (Km)	WIND SPEED (M/Sec)	α_{ss} (Deg)	ΔSHEAR (Deg)	ΔGUSTS (Deg)	$\Delta C_1, C_2$ (Deg)
56.0	6	51.0	-3.90	-2.80	-1.75	.01
63.1	8	63.0	-3.60	-2.95	-1.50	.01
69.4	10	75.0	-3.65	-3.25	-1.28	.01
72.2	11	75.0	-2.96	-3.59	-1.25	.01
75.5	12	75.0	-2.60	-3.68	-1.24	.01
77.6	13	75.0	-2.50	-3.65	-1.16	.01
80.0	14	75.0	-2.35	-3.34	-1.19	.01

TIME (Sec)	ALTITUDE (Km)	WIND SPEED (M/Sec)	β_{ss} (Deg)	ΔSHEAR (Deg)	ΔGUSTS (Deg)	$\Delta C_1, C_2$ (Deg)
57.0	6	51.0	- .31	- .64	- .57	-1.80
64.1	8	63.0	- .85	-1.03	- .83	-2.07
70.2	10	75.0	-1.61	-2.22	-1.22	-2.05
73.0	11	75.0	-1.49	-3.10	-1.22	-1.91
75.8	12	75.0	-1.70	-3.51	-1.22	-1.85
78.0	13	75.0	-1.80	-3.62	-1.15	-1.73
80.5	14	75.0	-1.75	-3.37	-1.09	-1.54

TABLE 7

AS-205/CSM-101 POST SEPARATION S-IVB PEAK DYNAMIC RESPONSES TOLERANCES

ITEM	DEVIATION
Thrust Misalignment (Pitch)	±1.75 Degrees (Not Composite)
Thrust Misalignment (Yaw)	±1.75 Degrees (Not Composite)
Thrust Misalignment (Roll)	±1.75 Degrees (Not Composite)
Center of Gravity Offset (Z)	±0.05 Meters
Center of Gravity Offset (X)	±0.05 Meters
Thrust Misalignment (Pitch)	±1.24 Degrees
Thrust Misalignment (Yaw)	±1.24 Degrees

TABLE 8

STAGE SEPARATION TOLERANCES CONSIDERED IN THE AS-205/CSM-101

SINGLE RETRO OUT COLLISION ANALYSIS

ITEM	DEVIATION
Retro Thrust Variation (Not Composite)	±13.28%
Retro Thrust Misalignment (Not Composite)	± .50 Degrees
S-IB Lateral CG Offset	± 1.1 Inches

TABLE 9

AS-205/CSM-101 SINGLE RETRO ROCKET FAILURE STAGING ANALYSIS

Retro Failures Are Simulated During an Otherwise Nominal Separation

Retro Failed	Lateral Clearance Assuming 1025 Kgm. of Residual S-IB Propellants Become Unseated * (Meters)
No. 1	.301
No. 2	.288
No. 3	.255
No. 4	.270

* Lateral clearance of the undeflected J-2 bell bottom (at Interstage Exit Plane with the S-IB Interstage)

Retro Failed	Lateral Clearance Assuming Fully Seated Residual S-IB Propellants * (Meters)
No. 1	.238
No. 2	.224
No. 3	.190
No. 4	.207

TABLE 10

PROPOSED MANEUVERS TO QUALIFY MANUAL CONTROL OF S-IVB ON AS-205/CSM-101 MISSION

		TIME *	
		SEC	MIN:SEC
1.	PULSE IN EACH AXIS	30 SEC	0:30
2.	-PITCH FOR 9°	30 SEC	1:00
3.	STOP RATE, HOLD INERTIAL ATTITUDE	10 SEC	1:10
4.	+PITCH FOR 30°	100 SEC	2:50
5.	STOP RATE, HOLD INERTIAL ATTITUDE	10 SEC	3:00
6.	-ROLL FOR 20°	40 SEC	3:40
7.	STOP RATE, HOLD INERTIAL ATTITUDE	20 SEC	4:00
8.	+ROLL FOR 20°	40 SEC	4:40
9.	STOP RATE, HOLD INERTIAL ATTITUDE	20 SEC	5:00
10.	-YAW FOR 15°	50 SEC	5:50
11.	STOP RATE, HOLD INERTIAL ATTITUDE	10 SEC	6:00
12.	+YAW FOR 15°	50 SEC	6:50
13.	STOP RATE, HOLD INERTIAL ATTITUDE	10 SEC	7:00

* TIME FROM INITIATION OF MANUAL CONTROL (2:30:00 GET) OR $(8406.17)_4$

NOTE: DURING CREW TRAINING CHANGES TO THIS SEQUENCE WILL BE MADE IF FOUND TO BE NECESSARY.

GOVERNMENT FURNISHED DOCUMENTATION

DELIVERABLE ITEM NO.

GFDA NO.	DATE MSFC APPROVAL	DESCRIPTION OF GFD REQ'D	IDENTIFICATION OF GFD
05A00024	4/18/68	L/V Reference Trajectory	MSFC R-AERO-FMR-199-67
		Control System Specifications	a) MSFC R-ASTR-FD-67-15 b) MSFC R-ASTR-F-66-195 c) MSFC R-ASTR-NFM-128-65
		Prescribed Wind Data	a) NASA TM X-53328 b) MSFC R-AERO-Y-118-66
		L/V Systems Tolerances for Liftoff Control Studies	a) MSFC R-AERO-FF-96-67 b) MSFC R-AERO-DCC-15-64 c) MSFC J Dwg. 75M15223 d) MSFC J Dwg. 75M10701 e) KSC D Dwg. 75M13158 f) MSFC J Dwg. 75M14011 g) MSFC J Dwg. 75M14010 h) MSFC J Dwg. 75M02877 i) MSFC J Dwg. 75M02883 j) Corps of Engs. Dwg. U-34 M-7
		Reference Propulsion Data	MSFC Propulsion Tape 1416
		Reference Mass Characteristics	MSFC Mass Tape 2117
		Final Non-Linear Aerodynamics	a) MSFC TM X-53657 b) NASA TM X-53401
		S-IVB Stage Control System Specifications	a) MSFC R-ASTR-NG-88-66 b) MSFC R-ASTR-NG-74-66

GOVERNMENT FURNISHED DOCUMENTATION

DELIVERABLE ITEM NO.

GFDA NO.	DATE MSFC APPROVAL	DESCRIPTION OF GFD REQ'D	IDENTIFICATION OF GFD
05A00023	5/21/68	Propulsion Tape (B-9 Input Tape)	CCSD Edited Propulsion Tape 5351 Merge of CCSD B50263 (S-IB Stage) Propulsion Tape and MSFC 4116 (S-IVB Stage) Propulsion Tape
		Launch Vehicle Operational Flight Trajectory - S-IB and S-IVB Stages	a) Trajectory Printout of S-IB & S-IVB Stages b) MSFC R-ASTR-F-68-15
		Launch Vehicle Operational Flight Trajectory - Orbital Phase Including Orbital Flight Mass Characteristics (CG's and Moments of Inertia)	a) Orbital Trajectory Printout of Inertial Attitudes (Unpublished) b) S-IVB Orbital Attitude and Venting Time Lines for AS-205/CSM-101 Revision B

GOVERNMENT FURNISHED DOCUMENTATION

DELIVERABLE ITEM NO.

GFDA NO.	DATE MSFC APPROVAL	DESCRIPTION OF GFD REQ'D	IDENTIFICATION OF GFD
05A00023 Rev. A	7/2/68	Bending Vibration Modes Frequencies, and Generalized Masses	TN-AP-68-326, Part I, Volume I, Addendum dated May 15, 1968
05A00022	5/18/68	Structural Flight Limits	MSFC R-P&VE-SJ-67-323
05A00023 Rev. C	7/31/68	Updated Orbital Flight Phase Time Lines	a) Apollo Inter-City Interface Control Document 80M92051, Rev. C b) R-ASTR-S-67-82
05A00024 Rev. A	7/31/68	H-1 Engine Thrust Misalignment Due to Vehicle Electrical & Mechanical Tolerances	R-ASTR-NG-170-66
05A00099	8/29/68	AS-205/CSM-101 Launch Vehicle Operational Trajectory (Open Loop PU System)	a) MAVRIK Punch Card Data (S-IB & S-IVB) b) B-9 Propulsion Tape (S-IB & S-IVB) c) S-IB and S-IVB Trajectory Printout d) Sequence of Events (Table from the Report)
		Revised Structural Limits	R-P&VE-SJ-68-186, "Revised Structural Limits for the Saturn IB AS-205 Vehicle", dated 7/16/68

REFERENCES

1. MSFC Operational Trajectory Data Report, "AS-205/CSM-101 Launch Vehicle Operational Trajectory", dated 15 May, 1968

2. MSFC Dwg. 75M-10701, "Saturn IB Vehicle No. 201 LC-34".

3. MSFC Dwg. 75M-12492, "Apollo Access Arm Installation".

4. MSFC Dwg. 75M-02883, "Fuel Filling Mast Installation, C-1 Block II Complex 34".

5. MSFC Dwg. 75M-02877, "LOX Fill Mast Installation Complex 34 S-IB".

6. MSFC Dwg. 75M-14010, "Short Cable Mast Installation Pos. IV Complex 34 S-IB".

7. MSFC Dwg. 75M-14011, "Short Cable Mast Installation Pos. II Complex 34 S-IB".

8. MSFC Dwg. 75M-15223, "Complex 34 Firing Accessories Saturn IB".

9. MSFC R-AERO-AD-67-40, "Design Criteria: Apollo/Saturn IB Vehicle Liftoff Aerodynamics", dated 26 April 1967.

10. NASA TMX-53328, "Terrestrial Environment (Climatic) Criteria Guidelines for Use in Space Vehicle Development, 1966 Revision", dated 1 May 1966.

11. CCSD TB-AE-56-639, "Saturn IB Liftoff Motion Parametric Analysis", dated 5 August 1965.

12. MSFC R-AERO-DCC-15-64, "Saturn IB Liftoff Tower Clearance Study", dated 9 September 1964.

13. MSFC Letter, R-AERO-FF-96-67.

14. NASA TMX-53657, "Static Aerodynamic Characteristics of the Apollo-Saturn IB Vehicle", dated 25 September 1967.

15. CCSD TN-AP-68-302, Addendum-1, "Revised Saturn IB, SA-205/CSM Aerodynamic Axial Force Characteristics", dated 1 April 1968.

16. MSFC R-ASTR-F-68-15, "Control Gains and Shaping Networks for AS-205, AS-207, and AS-209, S-IB and S-IVB Stages", dated 7 February 1968.

17. MSFC R-ASTR-NFM-128-65, "The Linear Equations and Nonlinear Models for Saturn IB Thrust Vector Control System", dated 18 March 1965.

18. R-P&VE-SJ-67-323, "Structural Limits on Saturn IB, AS-205 Vehicle", dated 24 October, 1967

19. MSFC R-AERO-Y-118-66, Amendment No. 1, "Addendum to Cape Kennedy Wind Component Statistics 0-60 KM. Altitude, for all Flight Azimuths for Monthly and Annual Reference Periods", dated 5 December 1966.

20. CCSD TB-AE-65-313, "Saturn IB Preliminary Engine Out Controllability Study", dated 7 December 1965

21. CCSD BB 3.6.1-1-101, "Saturn IB Vehicle Thrust Vecto· Control (TVC) System Mathematical Model and Load Analysis", dated 31 March 1967.

22. CCSD TN-AP-66-46, "AS-202 Launch Vehicle Dynamics Analyses".

23. NASA TMX-53042, "A Technique for Including the Effects of Vehicle Parameter Variations in Wind Response Studies", dated 1 May 1964.

24. CCSD TB-AP-68-145, "Bending Moment Coefficients for the AS-205 Vehicle", dated 6 February 1968.

25. MSFC R-P&VE-SJ-67-288, "Upper Stage Capability for Saturn IB Vehicle", dated 11 September 1967.

26. MSFC R-AERO-DCC-12-66, "Chi-freeze Values for Single Engine Out on AS-204", dated 7 December 1965.

27. MSFC Dwg. 1B31436, "Frame Installation Forward Interface, Aft Interstage".

28. MSFC Dwg. 1B32282, "Inboard Cap, Forward Closing Frame, Aft Interstage".

29. Thiokol TEMS-17, "Model Specification Rocket Motor, Solid Propellant, Recruit, Thiokol Chemical Corporation, Model No. TE-M-29-5", dated 31 May 1966.

30. Thiokol SP-544A, "Model Specification Motor, Rocket, Solid Propellant", dated 23 February 1966.

31. CCSD TB-P&VE-67-235A, "S-IB Thrust Decay Characteristics During Flight Revision A", dated 21 March 1968.

32. NASA TMX-53657, "Static Aerodynamic Characteristics of the Apollo-Saturn IB Vehicle", dated 25 September 1967.

33. CCSD BB-3.8.0-2-201, "Final Predicted Mass Characteristics Saturn IB Vehicle AS-205", dated 11 March 1968.

34. CCSD TN-AP-66-156, "AS-206A Launch Vehicle Operational Flight Trajectory Dispersion Analysis", dated 29 December 1966.

35. MSFC R-AERO-DCC-16-64, "Saturn IB Separation-Clearance Phase", dated 8 July 1964.

36. MSFC R-P&VE-VAW-66-30, "SA-203 Center of Gravity and Moment of Inertia Three Sigma Deviations for Separation Studies", dated 29 March 1966.

37. MSFC Dwg. 80M92051, "S-IVB/CSM Orbital Attitude Timelines and Vent Schedule for the AS-205", dated 16 November 1966 (Original), dated 8 July 1968 (Revision C).

38. MSFC R-AERO-FMR-170-68, "AS-205/CSM-101 Launch Vehicle Trajectory Listing with an Open Loop Propellant Utilization System", dated 2 August 1968.

39. MSFC R-P&VE-VOO-68-76, "SA-205 Flight Sequence", dated 12 July, 1968.

40. MSFC R-P&VE-SJ-68-186, "Revised Structural Limits for the Saturn IB, AS-205 Vehicle", dated 16 July 1968.

DISTRIBUTION

Marshall Space Flight Center

Mr. Germany I-I/IB-E (1)
Mr. Mann I-I/IB-E (1)
Mr. Jackson R-AERO-P (101) and (1) Reproducible